Environmental effects on the dynamics of coupled nonlinear systems

A thesis

submitted in partial fulfilment of the requirements

of the degree of

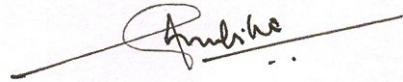Doctor of Philosophy

by

V. Resmi

20073002

INDIAN INSTITUTE OF SCIENCE EDUCATION AND RESEARCH PUNE

April 2012

CERTIFICATE

Certified that the work incorporated in the thesis entitled **Environmental effects on the dynamics of coupled nonlinear systems** submitted by **V. Resmi** was carried out by the candidate, under my supervision. The work presented here or any part of it has not been included in any other thesis submitted previously for the award of any degree or diploma from any other University or institution.

Dr. G. Ambika

(Supervisor)

Date: 23 April 2012

DECLARATION

I declare that this written submission represents my ideas in my own words and where other's ideas have been included, I have adequately cited and referenced the original sources. I also declare that I have adhered to all principles of academic honesty and integrity and have not misrepresented or fabricated or falsified any idea / data / fact / source in my submission. I understand that violation of the above will be cause for disciplinary action by the Institute and can also evoke penal action from the sources which have thus not been properly cited or from whom proper permission has not been taken when needed.

V . Resmi
20073002

Date: 23 April 2012

Acknowledgements

I have known Dr. G. Ambika since my M.Sc. days. She has introduced me to nonlinear dynamics and chaos and has been a great advisor to me. I am impressed by her dedication to science and very organized way of doing research. My teacher, thank you for the encouragement, guidance and support you have been giving me all these years.

I consider it an honour to have collaborated with Prof. R.E. Amritkar (Physical Research Laboratory, Ahmedabad) and Prof. G. Rangarajan (Indian Institute of Science, Bangalore). I have benefited greatly from the discussions I had with them on various aspects of my work. I sincerely thank them for their contribution to this thesis. It is a pleasure to thank Prof. A.D. Gangal, Dr. M.S. Santhanam and Dr. T.S. Mahesh who were in my research advisory committee for their valuable feedback and suggestions. I am grateful to Dr. Pranay Goel for teaching me the basics of mathematical biology. I wish to thank Dr. Amitabha Bose (New Jersey Institute of Technology, United States) for discussions.

Dr.V.S. Rao, Registrar, IISER-Pune, has always been approachable and encouraging. My sincere thanks to him. I would like to thank Dr. K. N. Ganesh, Director, IISER-Pune, for the excellent research facilities and academic environment here. I acknowledge the financial support from IISER-Pune in the form of research fellowship. Many thanks to IISER administration, library, computer, transport and house-keeping staff. In particular, I would like to thank Prabhakar who was very helpful in various ways.

I would like to the thank the organizers of DST-SERC Schools Kolkata, Bangalore and Delhi, and IMSc Complex systems school, Chennai for providing with excellent intellectual environment. I have learned many valuable lessons from the lectures and practice sessions. I would like to thank Rajeev, Sridhar, Vikram, Suman and Vimal for their company during those schools. Special thanks to Rajeev for being a great host in Chennai. Many thanks to Vimal for the pleasant time we spent together. I am thankful to the organizers of the Sokendai life science retreat for the opportunity to present my work there. Special thanks to Dr. L.S. Shashidhara and Prof. Yasushi Hiromi (National Institute of Genetics, Japan) for

It is really a nice experience to be in a group with Madhuri, Snehal, Kajari and Abhijith. I have enjoyed the group meetings and many discussions with them. Madhuri has assisted me in writing this thesis. My sincere thanks to her. Special thanks to Sheekha for starting an excellent piece of work during her summer project with Dr. Ambika.

It was fun to be with my fellow students. I thank Arun, Mayur, Kanika, Hardik, Keerthi, Vimal, Neeraj, Madhan, Usha, Murthy, Arthur, Yogesh, Peepi, Somu, Abhishek, Swati, Kajari, Snehal and Shweta for all the fun we had in common room. I cherish those Ludo games, ice-cream treats, Saturday-talks, sweets, and many celebrations. Mayur, Arun and Madhan, I really enjoyed the many heated arguments we had on varied social, political issues and philosophy. Hardik, thank you so much for trying to teach me some math. Thanks to Kanika for insisting that we attend all the seminars. I would like to thank Savita and Mubeena for tolerating my unorganized room. It was nice to be with Anurag, Viral and Karthik during my first few months in IISER. Many thanks to Gayathri, Sheekha, Murthy, Ramya and Peepi for the wonderful company in kitchen. Murthy, special thanks to you for the many dinners you cooked for me, whenever I stayed late in the institute or was just too lazy.

The story of my PhD life is not without sleepless nights, insecurities, illnesses, cries and the many shoulders I could lean on to. I am grateful to Gayathri, Mayur, Peepi and Ramya for the many hours they spend consoling me, whenever I approached them with a problem. My sincere thanks to Murthy, Arun and Vimal for their support. Many thanks to Delmy and Akhila for occasional hospitality. I would like to thank Priya, Anandhi, Arul, Jibin, Jeslin and Jiju for the support they extended from miles away. A big thanks to Acha, Annan, Chinnu, Salkuna, Bindu and Kochu for being there for me. Ammachi and Pravy have provided me with emotional and financial support whenever I asked for them, and at times without even asking. I am indebted to them for their patience and understanding. Since I have always taken them for granted, I choose not to thank them here !

Resmi

Abstract

Most of the real world systems are complex and their dynamics is studied by modeling them by many subunits interacting with one another. Such systems with interactions are well studied in the last few decades and are found to exhibit many emergent phenomena. In real world situations, the systems are not isolated, but are in contact with some environment. Studies of nonlinear systems in interaction with the environment are very rare. There are many cases where the different dynamical activities are regulated, monitored or triggered by a common medium or environment. The actual mechanism in such cases are not fully understood and hence this forms a topic of great relevance for a detailed study.

In this thesis, we report the study of emergent phenomena such as synchronization and amplitude death in nonlinear dynamical systems caused by coupling via a common shared environment. We first consider a simple case where, an environment interacts with two uncoupled chaotic systems. The environment has an intrinsic damped dynamics of its own, which is modulated via feedback from the systems. The environment in turn, gives feedback to both the systems. Taking standard chaotic systems such as Rössler and Lorenz systems as examples, we show that such an interaction can be tuned to induce a variety of synchronization phenomena such as in-phase, anti-phase, complete and antisynchronization.

We then consider a case where, two systems are coupled directly such that with sufficient strength of coupling, they can exhibit synchronous behaviour.

The indirect feedback coupling through the environment is introduced in them in such a way as to induce a tendency for anti-synchronization. We show that, for sufficient strengths, these two competing effects can lead to amplitude death. By choosing a variety of dynamics such as periodic, chaotic, hyperchaotic and time-delay systems, we illustrate that this mechanism is quite general and works for different types of direct coupling such as diffusive, replacement and synaptic and different damped dynamics for environment. The specific systems considered in this study are chaotic Rössler and Lorenz systems, Landau-Stuart and van der Pol oscillators, hyperchaotic systems such as hyperchaotic Rössler and Mackey-Glass time-delay systems, non-autonomous systems such as driven van der Pol and Duffing systems.

We further extend the study to the case of a complex network of nonlinear oscillators, in interaction with a common environment. We study the onset of amplitude death in networks of Rössler systems and Landau-Stuart oscillators. An important result of our analysis is that there exists a universal relation between the critical value of coupling strength for amplitude death and the largest non-zero eigenvalue of the coupling matrix for different network topologies.

We develop the stability analysis for all these cases independent of system dynamics and network topology to obtain the criteria for transition to synchronization or amplitude death in each case. Extensive numerical simulations are provided to illustrate the generality of the mechanisms. The results from direct numerical simulations are found to support the results from the stability analysis.

We apply the theory developed in the general case, to the special case of neuronal systems. using Hindmarsh-Rose system as the nodal dynamics, we study in detail the occurrence of synchronized and suppressed neural activity in neurons coupled via gap-junctions and synapses.

Keywords: Coupled oscillators, Complex networks, Environmental coupling, Synchronization, Amplitude death.

Publications

The research work presented in this thesis has appeared in the following publications.

1. V. Resmi, G. Ambika, and R. E. Amritkar, Phys. Rev. E **81**, 046216 (2010)

2. V. Resmi, G. Ambika, and R. E. Amritkar, Phys. Rev. E **84**, 046212 (2011).

3. V. Resmi, G. Ambika, R. E. Amritkar, and G. Rangarajan, Phys. Rev. E **85**, 046211 (2012).

Contents

Chapter 1

Introduction

Nonlinear dynamical systems have been in the focus of intense research activity since the 1960's. Research in this area has lead to many path breaking discoveries like chaos, solitons, stochastic resonance etc. Studies of such nonlinear phenomena have been extremely useful in analysing and understanding the complexity of many real world systems which are inherently nonlinear in nature. Such studies have led to many new fundamental and useful techniques and methods like bifurcation analysis, time series analysis and control theory. Moreover, nonlinear systems are found useful in many practical applications like secure communication [1–4], logic gates [5–9], and optimal control and resonances [10–12].

Nonlinear dynamical systems arise in all branches of science, engineering and technology and in diverse fields such as economics and social dynamics. Such systems in general can be modeled by nonlinear differential equations that occur in several forms, ordinary, partial, delay, difference etc., depending on the nature of the dynamics of the system. The nature of the underlying dynamics derived from these systems has interesting variety depending on the number of independent variables, order of the highest derivative, degree of nonlinearity, numerical value of the control parameter and initial conditions.

In our work, we deal with continuous dynamical systems which are rep-

resented by nonlinear differential equations of the form

$$\dot{x} = F(a, x), \tag{1.1}$$

where, x is an m-dimensional vector defining the phase space of the system, F is the nonlinear function governing the dynamics and a is the set of control parameters involved in the dynamics.

For a given set of initial values of x at time $t = 0$, $x(0)$, the above equation can be analysed either analytically or numerically to study the evolution of the system in its phase space. Most of the systems are dissipative in nature, which means,

$$\nabla \cdot F < 0. \tag{1.2}$$

Therefore, the phase space volume contracts as the system evolves and asymptotically reaches a state called attractor. Depending on the nonlinearity of F and the values of the control parameters a, different types of attractors can arise in the systems, viz, steady state or fixed point, periodic limit cycle, quasiperiodic, chaotic and hyperchaotic behaviors. The nature of this attractor determine the asymptotic dynamics of the system. The set of initial conditions that settle to a given attractor is called the basin of that attractor. If more than one attractor exist for a given set of parameter values, the system is said to have multistability, with basins separated by basin boundaries.

The set of parameters a, called control parameters, controls the asymptotic state of the system and often such systems undergo transitions from one type of attractor to another as these parameters are changed. Such transitions, called bifurcations can explain the change of a dynamical system from fixed point behavior to chaotic behavior.

If the system asymptotically settles to steady state behavior,

$$\dot{x} = 0. \tag{1.3}$$

Therefore, the steady state or fixed point, x^*, can be obtained by solving,

$$F(x^*) = 0. \tag{1.4}$$

Depending on the nonlinearity of F, the system in general can have p fixed points. However, all of them need not be stable. The stability of a fixed point is decided by the eigenvalue of the Jacobian of the system evaluated at the fixed point. The Jacobian is defined as the matrix J, whose elements are given by

$$J_{ij} = \left.\frac{\partial F_i}{\partial x_j}\right|_{x^*}. \tag{1.5}$$

Based on the nature of eigenvalues of the Jacobian, the fixed points can be classified as nodes, spiral nodes, repellers, saddle point etc. [13]. If all the eigenvalues have negative real parts, the fixed point is stable.

When the control parameters change, the stable fixed point can become unstable giving rise to another type of fixed point or limit cycle. Such transitions, or bifurcations can be identified by studying the eigenvalue of the Jacobian as the parameter changes. In general, a limit cycle can undergo a series of bifurcations called period doubling bifurcations to reach aperiodic or chaotic behavior. This is called the period doubling route to chaos [13]. There are other routes like intermittency and Ruelle-Takens-Newhouse scenario or quasiperiodic route [13] by which a dynamical system can exhibit chaotic behavior as the control parameter is changed. Such phenomena will be described in detail by taking specific examples later, in section 1.1.1

1.1 Chaos and its characterization

Among the various attractors possible for nonlinear dynamical systems, the chaotic attractor is highly special with peculiar properties like irregularity, aperiodicity, and sensitive dependence on initial conditions. [14, 15]. Chaos represents the third revolutionary concept and paradigm shift in the history

of physics in the last century, and the modern history of chaos starts from E. Lorenz who discovered the existence of long term unpredictability in a system of equations called the Lorenz system [16].

As mentioned earlier, chaotic systems are sensitive to initial conditions, such that, two identical systems starting from very near initial conditions separate or diverge as they evolve in time. This phenomena, called the butterfly effect by Lorenz, can be characterized using an index called Lyapunov exponent. If $\Delta x(0)$ represent the difference in initial conditions, $\Delta x(t)$ the separation of their trajectories at time t, then, in general

$$\Delta x(t) = \Delta x(0)e^{\lambda t}, \tag{1.6}$$

where λ representing the average separation, is called the Lyapunov exponent. Lyapunov exponents are computed numerically by integrating the dynamical equations and their variations and computing $\Delta x(t)$. The details of these are given by Wolf algorithm [17] which is often used for computing the Lyapunov exponents of a system. An m-dimensional system will have m such exponents and if all of them are negative, the system asymptotically will go to a steady state behavior. If one of them is zero, and all others are negative, the system's dynamics will be periodic motion. If more than one Lyapunov exponents are zero, and all others are negative, the motion is quasiperiodic. If one of the Lyapunov exponents are positive, the motion is chaotic and if more than one Lyapunov exponents are positive, the motion is said to be hyperchaotic [14]. These different dynamical states of nonlinear systems are illustrated in Fig. 1.1. Transitions from one dynamical behavior to another, or bifurcations, as the control parameter is changed can therefore be traced by calculating the Lyapunov exponent of the system. Especially in the context of chaotic attractors, Lyapunov exponent gives a dynamical characterization of a chaotic attractor, while a geometric characterization is possible by using the concept of fractal dimensions [13, 14]. Now, we discuss in detail the concepts introduced above by taking specific examples.
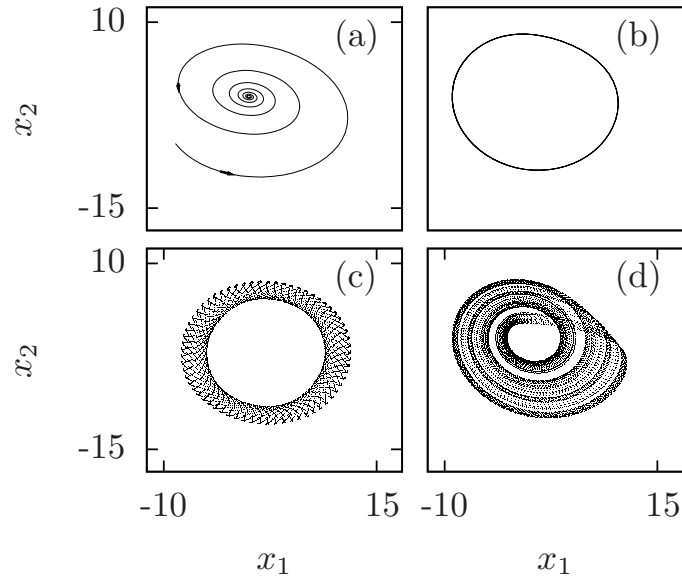
Figure 1.1: Different dynamical states of nonlinear systems. (a) Fixed point, (b) limit cycle, (c) quasiperiodic orbit and (d) chaotic attractor.

1.1.1   Chaotic dynamical systems

Rössler system

Rössler system was introduced by O. Rössler in 1976 [18]. The dynamics of this system is given by the following equations

$$
\begin{aligned}
\dot{x}_1 &= -x_2 - x_3, \\
\dot{x}_2 &= x_1 + ax_2, \\
\dot{x}_3 &= b + x_3(x_1 - c).
\end{aligned}
\tag{1.7}
$$

The fixed points of this system are given by

$$
\begin{aligned}
x_1^* &= \frac{c \pm \sqrt{c^2 - 4ab}}{2} \\
x_2^* &= -\left(\frac{c \pm \sqrt{c^2 - 4ab}}{2a}\right) \\
x_3^* &= \frac{c \pm \sqrt{c^2 - 4ab}}{2a}
\end{aligned}
\tag{1.8}
$$
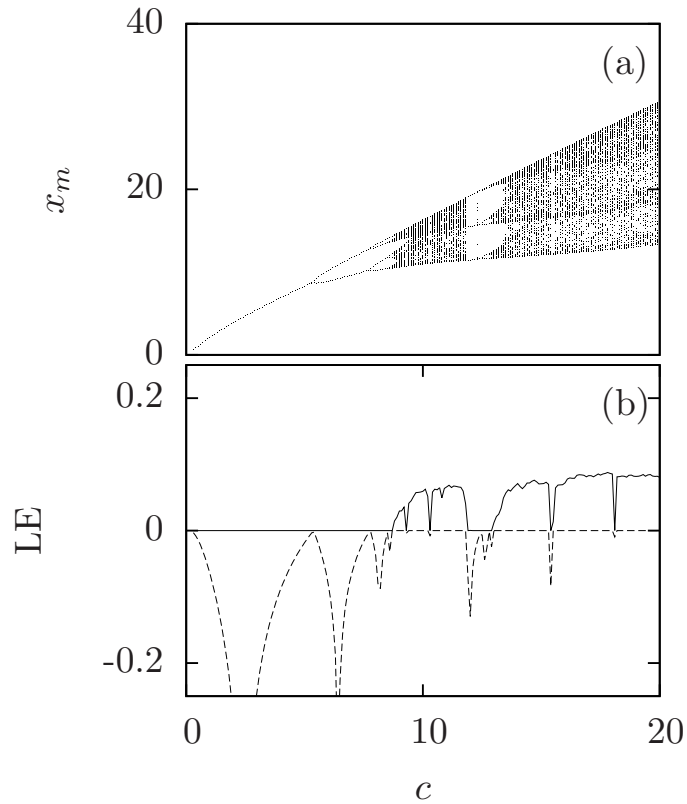
Figure 1.2: (a) Bifurcation diagram for Rössler system given in Eq. (1.7) for increasing c. The maxima of the x_1 variable, x_m, is plotted for sufficiently long interval of time. (b) Lyapunov exponents for Rössler system for increasing c. Other parameters are fixed at $a = b = 0.1$.

We analyse the system by fixing the parameters $a = b = 0.1$ and increasing c. For $c < 0.2$, the fixed points are not real. At $c = 0.3$, we see that the trajectory is a periodic limit cycle. As c is increased, the system undergoes a series of period-doubling bifurcations to chaos. The bifurcation diagram for this is shown in Fig. 1.2(a). Transitions between periodic and chaotic states can also be identified from the Lyapunov exponents, as shown in Fig. 1.2(b). When the system is in chaotic state, the largest Lyapunov exponent is positive. The phase-space plot of representative states are shown in Fig. 1.3(a)-(d).

6
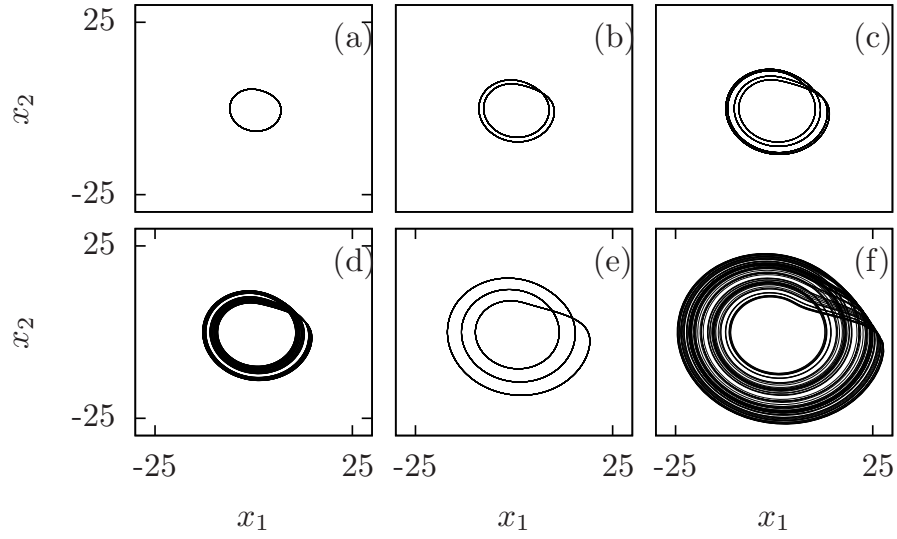
Figure 1.3: Phase space plots of different dynamical states of Rössler system for $a = b = 0.1$. (a) 1-cycle at $c = 4$, (b) 2-cycle at $c = 6$, (c) 4-cycle at $c = 8.5$, (d) chaos at $c = 9$, (e) 3-cycle at $c = 12$, (f) chaos at $c = 18$.

Lorenz system

Lorenz system wad introduced by E.Lorenz in 1963 as a simplified mathematical model for atmospheric convection [16]. The dynamics of this system is given by the following equations

$$
\begin{aligned}
\dot{x}_1 &= \sigma(x_2 - x_1) \\
\dot{x}_2 &= x_1(r - x_3) - x_2 \\
\dot{x}_3 &= x_1 x_2 - b x_3
\end{aligned}
\tag{1.9}
$$

Later, these equations were shown to describe dynamics of a single mode laser [19] and a segmented disc dynamo in the presence of friction [20].

The fixed points of Eq. (1.9) are given by

$$
\begin{aligned}
x_1^* &= \pm\sqrt{(b(r-1))}, \\
x_2^* &= \pm\sqrt{(b(r-1))}, \\
x_3^* &= r - 1.
\end{aligned}
\tag{1.10}
$$

7
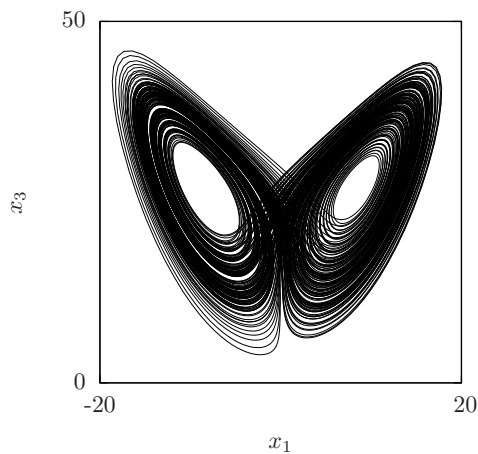
Figure 1.4: The chaotic attractor of the Lorenz system at $\sigma = 10$, $b = 8/3$ and $r = 28$.

For $\sigma = 10$, $b = 8/3$ and $0 < r < 1$, the only real fixed point is $(0,0,0)$ and is stable. At $r = 1$, this fixed point becomes unstable, and the fixed points $(\pm\sqrt{(b(r-1))}, \pm\sqrt{(b(r-1))}, r-1)$ becomes real and stable. At $r \sim 24.73$ these fixed points becomes unstable and the system settles to a chaotic attractor. The chaotic attractor at $r = 28$ is well-studied and a phase space plot of the same is shown in Fig. 1.4

Some of the other dynamical systems of interest that are often encountered are discussed below.

van der Pol oscillator

The van der Pol oscillator is a damped nonlinear oscillator [14], whose dynamics is described by

$$\ddot{x} - a(1 - x^2)\dot{x} + x = b\sin(\omega t), \tag{1.11}$$

where, a is the strength of damping, b and ω are the strength and frequency of forcing respectively. This is a system with nonlinear damping term and hence capable of limit cycle motion in the absence of forcing. In the absence of forcing ($b = 0$), the origin is the fixed point of the system. This fixed point

8
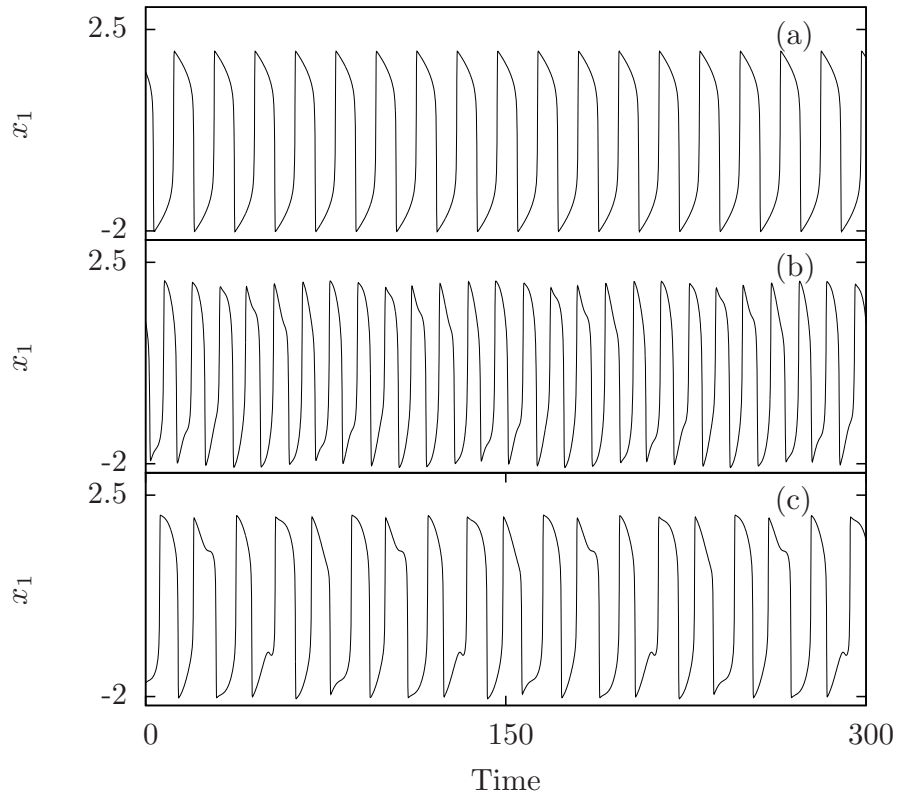
Figure 1.5: The time series of the x_1 variable of the van der Pol oscillator (Eq. (1.11)) showing different dynamical states. (a) Periodic at $a = 8.53$, $b = \omega = 0$, (b) quasiperiodic at $a = 5$, $b = \omega = 1$ and (c) chaotic at $a = 8.53$, $b = 1.2$ and $\omega = 0.63$.

is unstable for $0 < b < \infty$, and the system exhibits a periodic limit cycle. In the presence of forcing, the system can exhibit quasiperiodicity and chaos, depending on the values of b and ω. In Fig. 1.5(a)–(c), we show the time series of periodic, quasiperiodic and chaotic states in van der Pol oscillators for specific values of the parameters.
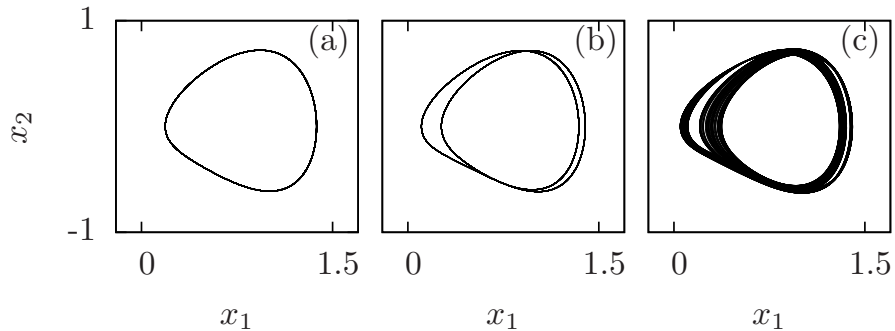
Figure 1.6: Phase space plots of different dynamical states of Duffing oscillator for $a = 0.5$, $\omega_0^2 = 1$. (a) 1-cycle at $b = 0.34$, (b) 2-cycle at $b = 0.35$, (c) chaos at $b = 0.36$.

Duffing oscillator

The Duffing oscillator is another example of a damped and driven nonlinear oscillator [14]. The dynamics is given by

$$\ddot{x} + a\dot{x} - \omega_0^2 x + x^3 = b\cos(\omega t) \tag{1.12}$$

This represents an oscillator with a double-well potential and hence appears in many situations including doubly clamped nano-mechanical oscillators. The fixed points of this system in the absence of forcing ($b = 0$) are given by

$$x^* = 0, \tag{1.13}$$

and

$$x^* = \pm\omega_0. \tag{1.14}$$

The fixed point $x^* = 0$ is unstable for all $a > 0$. The other two fixed points, $x^* = \pm\omega_0$ are stable, and the system settles to any one of them depending on the initial conditions. In the presence of forcing, the system undergoes period doubling sequence to chaos [21]. This is illustrated in the phase space plots in Fig. 1.6.
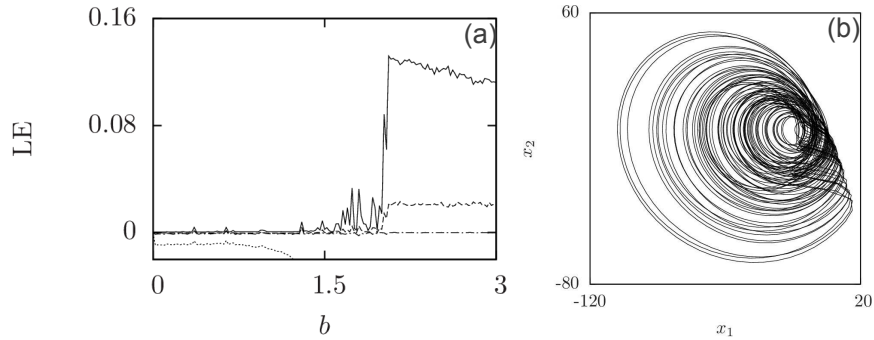
Figure 1.7: (a) Lyapunov exponents of the hyperchaotic Rössler system for $a = 0.25$, $c = 0.5$ and $d = 0.05$ and increasing b. (b) Phase space plot of hyperchaotic Rössler sytem for $a = 0.25$, $b = 3$, $c = 0.5$ and $d = 0.05$

1.1.2 Hyperchaotic systems

The hyperchaotic Rössler equations were introduced by Rössler in 1979 [22].

$$
\begin{aligned}
\dot{x}_1 &= -x_2 - x_3 \\
\dot{x}_2 &= x_1 + ax_2 + x_4 \\
\dot{x}_3 &= b + x_3 x_1 \\
\dot{x}_4 &= -cx_3 + \sigma x_4
\end{aligned}
\tag{1.15}
$$

The system has hyperchaotic trajectory for the following parameters $a = 0.25$, $b = 3$, $c = 0.5$ and $d = 0.05$ with two positive Lyapunov exponents as shown in Fig. 1.7(a). The phase space plot for this state is shown in Fig. 1.7(b).

1.1.3 Time-delay systems

Time-delay systems are a special class of nonlinear dynamical systems, which are capable of exhibiting rich variety of dynamics such as periodic, chaotic and hyperchaotic motion, depending on the value of delay. The Mackey-Glass system is one of the frequently studied time-delay system. It was first introduced by Mackey and Glass in 1977 as a model for blood generation
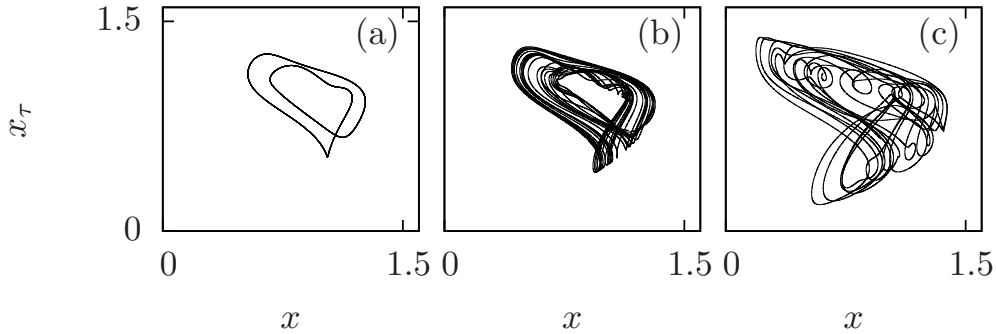
Figure 1.8: Different dynamical states in Mackey-Glass system for fixed $a = 0.1$, $b = 0.2$, $m = 10$ and varying τ. (a) Periodic state for $\tau = 14$, (b) chaotic state for $\tau = 17$, (c) hyperchaotic state for $\tau = 32$.

in patients with leukemia [23]. The equation representing the Mackey-Glass system is given by

$$\dot{x} = -ax + \frac{bx_\tau}{1 + x_\tau^m}, \tag{1.16}$$

where, x_τ is the value of the variable x at a delayed time $x(t - \tau)$. The presence of large time-delays in the equation makes the system effectively high dimensional. Depending on the values of the parameters a,b and delay τ, the system can exhibit fixed point,periodic, chaotic and hyperchaotic behavior. In Fig. 1.8, we show the different dynamical states of Mackey-Glass systems for different τ values.

1.1.4 Excitable systems

Excitable systems form an interesting class of nonlinear dynamical systems that exhibit spikes of oscillatory behavior and finds applications in switching and control phenomena. These systems normally remain in a steady state and can be excited to spiking behavior by large enough external perturbation. Such systems can be modeled by discrete or continuous dynamical equations which often include slow and fast dynamics. A typical example of an excitable system is the dynamics of a neuron. There are different models like Hodgkin-Huxley [24], FitzHugh-Nagumo [25], Hindmarsh-Rose [26]

12

etc. that can describe the spikes and burst characteristics of neuronal dynamics. Among these, Hindmarsh-Rose model is special, in the sense, it is computationally simple, while able to reproduce many different dynamical states exhibited by biological neurons, such as quiescent states, regular and irregular spiking and bursting states etc. [27]. We describe this model below.

Hindmarsh-Rose neuron model

$$
\begin{aligned}
\dot{x}_1 &= x_2 + ax_1^2 - x_1^3 - x_3 + I, \\
\dot{x}_2 &= 1 - bx_1^2 - x_2, \\
\dot{x}_3 &= -\rho(x_3 + s(x_1 + \chi)).
\end{aligned}
\tag{1.17}
$$

Here, x_1 represents the membrane potential, x_2 and x_3 corresponds to fast and slow ion channel currents respectively, and a, b, s, ρ, χ and I are the parameters of the model. The parameter I represents the membrane input current and is usually taken as the control parameter while keeping the other parameters fixed. The parameter ρ is usually chosen to be very small, to make the timescales of the variable x_3 to be slow. As mentioned earlier, different states such as fixed points, periodic spiking, periodic bursting, chaotic spiking, chaotic bursting and multistable states are possible, depending on the parameter values. Different dynamical regimes and bifurcations in Hindmarsh-Rose neuron models are studied in detail in [27–30]. We show the time series of the representative states in Fig. 1.9. Fig. 1.9(a) illustrates periodic or tonic spiking. Time series of chaotic spiking behavior is shown in Fig. 1.9(b). It is interesting to note that, here the chaos is in the inter-spike interval while the amplitude of the spikes remains almost the same. The periodic bursting state has same number of spikes per burst with the inter-burst interval a constant (Fig. 1.9(c)). In the chaotic bursting state, both the number of spikes per burst, and the inter-burst interval may vary (Fig. 1.9(d))
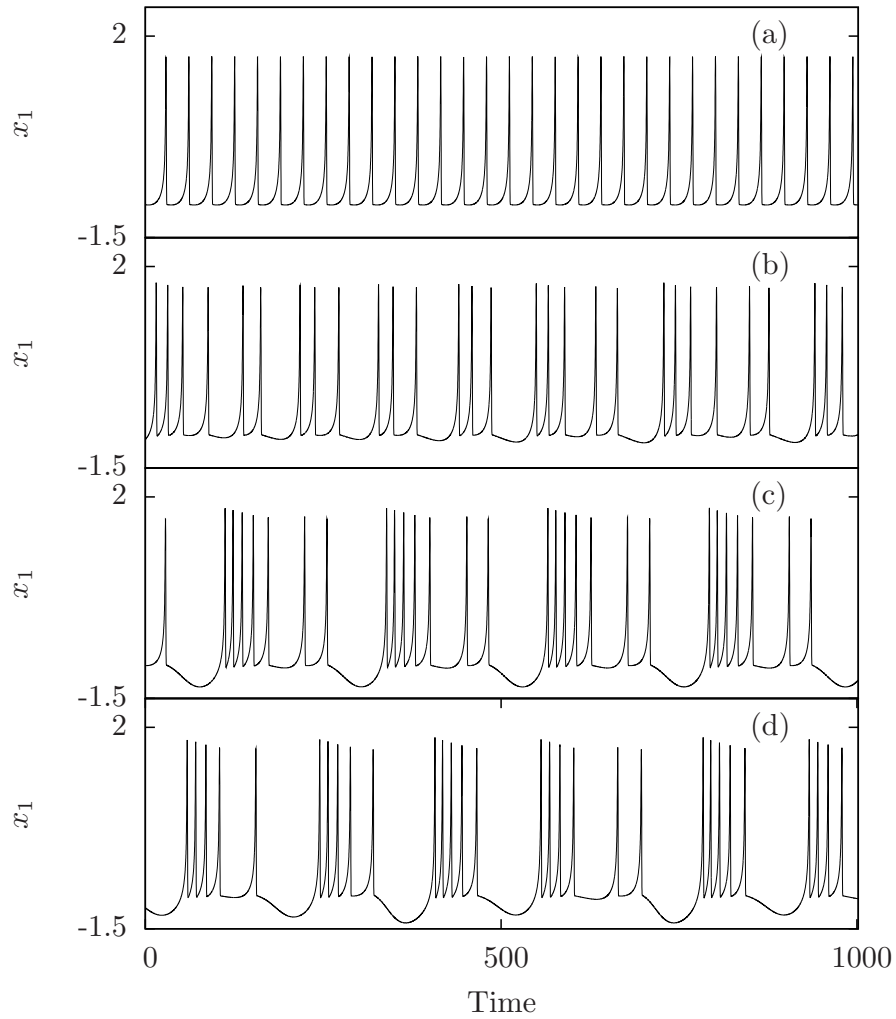
Figure 1.9: The time series of the x_1 variable of the Hindmarsh-Rose neuron model given in Eq. (1.17). (a) Periodic spikes at $I = 3.50$, (b) chaotic spikes at $I = 3.33$, (c) periodic burst at $I = 3.20$ and (d) chaotic burst at $I = 3.05$. The other parameters are taken to be $a = 3$, $b = 5$, $s = 4$, $\rho = 0.005$ and $\chi = 1.6$.

1.2 Summary

In this chapter, we have discussed some of the typical nonlinear dynamical systems capable of exhibiting different dynamical states such as periodic, chaotic and hyperchaotic. In any real-world system, there are many such units that act together to produce collective behavior. We will discuss the interactions among these systems and some of the interesting consequences of these interactions in the next chapter.

Chapter 2

Emergent phenomena in coupled systems

The complex dynamical behavior of many real world systems can be understood as a collective behavior of a number of subsystems or units which are in interaction with each other. The subsystems, in general, can have a dynamics modeled by any of the systems discussed in the preceding chapter. Due to interactions among themselves, coordinated actions of such systems are possible, leading to collective dynamical behavior know as emergent phenomena. Emergence of such collective behavior is hence a relevant problem in the theory of complex systems. Different types of emergent phenomena are known, two important ones being synchronization and amplitude death. We discuss below the salient features of these phenomena.

2.1   Coupled systems

The dynamics of two coupled systems can be written as

$$
\begin{aligned}
\dot{x}_1 &= f_1(x_1) + g(x_1, x_2), \\
\dot{x}_2 &= f_2(x_2) + g(x_2, x_1).
\end{aligned}
\tag{2.1}
$$
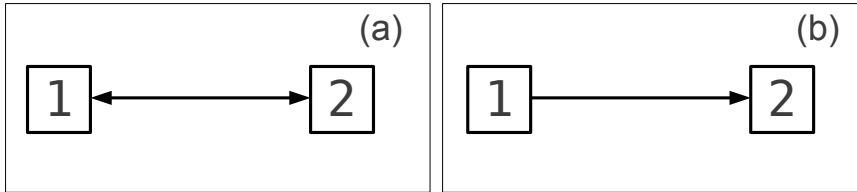
Figure 2.1: Schematic representation of coupling schemes. (a) Bidirectional coupling and (b) unidirectional coupling.

Here the coupling is bidirectional or mutual, as illustrated in Fig. 2.1(a). The coupling can be unidirectional as shown in Fig. 2.1(b). In that case, the dynamics of the coupled systems is given by the following equations

$$
\begin{aligned}
\dot{x}_1 &= f_1(x_1), \\
\dot{x}_2 &= f_2(x_2) + g(x_2, x_1).
\end{aligned}
\tag{2.2}
$$

Here, x_1 is called the drive and and x_2 is called the response system. The intrinsic dynamics of the systems are given by the functions, f_1 and f_2, and can either be identical or mismatched. The coupling between the systems is given by the coupling function g. A commonly used form of the coupling function, called diffusive coupling [31, 32] is given by

$$
g(x_1, x_2) = \epsilon\beta(x_2 - x_1),
\tag{2.3}
$$

where, ϵ is the coupling strength and β is an $m \times m$ matrix, whose elements decide the components of x_1 and x_2 which takes part in the coupling. However, the coupling function g, can take many forms such as replacement [33], subsystem decomposition [34, 35], active-passive decomposition [36, 37] etc. In addition to this, nonlinear coupling schemes such as synaptic coupling are also studied [38, 39]. The diffusive type of coupling in the context of Rössler and Lorenz systems is used in our study given in chapter 4, and the synaptic coupling in the case of Hindmarsh-Rose neurons is used in chapter 7.
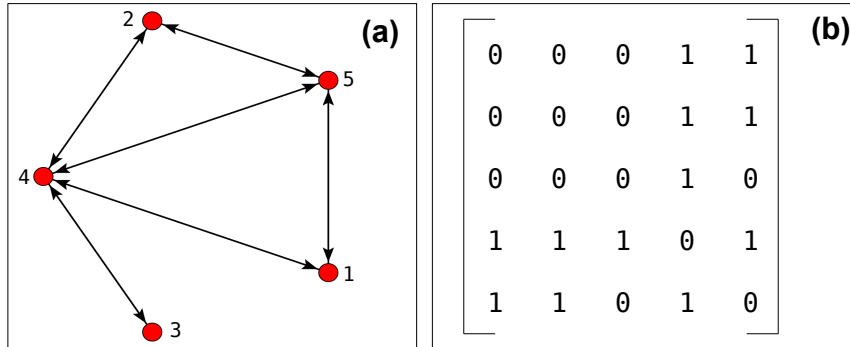
Figure 2.2: (a) Illustration of a network with 5 nodes and (b) the corresponding adjacency matrix.

2.1.1 Networks

In real world systems, a large number of subsystems are connected to form complex networks. The dynamics of such a network can be written as

$$\dot{x}_i = f_i(x_i) + \epsilon \sum_{j=1}^{N} A_{ij} H(x_j), \tag{2.4}$$

where H is an $m \times m$ matrix whose elements determine the coupling function and A is an $N \times N$ matrix called adjacency matrix. If A is symmetric, the coupling is bidirectional. The elements of A are decided by the network topology. If $A_{ij} = 1$ for all $i \neq j$, the network is said to be all-to-all coupled. This configuration is also known as the global coupling [40–42]. The configuration where $A_{ij} = 1$ if $|i - j| = 1$ is known as the linear array or chain with nearest neighbour interactions. A chain network with periodic boundary conditions is called a ring. There are other regular network configurations such as tree, lattice etc. The elements of A can be chosen randomly, to form a random network. In Fig. 2.2, we show an illustration of a random network and the corresponding adjacency matrix. Details of the dynamics on such networks in the context of our study are given in chapter 6.

The real world networks are found to exhibit characteristics that are between those of regular and random networks. The small world model

proposed by Watts and Strogatz in 1998 was one of the first models that could explain the co-existence of high clustering and small path lengths exhibited by real world networks. [43]. However, the small-world model of network does not explain the power-law degree distribution exhibited by many real world networks. To explain this, the scale-free network was introduced in 1999 by Barabási and Albert [44]. The study of complex networks is important in many contexts, including biological networks [45–53], epidemics [54–58], traffic networks [59, 60] internet [61, 62], power-grids [63–65]etc.

Due to interactions among the systems in the network, coordinated actions of such systems are possible, leading to collective dynamical behavior known as emergent phenomena. In such cases, the global dynamics depends on the interplay between the network structure and nodal dynamics. Emergence of such collective behavior is hence a relevant problem in the theory of complex systems. In the context of complex networks, synchronization and amplitude death are the most well-studied emergent phenomena [48, 66–69].

2.2 Synchronization in coupled systems

Synchronization refers to the coordinated dynamical activity of two or more systems. This is a form of self organization leading to dynamical order. Synchronization of periodic systems was first observed by Christian Huygens [48]. Synchronization is especially relevant in the context of chaotic systems, since even a single chaotic system with slightly different initial conditions evolve very differently. Since the first paper by Pecora and Carol in 1990 [34], the field of chaotic synchronization has grown considerably and is still an area of intense research activity due to its basic role in many real world phenomena and useful technological applications. Synchronous flashing of fireflies [48], cardio-respiratory system [70, 71], collective rhythmic firing of neurons [72] etc. are some of the widely cited examples of synchronization.

Synchronization can be of different types such as complete or identical

synchronization [34, 73], generalized synchronization [74, 75], phase synchronization [76, 77], lag synchronization [78, 79] etc. These states can be achieved by proper choice of the coupling terms and system parameters.

Complete synchronization

The diffusive type of coupling in identical systems can lead to a solution given by

$$x_1(t) = x_2(t) = x(t). \tag{2.5}$$

This is called complete synchronization. This occurs above a critical value of the coupling strength, $\epsilon > \epsilon_c$. In the synchronized state, $|x_2 - x_1| \rightarrow 0$ as $t \rightarrow \infty$. The different types of synchronized states in the case of two coupled systems is illustrated in the time series in Fig. 2.3. Fig. 2.3(a) shows two systems getting stabilized to complete synchronization. Antisynchronization is a special type of synchronization which occurs in the case of two coupled systems. This is the state where the state vectors of both systems have the same absolute values but are of opposite signs, $x_1 = -x_2$ as shown in Fig. 2.3(b). This has also been demonstrated in both numerical simulations and experimental systems [80–90].

Generalized synchronization is the type of synchronization which occurs in unidirectionally coupled non-identical systems [74, 75, 91]. Here, the dynamics of two systems share a functional relationship of the following form

$$x_2 = F(x_1). \tag{2.6}$$

If F is identity, this corresponds to complete synchronization given by 2.5.

Phase synchronization

Phase synchronization is a weaker form of synchronization, where the amplitude of the coupled systems remain uncorrelated, but the phases of both
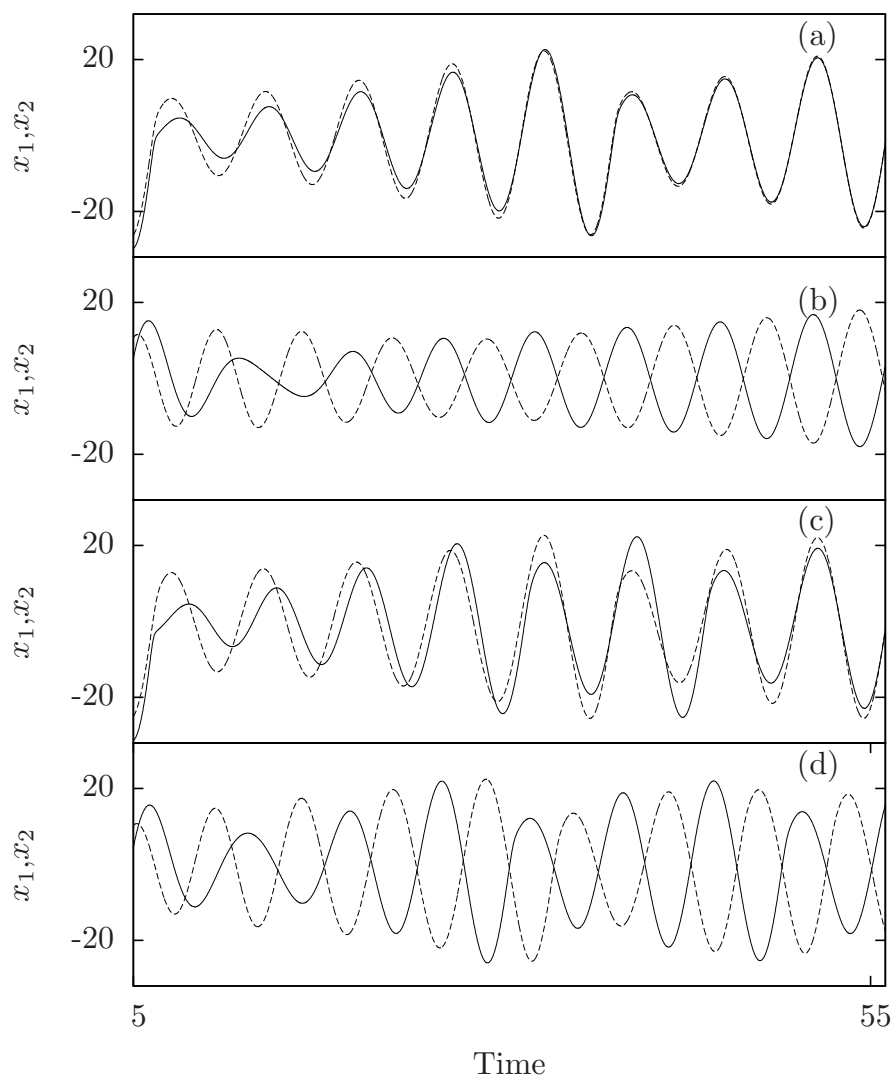
Figure 2.3: Time series showing different synchronization phenomena. (a) Complete synchronization, (b) antisynchronization, (c) in-phase synchronization and (d) antiphase synchronization.

the systems evolve together [76, 92–95]. It could either be in-phase synchronization where the phase difference between the systems is nearly zero (Fig. 2.3(c)), or antiphase synchronization where the phase difference between the systems in nearly π [96–100] (Fig. 2.3(d)).

Phase synchronization usually happens in non-identical systems under weak coupling [76, 77, 101]. This is very relevant in biological systems, since complete synchronization is difficult to achieve in the noisy background. Phase synchronization has been studied in the context of Parkinson's disease using magnetoencephalographic and electromyographic techniques [102]. So also, phase synchronization is demonstrated in cardio-respiratory system in rats [71], Lobster stomatogastric ganglion [103] and electrosensitive cells in paddle fish [104].The transition to phase synchronization is usually an intermittency transition [78, 105].

If the coupling involves a time-delay, corresponding to finite transmission time in communication channels,

$$g(x_1, x_2) = \epsilon \beta (x_{2\tau} - x_1) \tag{2.7}$$

where $x_{2\tau}$ is the state vector of the system x_2, at time $t - \tau$. Then, the synchronized state corresponds to delay or lag synchronization .

$$x_1(t) = x_2(t - \tau). \tag{2.8}$$

This also occurs in coupled non-identical systems with moderate strength of coupling [78, 79, 106]. Lag-synchronization has also been demonstrated in coupled lasers [107] and electroencephalogram of epilepsy patients during seizure [108]. The time-delayed coupling given in Eq. (2.7) can also lead to a state where the response system anticipates the future state of the drive system. This is called anticipatory synchronization [85, 109–111].

Stability of the synchronized state

When two coupled systems settle to a synchronized state the dynamics remains on the hyperplane defined by $x_1 = x_2$. This hyperplane is called the synchronization manifold and the stability of the synchronized state is studied by considering the variations from the synchronized manifold. Let $\xi_\parallel$ and $\xi_\perp$ represent the variations in the synchronization manifold and the transverse manifold respectively. Then, the dynamics of these variations are given by

$$\dot{\xi}_\parallel = \left. \frac{\partial f(x)}{\partial x} \right|_{x(t)} \cdot \xi_\parallel, \tag{2.9a}$$

$$\dot{\xi}_\perp = \left(\left. \frac{\partial f(x)}{\partial x} \right|_{x(t)} - 2\epsilon\beta \right) \cdot \xi_\perp. \tag{2.9b}$$

The synchronization manifold is stable, if the transverse Lyapunov exponent, corresponding to Eq. (2.9b) is negative [112, 113].

Characterization of synchronized state

The state of complete synchronization or antisynchronization can be identified using the asymptotic correlation coefficient as the index. The correlation coefficient is calculated using the equation

$$C = \frac{< (x_{11}(t) - < x_{11}(t) >)(x_{21}(t) - < x_{21}(t) >) >}{\sqrt{< (x_{11}(t) - < x_{11}(t) >)^2 >< (x_{21}(t) - < x_{21}(t) >)^2 >}}. \tag{2.10}$$

The state where $C \sim 1$ corresponds to complete synchronization, while the state where $C \sim -1$ corresponds to antisynchronization.

In phase synchronization, the amplitudes remain uncorrelated. Therefore, $|C| < 1$ in this state. Hence, we need to calculate the phase difference of the coupled oscillators to identify any phase synchrony between them. This is applied in our study of Rössler and Lorenz systems in chapter 3 and in the
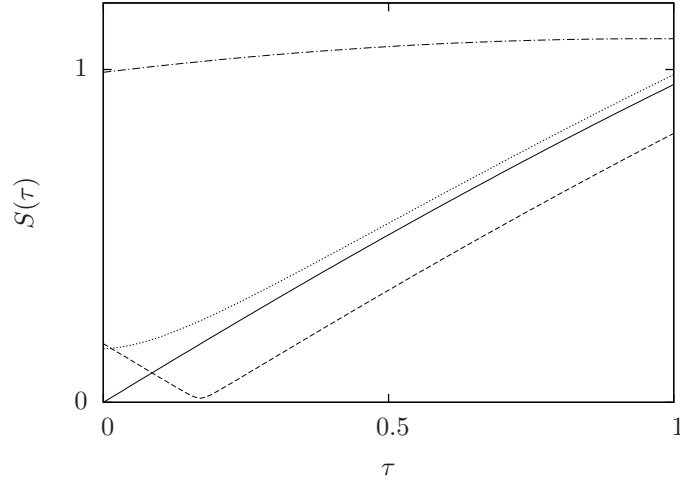
Figure 2.4: The similarity function for different types of synchronized states. The solid curve represents complete synchronization ($S(0) \sim 0$), the dashed curve represents lag synchronization ($S(\tau_L) \sim 0$), where τ_L is the time-lag, the dotted curve represents phase synchronization ($\S(0)$ is nonzero, but small) and the dotted-dashed curve represents no synchronization ($S(\tau) \sim 1$ for all τ).

case of Hindmarsh-Rose systems in chapter 7.

Another useful index to identify the different types of synchronizations between two time series x_1 and x_2 is the similarity function $S(\tau)$ given by [78],

$$S^2(\tau) = \frac{< [x_2(t+\tau) - x_1(t)]^2 >}{[< x_1^2(t) >< x_2^2(t) >]^{1/2}} \tag{2.11}$$

where τ a suitable time-delay. When $S(\tau) \sim 1$ for all values of τ, the systems are unsynchronized. The state with $S(0) \sim 0$ is the state of complete synchronization, and the state $S(\tau) \sim 0$ corresponds to lag synchronization with time-lag, τ. In the in-phase synchronized state, $0 < S(0) < 1$. This is illustrated in Fig. 2.4. To identify states of antisynchronization and antiphase synchronization, we use a modified similarity function S_1, which is defined as [114]

$$S_1^2(\tau) = \frac{< [x_2(t+\tau) + x_1(t)]^2 >}{[< x_1^2(t) >< x_2^2(t) >]^{1/2}} \tag{2.12}$$

The state with $S_1(0) \sim 0$ corresponds to antisynchronization and the state

with $0 < S_1(0) < 1$ corresponds to antiphase synchronization. We use these similarity functions to identify in-phase, antiphase, complete and anti-synchronized states of coupled Lorenz systems in chapter 3.

In the preceding chapter, we have mentioned that, using the Lyapunov exponents the different dynamical states of individual systems can be identified. The Lyapunov exponent is also used as an index to identify synchronized states [76, 78, 115] in coupled systems. In the absence of coupling, the systems evolve independently and each system have at least one zero Lyapunov exponent which correspond to the eigenvector along the direction of the trajectory. When the systems get phase (or antiphase) synchronized, all the zero Lyapunov exponents, except one becomes negative. Similarly, when the systems becomes synchronized, all positive Lyapunov exponents except one becomes negative. Thus, the strength of coupling at which the first zero-crossing of the Lyapunov exponents occurs, is the critical strength for phase synchronization and the strength of coupling at which the all positive Lyapunov exponents except one, become negative, is the critical coupling strength for complete, anti, lag or anticipatory synchronization [115]. In this thesis, the Lyapunov exponents are calculated using Wolf algorithm [17] and are used to identify the transitions to different types of synchronizations in Chapter 3.

2.2.1   Synchronization in networks

Collective and synchronized dynamics in complex networks of coupled units have been studied under different topologies such as small-world networks, scale-free networks , weighted complex networks and different coupling configurations [116, 117, 117–130]. This is also demonstrated in a variety of systems like array of lasers [131, 132], chemical oscillators [133], ensemble of living cells [134], cardio-respiratory system [71, 135], ecology [136, 137], climatology [138] etc. Many studies on synchronization of a large ensemble of systems were done by considering a model of phase oscillators coupled to each other via the sine of their phase differences. Transitions to synchro-

nization can be defined using an order parameter and variations of the order parameter with increase in coupling strength. This simple mathematical model, called Kuramoto model displays a large variety of synchronization patterns [139, 140].

The stability of the synchronized dynamics in coupled systems are developed for arbitrary topologies and coupling functions using the master stability function [141, 142]. The coupled system given in Eq. (2.4), in the case of identical oscillators, admits a solution given by

$$x_1(t) = x_2(t) = \ldots = x_N(t) = s. \tag{2.13}$$

This state is called the synchronization manifold. Linearization of Eq. (2.4) about the synchronized state will give

$$\dot{\xi} = \sum_{j=1}^{N} [\delta_{ij} \mathbf{D} f(s) + \epsilon A_{ij} \mathbf{D} H(s)] \xi_j, \tag{2.14}$$

where, $\mathbf{D}$ is the differential operator and ξ_j is the variation about the synchronized state, s. This can be simplified to get the variational equations in eigenmode form as

$$\dot{\zeta}_k = [\mathbf{D} f + \epsilon \mu_k \mathbf{D} H] \zeta_k, \tag{2.15}$$

where, μ_k is the kth eigenvalue of A. Eq. (2.15) for ζ_0 corresponds to the variations along the synchronization manifold and all other ζ_k corresponds to transverse eigenvectors. The stability of the synchronized state depends on the largest Lyapunov exponent of Eq. (2.15) for $k > 1$, which in turn, depends on both the intrinsic dynamics f and the network topology A. Partial synchronization is an interesting phenomenon which occurs in complex networks during the transition to complete synchronization [143–145].

Apart from the many forms of synchronization discussed above, other forms of synchronizations are studied recently. Synchronization has been achieved by a common stochastic drive in uncoupled chaotic systems [146–148]. Projective synchronization where the ratio of the corresponding vari-

ables becomes a constant is studied in the case of chaotic systems, with applications to secure communication [149–151]. So also, adaptive synchronization, where the strength of coupling varies with time has got applications in secure communication [152–154]. Another interesting synchronization studied recently is the remote synchronization, where two or more nodes in a network which are coupled indirectly through other nodes are phase synchronized, while the nodes along the path are not synchronized [155]. Design of coupling to achieve different forms of synchronization, enhancing the synchrony using an indirect dynamic relaying are some of the recent developments in the area of synchronization. Synchronization with variable delay with reset has been studied recently, which has application in secure communication [156–158].

2.3 Amplitude death

Quenching or suppression of dynamics, called the amplitude death is another emergent phenomenon observed in coupled systems. This occurs due to the stabilization of a steady state. The equilibrium states or fixed points can be either that of the uncoupled system or those evolved by coupling. The occurrence of amplitude death has been reported in many cases such as chemical reactions [159–162], biological oscillators [163–166], coupled laser systems [167, 168] and relativistic magnetrons [169]. This is often a useful control mechanism for stabilizing systems such as coupled lasers [170, 171].

The mechanisms so far reported to induce amplitude death in coupled systems are de-tuning of oscillators under strong coupling [172–174], coupling through conjugate variables [175, 176], dynamic coupling [177] and delay in the coupling due to finite propagation or information processing speeds [178–183]. Distributed delays rather than discrete or constant delays have been proposed as more realistic models in ecology and neurobiology, where the variance of the delay plays a relevant role [184]. So also, amplitude death has been studied in the context of attractive and repulsive couplings in two

28

chaotic Lorenz systems [185]. In addition to the study of amplitude death in regularly coupled systems, there has been a few recent studies on amplitude death in complex networks. In the specific context of networks, amplitude death has been studied for parameter mismatch or detuning of frequencies in an ensemble of limit cycle oscillators with mean field coupling [186], array of limit cycle oscillators [187–189],small-world networks [190] and scale-free networks [191]. So also, time-delay in coupling is found to induce amplitude death in networks of limit-cycle oscillators [182,192–194] and chaotic systems [195, 196]. Recently, it was shown that, it is possible to target amplitude death in a network of nonlinear oscillators by a proper choice of nonlinear coupling [197].

Since the amplitude death state corresponds to a stable fixed point of the coupled system, the transition to amplitude death can be identified by evaluating the eigenvalues of the Jacobian of the coupled system. At the transition, the real part of the largest eigenvalue becomes negative. This can also be studied using the Lyapunov exponents of the coupled system [175, 179]. We use the eigenvalues of the Jacobian of the coupled system and the Lyapunov exponents to identify the transition to amplitude death in the case of Rössler and Lorenz systems in Chapter 4.

The nature of the transition to the amplitude death state can be either sudden or continuous depending on the nature of the intrinsic dynamics of the coupled systems [179]. The transition to amplitude death is also associated with a phase-flip bifurcation in delay-coupled and conjugate coupled systems, where the phase difference between the oscillators change abruptly by π [198–200]. In the case of amplitude death in networks, the transition via a state of partial amplitude death is observed in both numerical studies [189, 201] and experimental systems [202].

2.4   Summary

We have discussed the occurrence of emergent phenomena like synchronization and amplitude death in coupled systems as well as networks and different ways of characterizing these states. In the following chapters, we will discuss our study on a new scheme for synchronization and amplitude death.

Chapter 3

Synchronization in chaotic systems coupled indirectly via environment

In the preceding chapter, we have discussed a few emergent phenomena such as synchronization and amplitude death, caused by the coupling between the systems. Most studies on synchronization and amplitude death consider two or more coupled units. However, in many real world cases, the sub-systems can synchronize even in the absence of any direct coupling between them. Two pendulum clocks getting antiphase synchronized with each other via the vibrations of the common wooden beam is a classic example of this [203]. This type of interactions via a common medium are relevant in biological systems. For example, in bacterial quorum sensing, the organisms interact via releasing chemicals to the surrounding medium, and sensing the concentration of the chemicals in the surrounding medium [204–206]. Synchronization due to chemical interactions via the intracellular medium is also found in circadian oscillators [207] as well as genetic oscillators [208, 209]. So also, synchronization is reported in chemical oscillations of catalyst-loaded reactants in a medium of catalyst free solution, where coupling is through exchange of chemicals with the surrounding medium [210]. This phenomenon has also

been studied in the context of laser systems [211, 212]. In all these cases, collective dynamics arises from an indirect coupling via an external agency, rather than a direct coupling among the units.

In the work presented in this thesis, we model this indirect interaction mediated by a common agent by considering an external system, which has an intrinsic dynamics different from that of the systems. Such an indirect coupling, leading to synchronization, has been reported in the context of periodic oscillators by Katriel [213]. Here, we consider two chaotic systems coupled indirectly through a common dynamic environment, with no direct coupling between them. We show that this type of coupling can lead to a rich variety of synchronous behavior such as antiphase, in-phase, identical and antisynchronization. This mechanism has the interesting feature that the common environment while capable of synchronizing the systems, does not cause major changes in their dynamics. In the synchronized state, the systems retain more or less the same phase space structure of the uncoupled system. We also develop an approximate stability analysis for the stability of the different synchronized states. We report detailed numerical studies for two standard chaotic systems, Rössler and Lorenz, and demonstrate the richness of the synchronization behavior. The transition to different stages of synchronization is studied by computing average phase differences, correlations, and Lyapunov exponents. From the numerical analysis, we verify the relation between the critical parameters for the transition to different synchronization states obtained from the stability analysis. The work presented in this chapter has been published in Phys. Rev. E **81**, 046216 (2010) [214].

3.1 Synchronization by indirect coupling via environment

We consider two chaotic systems coupled to a common environment through a linear coupling given by the following equations

$$\dot{x}_1 = f(x_1) + \epsilon_1 \gamma \beta_1 w, \tag{3.1a}$$

$$\dot{x}_2 = f(x_2) + \epsilon_1 \gamma \beta_2 w, \tag{3.1b}$$

$$\dot{w} = -\kappa w - \frac{\epsilon_2}{2} \gamma^T (\beta_1 x_1 + \beta_2 x_2). \tag{3.1c}$$

Here, x_1 and x_2 represents two m-dimensional nonlinear systems whose intrinsic dynamics are given by $f(x_1)$ and $f(x_2)$ respectively. The variable w represents the environment, whose dynamics is assumed to be decaying with κ as the damping parameter. Therefore, without feedback from the systems, it is incapable of sustaining itself for extended periods of time. For simplicity, we take w to be 1-dimensional environment. Here, ϵ_1 is the strength of feedback to the system and ϵ_2 is that to the environment. γ is a column matrix $(m \times 1)$, with elements zero or one, and it decides the components of x_i that take part in the coupling. The nature of feedback from and to the environment is adjusted by prescribing values for β_1 and β_2. When both β_1 and β_2 are of the same sign, i.e. $(\beta_1, \beta_2) = (1, 1)$, the coupling is repulsive and can drive the systems to anti-phase synchronization. When β_1 and β_2 are of different signs, i.e. $(\beta_1, \beta_2) = (1, -1)$, the coupling is of difference type leading to in-phase synchronization. We illustrate this behavior for the case of two chaotic Rössler systems coupled through environment as given by the equations $(i = 1, 2)$

$$\dot{x}_{i1} = -x_{i2} - x_{i3} + \epsilon_1 \beta_i w,$$

$$\dot{x}_{i2} = x_{i1} + a x_{i2},$$

$$\dot{x}_{i3} = b + x_{i3}(x_{i1} - c),$$

$$\dot{w} = -\kappa w - \frac{\epsilon_2}{2} \sum_{i=1,2} \beta_i x_{i1}. \tag{3.2}$$
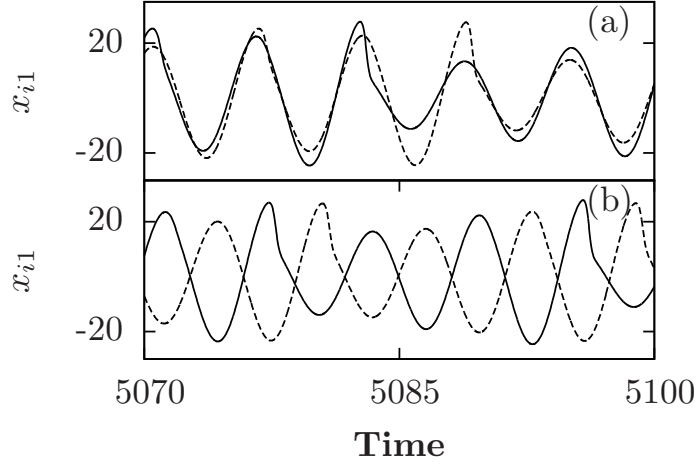
Figure 3.1: Time series of the first variable x_{i1} of two environmentally coupled chaotic Rössler systems (a) In-phase synchronization at ($\epsilon_1 = \epsilon_2 = 0.2$, $\beta_1 = -\beta_2 = 1$) (b) antiphase synchronization at ($\epsilon_1 = \epsilon_2 = 0.2$, $\beta_1 = \beta_2 = 1$). Rössler parameters are $a = b = 0.1$, $c = 18$, i.e. we have chaotic attractor. The damping parameter of the environment is taken to be $\kappa = 1$.

We find that, when $\beta_1 = -\beta_2 = 1$, the systems get phase-synchronized for suitable strengths of ϵ_1 and ϵ_2. When $\beta_1 = \beta_2 = 1$, the systems get antiphase synchronized for suitable strengths of couplings. The time series of the coupled Rössler systems for the in-phase synchronized and antiphase synchronized cases is shown in Fig. 3.1a and 3.1b.

We repeat the same analysis with two Lorenz systems coupled through environment as given by the following equations ($i = 1, 2$)

$$
\begin{aligned}
\dot{x}_{i1} &= \sigma(x_{i2} - x_{i1}) + \epsilon_1 \beta_i w, \\
\dot{x}_{i2} &= (r - x_{i3})x_{i1} - x_{i2}, \\
\dot{x}_{i3} &= x_{i1}x_{i2} - bx_{i3}, \\
\dot{w} &= -\kappa w - \frac{\epsilon_2}{2} \sum_{i=1,2} \beta_i x_{i1}.
\end{aligned}
\tag{3.3}
$$

We find that in-phase synchronization is possible for $\beta_1 = -\beta_2 = 1$ and antiphase synchronization is possible for $\beta_1 = \beta_2 = 1$. The in-phase synchronized state where the average phase difference between the systems is
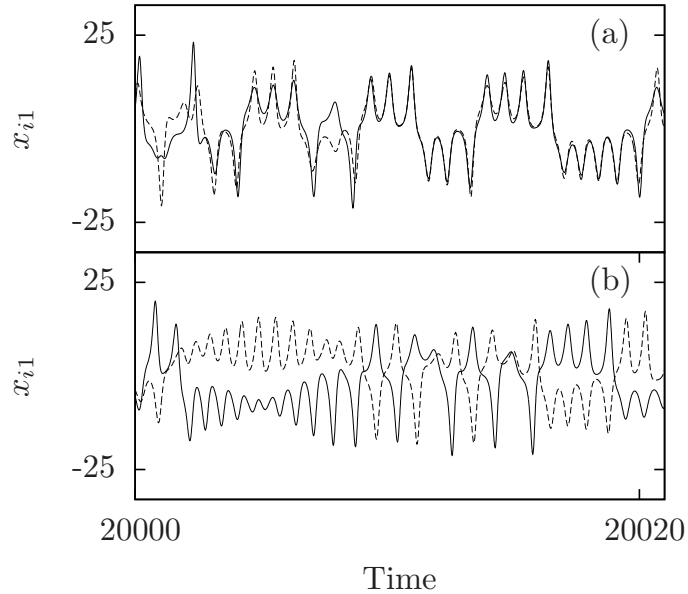
34

Figure 3.2: Time series of the first variable x_{i1} of two environmentally coupled chaotic Lorenz systems (a) In-phase synchronization at ($\epsilon_1 = \epsilon_2 = 9.0$, $\beta_1 = -\beta_2 = 1$) (b) antiphase synchronization at ($\epsilon_1 = \epsilon_2 = 8.0$, $\beta_1 = \beta_2 = 1$). Here, Lorenz parameters are ($\sigma = 10, r = 28, b = 8/3$). The damping parameter of the environment is chosen to be $\kappa = 1$.

~ 0, and antiphase synchronized states where the average phase difference between the systems is $\sim \pi$, of the coupled Lorenz systems are shown in Figs. 3.2(a) and 3.2(b) respectively.

3.2 Linear stability analysis

We analyze the stability of the synchronized state of two systems coupled via the scheme in Eq. (3.1). If ξ_1, ξ_2, and z represent the deviations from the synchronized state, their dynamics is governed by the linearized equations

obtained from Eqs. (3.1). They are

$$
\begin{align}
\dot{\xi}_1 &= f'(x_1)\xi_1 + \epsilon_1\gamma\beta_1 z, \tag{3.4a}\\
\dot{\xi}_2 &= f'(x_2)\xi_2 + \epsilon_1\gamma\beta_2 z, \tag{3.4b}\\
\dot{z} &= -\kappa z - \frac{\epsilon_2}{2}\gamma^T(\beta_1\xi_1 + \beta_2\xi_2). \tag{3.4c}
\end{align}
$$

In general, it is difficult to analyze the stability of the synchronized state from Eqs. (3.4). For the special case of the perfectly synchronized state, i.e. $x_1 = x_2$, Eqs. (3.4) can be simplified by defining

$$
\xi_0 = \beta_1\xi_1 + \beta_2\xi_2. \tag{3.5}
$$

Then Eqs. (3.4) can be written as

$$
\begin{align}
\dot{\xi}_0 &= f'(x_1)\xi_0 + \epsilon_1(\beta_1^2 + \beta_2^2)\gamma z \tag{3.6a}\\
\dot{z} &= -\kappa z - \frac{\epsilon_2}{2}\gamma^T\xi_0 \tag{3.6b}
\end{align}
$$

The synchronized state corresponding to the fixed point $(0,0)$ of Eqs. (3.6) will be stable if all the Lyapunov exponents obtained from Eqs. (3.6) are negative.

To proceed further, we assume that the time average values of $f'(x_1)$ and $f'(x_2)$ are approximately the same and can be replaced by an effective constant value α. In this approximation we treat ξ_1 and ξ_2 as scalars. This approximation simplifies the problem such that only the relevant features remain and is expected to give features near the transition. This type of approximation was used in Ref. [156] and it was noted that it describes the overall features of the phase diagram reasonably well. Thus, using ξ_0 defined by Eq. (3.5), Eqs. (3.4) can be written as

$$
\begin{align}
\dot{\xi}_0 &= \alpha\xi_0 + 2\epsilon_1 z \tag{3.7a}\\
\dot{z} &= -\kappa z - \frac{\epsilon_2}{2}\xi_0 \tag{3.7b}
\end{align}
$$

where we choose $\beta_1^2 + \beta_2^2 = 2$. Eliminating z from Eqs. (3.7a) and (3.7b), we

get an equation for ξ_0 as

$$\ddot{\xi}_0 = (\alpha - \kappa)\dot{\xi}_0 + (\kappa\alpha - \epsilon_1\epsilon_2)\xi_0 \tag{3.8}$$

Assuming a solution of the form

$$\xi_0 = Ae^{mt}$$

we get

$$m = \frac{(\alpha - \kappa) \pm \sqrt{(\alpha - \kappa)^2 - 4(\epsilon_1\epsilon_2 - \alpha\kappa)}}{2} \tag{3.9}$$

The synchronized state, defined by $\xi_0 = \beta_1\xi_1 + \beta_2\xi_2 = 0$, is stable if $\text{Re}[m]$ is negative for both the solutions. This gives the following criteria for the stability of the synchronized state.

1. If $(\alpha - \kappa)^2 < 4(\epsilon_1\epsilon_2 - \alpha\kappa)$, m is complex and the condition of stability is $\kappa > \alpha$.

2. If $(\alpha - \kappa)^2 > 4(\epsilon_1\epsilon_2 - \alpha\kappa)$, m is real and the stability condition becomes $\epsilon_1\epsilon_2 > \alpha\kappa$ and $\kappa > \alpha$.

In the first case above, the synchronized state is possible if we have an environment which has a sufficiently fast decay to compensate for the divergence of the system due to α. In the second case, both conditions must be satisfied. Here, the transition to stable synchronization is given by the threshold values of parameters satisfying the condition

$$\epsilon_{2c} = \frac{\alpha\kappa}{\epsilon_{1c}} \tag{3.10}$$

We now consider the properties of the synchronized state defined by $\xi_0 = \beta_1\xi_1 + \beta_2\xi_2 = 0$, i.e. $\beta_1 x_1 + \beta_2 x_2 = $ const.. Numerical simulations show that the constant is zero. Thus, for $\beta_1 = \beta_2 = 1$ we get $x_1 = -x_2$, i.e. antisynchronization while for $\beta_1 = -\beta_2 = 1$ we get $x_1 = x_2$, i.e. complete synchronization.

3.3 Numerical analysis

In this section, we apply the scheme of coupling through the environment given in Eqs. (3.1) to the standard Rössler and Lorenz systems in the chaotic regime. We study the two cases, $\beta_1 = +1$ and $\beta_2 = -1$ where in-phase synchronization is possible and $\beta_1 = \beta_2 = +1$ where antiphase synchronization is possible.

3.3.1 Indirectly coupled Rössler systems

Now, we apply the scheme of coupling introduced in Eqs. (3.1) to two Rössler systems in the chaotic regime (Eq. 3.2). When $\beta_1 = +1$ and $\beta_2 = -1$, we observe in-phase synchronization as shown earlier in Figs. 3.1(a). As the coupling strength is increased, systems go to a state of complete synchronization. When $\beta_1 = \beta_2 = +1$ we observe antiphase synchronization (Figs. 3.1(b)). As the strength of feedback is increased, control of chaos is observed and the systems become periodic, while the two coupled systems remaining in antiphase synchronization.

The transitions to in-phase (or antiphase) synchronization can be studied numerically using the average phase difference between the two systems. For this, we need to define phases of individual systems. In the case of Rössler systems, as the trajectory has a rotation around a fixed point in the x_1–x_2 plane, the phase $\phi(t)$ of the Rössler system can be defined [115] as the angle

$$\phi(t) = \tan^{-1}(x_2(t)/x_1(t)) \tag{3.11}$$

The phase $\phi(t)$ of the two Rössler systems coupled through environment are calculated using Eq. (3.11). Then the phase difference $\psi(t)$ between them, and its average over time $<\psi(t)>$ are calculated for increasing strengths of feedback for identical feedback strengths $\epsilon_1 = \epsilon_2 = \epsilon$. The state with $< \psi(t) >\sim 0$ corresponds to in-phase synchronized state and the state with $< \psi(t) >\sim \pi$ is identified as the antiphase synchronized state.
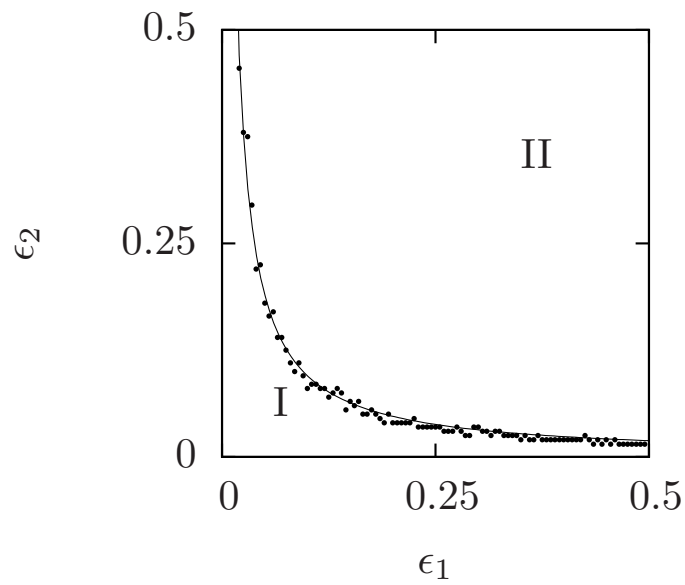
Figure 3.3: Transition from unsynchronized regions (I) to antiphase synchronized regions (II) in the parameter plane $\epsilon_1 - \epsilon_2$ for the coupled Rössler systems. The points are obtained numerically when the average phase difference becomes approximately π. Solid curve corresponds to the stability condition Eq. (3.10), i.e. $\epsilon_{2c} \propto 1/\epsilon_{1c}$.
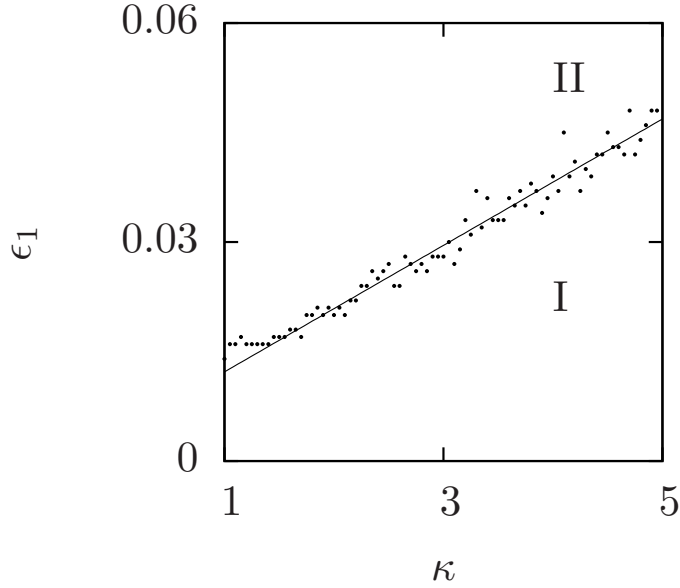
Figure 3.4: Transition from unsynchronized regions (I) to antiphase synchronized regions (II) in the parameter plane κ–ϵ_1 for coupled Rössler systems. Points are obtained from numerical simulation with $\epsilon_2 = 0.6$ and the solid curve is a linear fit corresponding to the stability condition Eq. (3.10) with the effective $\alpha = 0.009$.

For the coupled Rössler systems the average phase difference is calculated for the full parameter plane ϵ_1–ϵ_2 and the points where the average phase difference, $< \psi(t) >$, becomes approximately π are plotted in Fig. 3.3. These therefore correspond to the threshold values for onset of stability of antiphase synchronizaton. The solid line corresponds to the curve plotted using the threshold condition from our stability theory in Eq. (3.10). We observe that the agreement is quite good with $\alpha = 0.009$ and the relation $\epsilon_{2c} \propto 1/\epsilon_{1c}$ is clearly seen.

As seen in Eq. (3.10), we also have the relations $\epsilon_{2c} \propto \kappa$ and $\epsilon_{1c} \propto \kappa$. Fig. 3.4 shows the phase plot for the transition from unsynchronized to antiphase synchronized states in the $\epsilon_1 - \kappa$ plane. A linear relation is clearly seen and the solid line is drawn with the effective $\alpha = 0.009$, thus validating the transition criterion of Eq. (3.10) obtained from the stability theory.

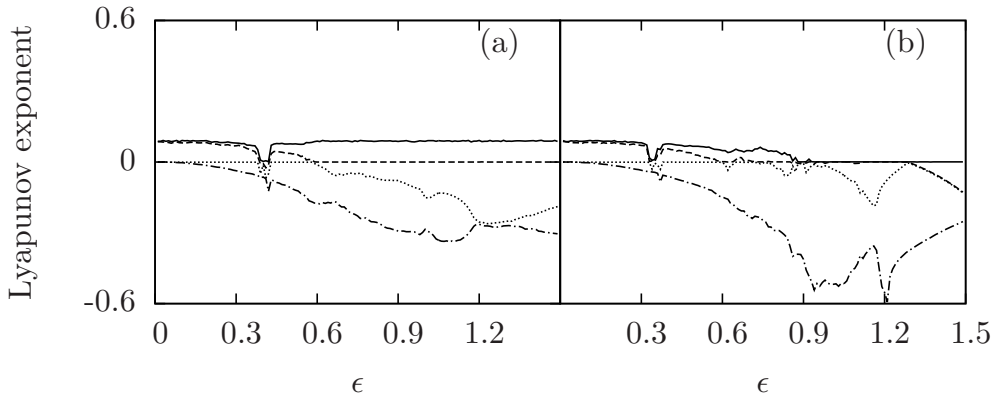The transitions to all the different types of synchronization described

Figure 3.5: Four largest Lyapunov exponents for the coupled Rössler systems as a function of the coupling strength. Here we take $\epsilon_1 = \epsilon_2 = \epsilon$. (a) $\beta_1 = +1, \beta_2 = -1$; the first crossing of 0 at $\epsilon \sim 0.12$ (fourth largest LE) indicates the transition to in-phase synchronization, while the second zero crossing at $\epsilon \sim 0.59$ (second largest LE) indicates the transition to complete synchronization (b) $\beta_1 = \beta_2 = +1$; the first crossing of 0 at $\epsilon \sim 0.12$ indicates antiphase synchronization and the region where all Lyapunov exponents are less than or equal to zero indicates the antiphase synchronized periodic states.

above can be tracked by calculating the Lyapunov exponents. Since the coupling here is indirect and through an environment, instead of calculating transverse Lyapunov exponents about the synchronized state, we calculate all the Lyapunov exponents of the coupled system. The two chaotic systems and the environment together form a seven-dimensional system and the Lyapunov exponents are calculated by considering variational equations using Wolf algorithm [17]. The four largest Lyapunov exponents for coupled Rössler systems are shown in Fig. 3.5 for various strengths of feedback. For the case $\beta_1 = +1$ and $\beta_2 = -1$, the zero crossing of the fourth largest Lyapunov exponent in Fig. 3.5(a) corresponds to the onset of in-phase synchronization, and the zero crossing of the second largest Lyapunov exponent corresponds to the onset of complete synchronization. Here, the narrow window where all Lyapunov exponents are less than or equal to zero corresponds to synchronized periodic states in Rössler systems as verified from the time series. In the case of antiphase synchronization similar results are seen (Fig. 3.5(b)). The region where all Lyapunov exponents are less than

41

or equal to zero in Fig. 3.5(b) corresponds to the antiphase synchronization in the periodic state.

The phase diagram showing regions of different dynamical regimes in the ϵ_1 – ϵ_2 plane for coupled Rössler systems is given in Fig. 3.6(a) for $\beta_1 = 1$, $\beta_2 = -1$. As the coupling strengths increase (along the diagonal) we see a transition from the unsynchronized state (dark gray) to the in-phase synchronized state (light gray) and then to the completely synchronized state (white). For large coupling constants, the system becomes unstable (black). It is seen that the critical coupling constants corresponding to the transitions between the different types of synchronization obey the relation Eq. (3.10) as obtained from the stability analysis. Fig. 3.6(b) shows a similar phase diagram for $\beta_1 = \beta_2 = 1$. Here dark gray region corresponds to unsynchronized states, region marked I corresponds to antiphase synchronization in chaotic state, regions II – IV corresponds to different regimes of synchronization in periodic states and black region corresponds to unstable states. We find that here, depending on the coupling strength, the coupled systems settle to two different periodic states A and B. The x_1–x_2 plane corresponding to the states A and B are shown in Fig. 3.7. In regions II and IV, both the Rössler systems are in state A, shown in Fig. 3.7(a). While in region III, one of the systems is in periodic state A and the other is in periodic state B(Fig. 3.7(b)).In regions II and IV, the synchronized states are such that $x_1(t + \tau) \simeq x_2(t)$, corresponding to lag synchronization, and in region III, the systems are in antiphase synchronization in the periodic state. The average error function calculated after shifting $x_1(t)$ by half the time period for the regions I, III and IV is shown in Fig. 3.7(c).

3.3.2   Indirectly coupled Lorenz systems

We repeat the same analysis for two chaotic Lorenz systems. From numerical simulations of Eq. 3.3, we find that when $\beta_1 = -\beta_2 = 1$, the systems are in in-phase synchronization (Fig. 3.2(b)). As the coupling strength is increased, the systems are in complete synchronization. When $\beta_1 = \beta_2 = 1$, the systems
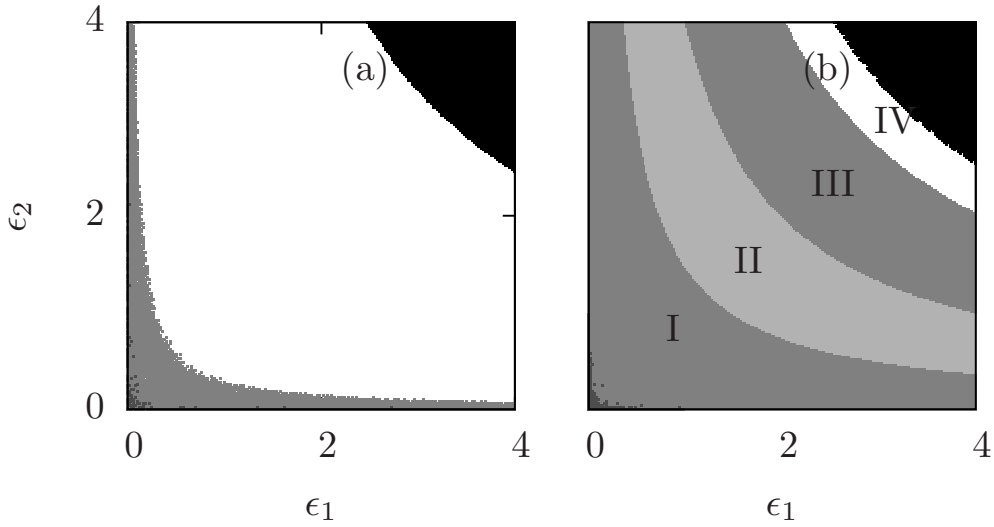
Figure 3.6: Regions of different states of synchronization marked out in the parameter plane $\epsilon_1 - \epsilon_2$ for the coupled Rössler systems. The different phase space regions are obtained by using the asymptotic correlation values C, average phase differences $< \psi(t) >$, and Lyapunov exponents. (a) $\beta_1 = +1, \beta_2 = -1$. White region corresponds to $|C| \sim 0.99$ indicating synchronized regions; light gray region corresponds to in-phase synchronized region. (b) $\beta_1 = \beta_2 = +1$ region I corresponds to antiphase synchronized chaotic states, regions II – IV correspond to different states of antiphase synchronized periodic states (see text). In both cases, the dark gray region corresponds to the unsynchronized states and the black regions in the upper right corner are the unstable states.
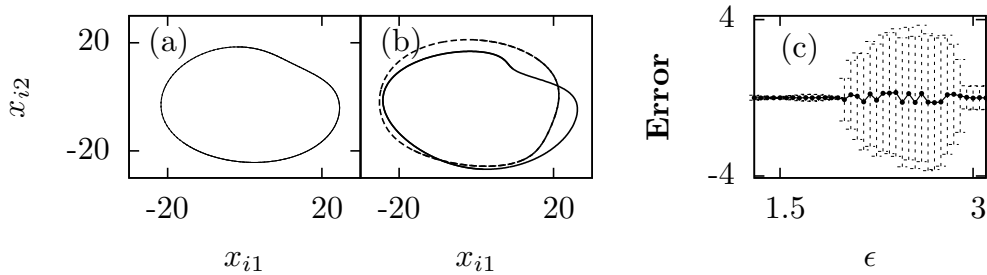

Figure 3.7: The x_1–x_2 phase plane of antiphase synchronized periodic states in regions II and III of Fig. 3.6(b). (a) $\epsilon_1 = \epsilon_2 = 1.5$ both systems are in state A (b) $\epsilon_1 = \epsilon_2 = 2.5$ systems are in different states A and B. (c) Average error function computed after shifting one of the time series by half the period in the synchronized periodic regions II – IV of Fig. 3.6(b). The average error ~ 0 for $\epsilon < 2$ and $\epsilon > 2.95$ indicating lag synchronization. The region $2 < \epsilon < 2.95$ corresponds to antiphase synchronization in the periodic state.

43

are in antiphase synchronization (Fig. 3.2(b)). When the coupling strength is increased from this state, the systems are found to be in antisynchronized state corresponding to $x_{11} = -x_{21}$, $x_{12} = -x_{22}$ and $x_{13} = x_{23}$.

Since the Lorenz system does not have such a proper rotation around any fixed point, the phase cannot be defined by Eq. (3.11). The phase of Lorenz system is calculated using the modified variables [92] as

$$\phi(t) = \tan^{-1}(\bar{z}/\bar{u}) \tag{3.12}$$

where $\bar{u} = u - u_p$, $\bar{z} = z - z_p$ and $u_p = \sqrt{2\beta(\rho - 1)}$, $z_p = \rho - 1$ and $u = \sqrt{x_1^2 + x_2^2}$. The dynamics in (u, z) looks like a rotation around some center point (u_p, z_p). The phase $\phi(t)$ of the individual Lorenz systems are calculated using Eq. (3.12). The phases show confinement due to coupling indicating in-phase (or antiphase) synchronization. It is evident that since we neglect the sign of x_1 and x_2 in the calculation of u, phase defined as in Eq. (3.12) can not distinguish between in-phase and antiphase cases. In this context, the similarity function S and a modified similarity function S' introduced in chapter 2 serve as useful indices for identifying the in-phase or antiphase synchronization. For $\beta_1 = 1, \beta_2 = -1$, at $\tau = 0$, $S = 0$ corresponds to the complete synchronization and S is finite for the in-phase synchronization. Similarly, for $\beta_1 = \beta_2 = 1$, at $\tau = 0$, S' is 0 indicating the antisynchronization and S' is finite for the antiphase synchronization.

We also calculate the Lyapunov exponents of the coupled Lorenz systems given in Eq. (3.3). The four largest lyapunov exponents are shown in Fig. 3.8. In Fig. 3.8(a), the case $\beta_1 = +1$ and $\beta_2 = -1$ is shown where the zero crossing of the fourth largest Lyapunov exponent corresponds to the onset of in-phase synchronization, and the zero crossing of the second largest Lyapunov exponent corresponds to the onset of complete synchronization. In Fig. 3.8(b), the case $\beta_1 = \beta_2 = 1$ is shown where the zero crossing of the fourth largest Lyapunov exponent corresponds to the onset of antiphase synchronization and the zero crossing of the second largest Lyapunov exponent corresponds to the onset of antisynchronization.
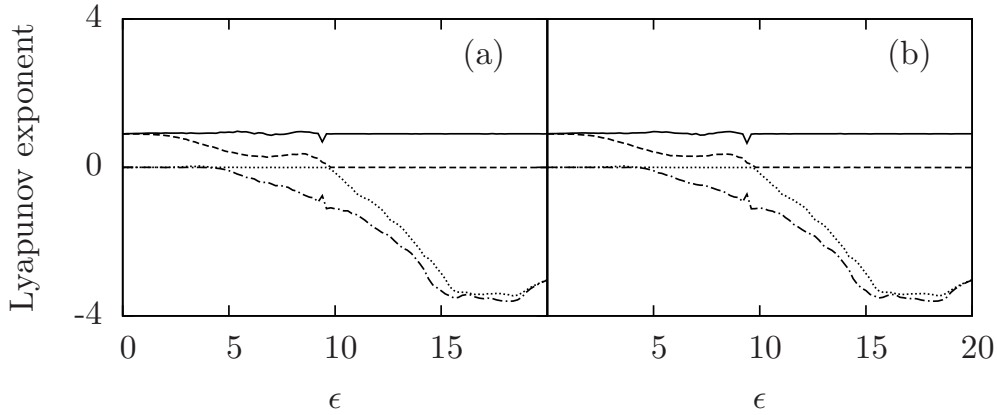
Figure 3.8: Four largest Lyapunov exponents of the two coupled Lorenz systems as a function of the feedback strength. We take $\epsilon_1 = \epsilon_2 = \epsilon$. (a) $\beta_1 = +1, \beta_2 = -1$; the first zero crossing of Lyapunov exponent at $\epsilon \sim 4.2$ indicates in-phase synchronization, the second zero crossing at $\epsilon \sim 9.8$ indicates complete synchronization (b) $\beta_1 = \beta_2 = +1$; the first zero crossing at $\epsilon \sim 4.4$ indicates antiphase synchronization, the second zero crossing at $\epsilon \sim 9.8$ indicates antisynchronization.

The parameter planes showing different synchronization regimes for coupled Lorenz systems are given in Figs. 3.9(a) and 3.9(b). As ϵ is increased along the diagonal, we observe transitions in the following sequence: unsynchronized state (dark gray) to in-phase/antiphase synchronized states (light gray) to complete/anti synchronized states (white) to unstable states (black). Here also, the critical coupling constants, corresponding to the transitions between the different types of synchronization, obey the theoretical relation, $\epsilon_{2c} \propto 1/\epsilon_{1c}$, obtained from the stability theory.

3.4 Summary

We report the synchronization of two nonlinear chaotic systems by coupling them indirectly through a common environment. The different types of synchronous behavior and the transitions among them are analyzed in the case of two standard chaotic systems, Rössler and Lorenz using the numerically computed Lyapunov exponents, average phase difference, correlation from
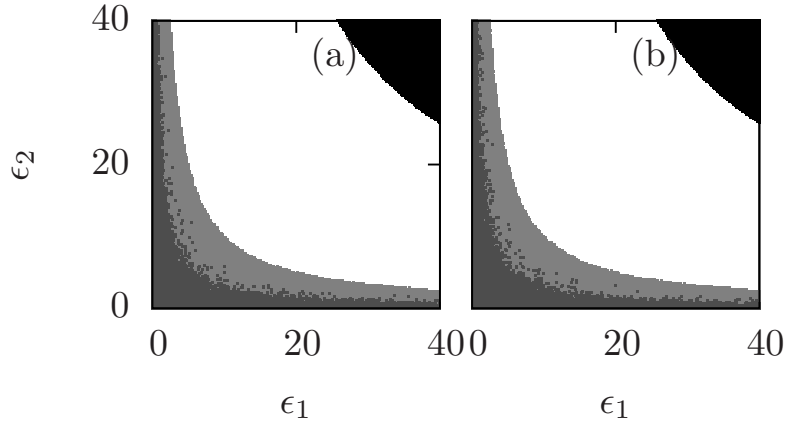
Figure 3.9: Regions of different states of synchronization marked out in parameter plane of coupling strengths ϵ_1– ϵ_2 by computing asymptotic correlation values C, average phase difference $< \psi(t) >$ and similarity functions for Lorenz systems. (a) $\beta_1 = +1, \beta_2 = -1$ (b) $\beta_1 = \beta_2 = +1$. In both cases, white region corresponds to $|C| \sim 0.99$ indicating synchronized/anti-synchronized regions. Light gray region is in-phase (or antiphase) syncrhonized state and dark gray region is unsynchronized state. Black region in the upper right corner corresponds to unstable states.

time series and similarity function. The salient features of the work reported in this chapter are

1. We show that, indirect coupling via a dynamic environment can lead to different types of synchronization in nonlinear systems.

2. The synchronized state has almost the same phase space structure as that of the uncoupled dynamics.

3. The coupling mechanism proposed here is general, and can be adjusted for in-phase and anti-phase or complete and anti- types of synchronization.

4. Using an approximate linear stability analysis, the threshold values of coupling strengths for onset of synchronization of the in-phase or anti-phase type are derived.

5. The transition curves obtained from numerical calculations agree with the curves from stability analysis.

Chapter 4

Amplitude death in chaotic systems coupled via both direct and indirect coupling

In chapter 3, we have shown that indirect feedback coupling through environment can induce anti-phase (or anti) synchronization in two systems which are not directly connected [214]. Here, we show that if in addition to the indirect feedback coupling through a dynamic environment, systems are coupled directly, then they can be driven to a state of amplitude death. We consider two systems coupled directly such that with adequate strength of coupling, they can exhibit synchronous behavior. Then we introduce an additional indirect feedback coupling through the environment or another external system such that it induces a tendency for antisynchronization. We find that, with sufficient strength of coupling, these two competing tendencies can lead to amplitude death. In the state of amplitude death, the subsystems stabilize to a fixed point of the coupled system. We find that, while it essentially explains quenching of activity or suppression induced by an external medium or agent, this novel method can also serve as a general mechanism to induce death in coupled synchronizable systems.

47

We develop an approximate stability analysis which provides the threshold or critical values of coupling strengths for amplitude death in the general context. Direct numerical simulations giving the regions of amplitude death in the space of coupling strengths agree well with the transition curves obtained from the stability analysis. We also analyse in detail the nature of transition to the amplitude death state. All the specific cases that we study basically exhibit two types of transitions, *viz*, continuous or discontinuous transitions to death. In the continuous case, as illustrated by two coupled Rössler systems, during the transition the full reverse period doubling scenario is observed reaching a one-cycle state before amplitude death occurs. The transition to death then occurs due to a super critical Hopf bifurcation. In the discontinuous case, the transition is sudden due to the disappearance of a distant attractor and stabilization of a fixed point. For two coupled Lorenz systems, we find the transition to death is probably via a sub-critical Hopf bifurcation with long transients and prior to this, the systems go through a state of frustration between synchronized and antisynchronized behavior. The work presented in this chapter and chapter 5 has been published in Phys. Rev. E **84**, 046212 (2011) [215].

4.1   Amplitude death via direct and indirect coupling

We start with two systems coupled mutually with two types of couplings, namely a direct diffusive coupling and an indirect coupling through an environment. The dynamics can be written as

$$\dot{x}_1 = f(x_1) + \epsilon_d \beta (x_2 - x_1) + \epsilon_e \gamma w \tag{4.1a}$$

$$\dot{x}_2 = f(x_2) + \epsilon_d \beta (x_1 - x_2) + \epsilon_e \gamma w \tag{4.1b}$$

$$\dot{w} = -\kappa w - \frac{\epsilon_e}{2} \gamma^T (x_1 + x_2) \tag{4.1c}$$

Here, x_1 and x_2 represent two m-dimensional oscillators whose intrinsic dynamics is given by $f(x_1)$ and $f(x_2)$ respectively. The systems are mutually coupled using diffusive coupling (second term in Eq. (4.1a) and (4.1b)). The environment is modelled by a one dimensional over damped oscillator w with a damping parameter κ. The environment is kept active by feedback from both the systems as given by the last term in Eq. (4.1c). Both the systems also get feedback from w (last term in Eq. (4.1a and 4.1b)). β is a matrix $(m \times m)$ with elements 0 and 1 and defines the components of x_1 and x_2 which take part in the diffusive coupling. For simplicity, we take β to be diagonal, $\beta = diag(\beta_1, \beta_2, ..., \beta_m)$ and in our numerical simulations only one component β_1 is assumed to be nonzero. γ is a column matrix $(m \times 1)$, with elements zero or one, and it decides the components of x_1 and x_2 that gets feedback from the environment. γ^T is the transpose of γ and it decides the components of x_1 and x_2 which gives feedback to the environment. We take ϵ_d to be the strength of direct diffusive coupling between the systems, and ϵ_e be the strength of feedback coupling between the systems and the environment.

The direct coupling ϵ_d, gives a synchronizing tendency between the two systems while the coupling through the environment ϵ_e, gives an antisynchronizing tendency. Thus, when both the couplings are above their critical values, there is a competition between the two tendencies, and the net effect is to drive the coupled systems to a fixed point, resulting in amplitude death.

We illustrate the above scheme for two coupled chaotic Rössler systems represented by the following equations $(i, j = 1, 2, \ i \neq j)$.

$$
\begin{aligned}
\dot{x}_{i1} &= -x_{i2} - x_{i3} + \epsilon_d(x_{j1} - x_{i1}) + \epsilon_e w \\
\dot{x}_{i2} &= x_{i1} + a x_{i2} \\
\dot{x}_{i3} &= b + x_{i3}(x_{i1} - c) \\
\dot{w} &= -\kappa w - \frac{\epsilon_e}{2} \sum_i x_{i1}
\end{aligned}
\tag{4.2}
$$

The resulting time series for synchronized state with only direct coupling,
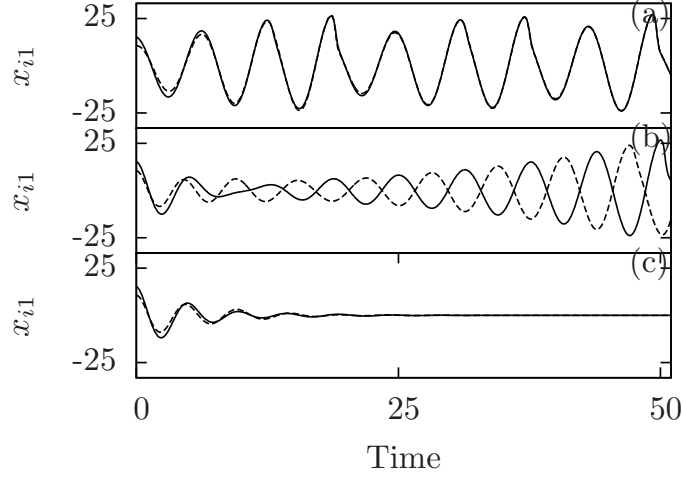
Figure 4.1: Time series of the first variables $x_{i1}, i = 1, 2$ of two coupled Rössler systems. (a) Synchronization for $(\epsilon_d, \epsilon_e) = (0.2, 0.0)$. (b) Anti-phase synchronization $(\epsilon_d, \epsilon_e) = (0.0, 1.0)$. (c) Amplitude death for $(\epsilon_d, \epsilon_e) = (0.2, 1.0)$. Here, the Rössler parameters are $a = b = 0.1, c = 18$. The damping parameter of the environment is taken to be $\kappa = 1$.

anti-phase synchronized state with only indirect coupling and amplitude death state with both direct and indirect couplings are shown in Fig. 4.1. When $\epsilon_e = 0$, and ϵ_d is sufficiently large, we observe synchronization (Fig. 4.1(a)). When ϵ_e is increased for $\epsilon_d = 0$, the systems are in anti-phase synchronized state (Fig. 4.1(b)). When both ϵ_e and ϵ_d are sufficiently large, the systems stabilize to a state of amplitude death (Fig. 4.1(c)).

We apply the same scheme to two coupled chaotic Lorenz systems as given by the following equations $(i, j = 1, 2, \ i \neq j)$

$$
\begin{aligned}
\dot{x}_{i1} &= \sigma(x_{i2} - x_{i1}) + \epsilon_d(x_{j1} - x_{i1}) + \epsilon_e w \\
\dot{x}_{i2} &= (r - x_{i3})x_{i1} - x_{i2} \\
\dot{x}_{i3} &= x_{i1}x_{i2} - bx_{i3} \\
\dot{w} &= -\kappa y - \frac{\epsilon_e}{2}\sum_i x_{i1}
\end{aligned}
\tag{4.3}
$$

We find that amplitude death occurs in this case also. This is shown in Fig. 4.2, where time series for a synchronized state (Fig. 4.2(a)), antisyn-
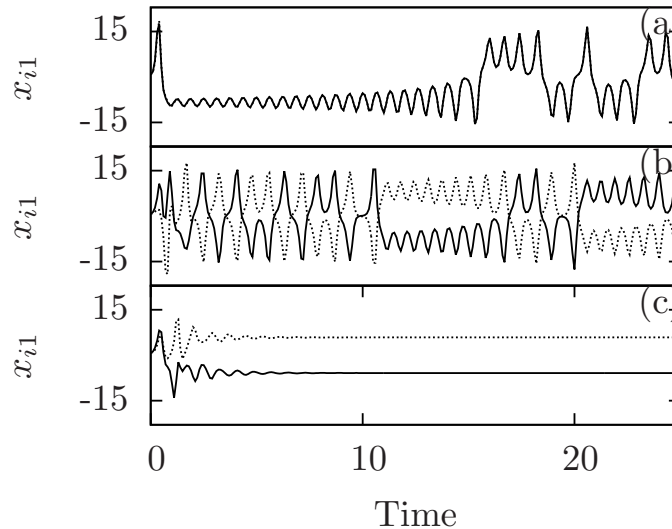
50

Figure 4.2: Time series of the first variables x_{i1} of the coupled Lorenz systems for the parameters ($\sigma = 10, r = 28, b = 8/3$) and $\kappa = 1$. (a) Synchronization for $(\epsilon_d, \epsilon_e) = (5, 0)$. (b) antisynchronization for $(\epsilon_d, \epsilon_e) = (0, 12)$. (c) Amplitude death for $(\epsilon_d, \epsilon_e) = (5, 12)$.

chronized state (Fig. 4.2(b)) and an amplitude death state (Fig. 4.2(c)) are shown.

So far we have presented the method for identical systems. However, the method also works for nonidentical systems. In general, for nonidentical systems the direct coupling will give a generalized synchronization between the coupled systems. Similarly, the antisynchronization due to the indirect coupling will also become of a generalized type. The combination of direct and indirect coupling still leads to the amplitude death. As an example, we consider two coupled Rössler systems as in Eq. (4.2). We keep the parameters of one system fixed and vary the parameter c of the other system. We find that for sufficient strength of coupling the systems go to the amplitude death state even for large deviation in c. Also, the amplitude death state occurs when the individual non-interacting systems are in different dynamical regimes. This is shown in Fig. 4.3, where time series for a generalized synchronized state (Fig. 4.3(a)), anti-phase synchronized state (Fig. 4.3(b)) and an amplitude death state (Fig. 4.3(c)) are shown for two non-identical
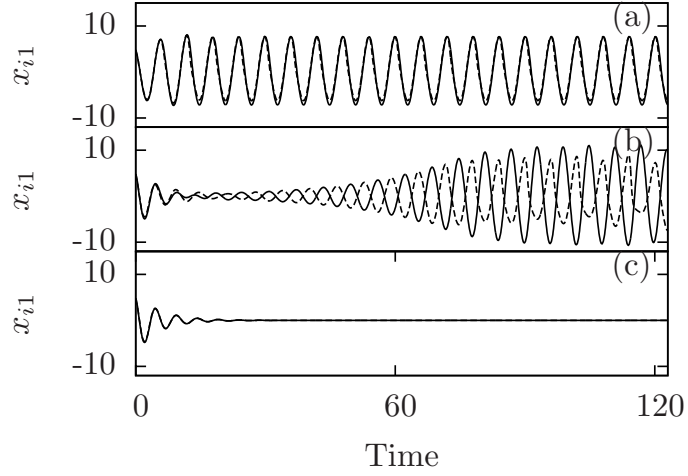
51

Figure 4.3: Time series of the first variables $x_{i1}, i = 1, 2$ of two coupled non-identical Rössler systems. Here, the parameters a and b of the two Rössler systems are chosen to be same ($a = b = 0.1$), while the parameter c of the systems are chosen such that one of the systems is in chaotic state ($c = 18$) and the other in periodic state ($c = 4$). The damping parameter of the environment is chosen to be $\kappa = 1$ (a) Generalized synchronization for $(\epsilon_d, \epsilon_e) = (1.0, 0.0)$.(b) Anti-phase synchronization $(\epsilon_d, \epsilon_e) = (0.0, 1.0)$.(c) Amplitude death for $(\epsilon_d, \epsilon_e) = (1.0, 1.0)$.

Rössler systems.

4.2   Linear stability analysis

We develop the stability analysis of the steady state of two systems coupled via the scheme given in Eq. (4.1). For this, we write the variational equations formed by linearizing Eq. (4.1) as

$$
\begin{aligned}
\dot{\xi}_1 &= f'(x_1)\xi_1 + \epsilon_d \beta(\xi_2 - \xi_1) + \epsilon_e \gamma z \\
\dot{\xi}_2 &= f'(x_2)\xi_2 + \epsilon_d \beta(\xi_1 - \xi_2) + \epsilon_e \gamma z \\
\dot{z} &= -\kappa z - \frac{\epsilon_e}{2}\gamma^T(\xi_1 + \xi_2)
\end{aligned}
\tag{4.4}
$$

where ξ_1, ξ_2 and z are small deviations from the respective values. We denote synchronizing and antisynchronizing tendencies through the variables ξ_s and

ξ_a respectively as given by

$$
\begin{aligned}
\xi_s &= \xi_1 - \xi_2 \\
\xi_a &= \xi_1 + \xi_2
\end{aligned}
\tag{4.5}
$$

Then Eq. (4.4) can be written as

$$
\begin{aligned}
\dot{\xi}_s &= \frac{f'(x_1) + f'(x_2)}{2}\xi_s + \frac{f'(x_1) - f'(x_2)}{2}\xi_a - 2\epsilon_d\beta\xi_s \\
\dot{\xi}_a &= \frac{f'(x_1) - f'(x_2)}{2}\xi_s + \frac{f'(x_1) + f'(x_2)}{2}\xi_a + 2\epsilon_e\gamma z \\
\dot{z} &= -\kappa z - \frac{\epsilon_e}{2}\gamma^T\xi_a
\end{aligned}
\tag{4.6}
$$

For stability, all the Lyapunov exponents obtained from Eq. (4.6) should be negative.

In general, it is not easy to analyse the stability of the synchronized state from Eqs. (4.6). However, considerable progress can be made if we assume that the time average values of $f'(x_1)$ and $f'(x_2)$ are approximately the same and can be replaced by an effective constant value α. This type of approximation was used earlier in Ref. [156] and in chapter 3 and it was noted that it describes the overall features of the phase diagram reasonably well. Thus, Eq. (4.4) becomes

$$
\begin{aligned}
\dot{\xi}_s &= \alpha\xi_s - 2\epsilon_d\xi_s & \text{(4.7a)} \\
\dot{\xi}_a &= \alpha\xi_a + 2\epsilon_e z & \text{(4.7b)} \\
\dot{z} &= -\kappa z - \frac{\epsilon_e}{2}\xi_a & \text{(4.7c)}
\end{aligned}
$$

We note that Eqs. (4.7b) and (4.7c) are coupled while Eq. (4.7a) is independent of the other two. The synchronizing tendency is given by Eq. (4.7a) and the corresponding Lyapunov exponent is

$$
\lambda_1 = \alpha - 2\epsilon_d
\tag{4.8}
$$

The antisynchronizing tendency is given by Eqs. (4.7b) and (4.7c). The

corresponding Jacobian is

$$J = \begin{pmatrix} \alpha & 2\epsilon_e \\ -\epsilon_e/2 & -\kappa \end{pmatrix}$$

and the eigenvalues are

$$\lambda_{2,3} = \frac{(\alpha - \kappa) \pm \sqrt{(\alpha - \kappa)^2 - 4(\epsilon_e^2 - \alpha\kappa)}}{2} \qquad (4.9)$$

As noted in the previous section, the amplitude death is obtained when both the synchronizing and antisynchronizing tendencies are present and the corresponding coupling constants are greater than the critical values required for the respective phenomena. The synchronizing and antisynchronizing tendencies become effective when the corresponding Lyapunov exponents i.e. the real parts of the eigenvalues are negative. From Eq. (4.8) we obtain the condition

$$\epsilon_d > \alpha/2 \qquad (4.10)$$

while from Eq. (4.9) we get the following conditions.
1. If $(\alpha - \kappa)^2 < 4(\epsilon_e^2 - \alpha\kappa)$, $\lambda_{2,3}$ are complex. Then the condition of stability is

$$\kappa > \alpha \qquad (4.11)$$

2. If $(\alpha - \kappa)^2 > 4(\epsilon_e^2 - \alpha\kappa)$, $\lambda_{2,3}$ are real. Then, the stability condition becomes

$$\kappa > \alpha \quad \text{and} \quad \epsilon_e^2 > \alpha\kappa \qquad (4.12)$$

If Eqs. (4.10) and (4.11) or (4.12) are simultaneously satisfied, then the oscillations can not occur and the systems stabilize to a steady state of amplitude death. For a given κ and α, the transition to amplitude death occurs at critical coupling strengths ϵ_{dc} and ϵ_{ec} independent of each other. That is

$$\epsilon_{dc} = const \qquad (4.13)$$

and

$$\epsilon_{ec} = const \qquad\qquad (4.14)$$

These general stability criteria are numerically verified for different systems in the following section.

We can also analyse the stability of amplitude death by noting that the amplitude death corresponds to a fixed point of the coupled system (Eq. 4.1) given by $\dot{x}_1 = \dot{x}_2 = \dot{w} = 0$. Then, the condition for the stability of amplitude death is that the real parts of the eigenvalue of the Jacobian evaluated at the fixed point are negative. This can be done for different systems numerically and is discussed in the next section.

4.3 Numerical Analysis

In this section, we apply our scheme to two standard chaotic systems Rössler and Lorenz and analyze the onset of amplitude death using numerical simulations.

4.3.1 Coupled Rössler systems

Now, we apply the scheme of coupling introduced in Eq. (4.1) to the case of two chaotic Rössler systems. The occurrence of amplitude death in this case is illustrated in Fig. 4.1(c). This is further confirmed by calculating the Lyapunov exponents [17]. When the systems are in amplitude death state, all the Lyapunov exponents of the coupled system are found to be negative. Fig. 4.9(b) shows the largest Lyapunov exponent of the coupled system as a function of coupling strength ϵ_e.

We study the transition to death by identifying regions of amplitude death in the parameter plane of coupling strengths $\epsilon_e - \epsilon_d$ for a chosen value of κ. To characterize the state of amplitude death, we use an index A, defined as
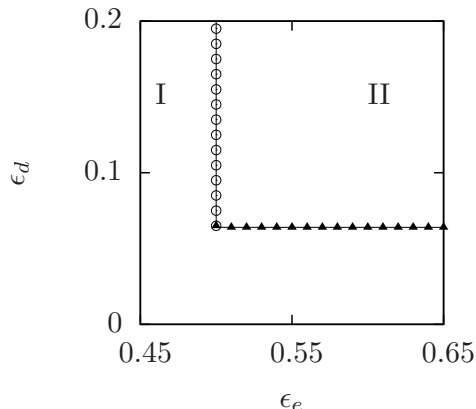
Figure 4.4: Transition from region of oscillations (I) to region of amplitude death (II) is shown in the parameter plane ϵ_e-ϵ_d for the coupled Rössler systems. Numerical simulations are done with $\kappa = 1$. The points mark the parameter values $(\epsilon_{ec},\epsilon_{dc})$ at which the transition to amplitude death occurs. Solid triangles show the transition to amplitude death as ϵ_d is increased for a constant ϵ_e. The horizontal line formed by these triangles confirms the stability condition Eq. (4.13). Similarly, circles correspond to transition to amplitude death state as ϵ_e is increased for a constant ϵ_d and confirm the stability condition of Eq. (4.14).

the difference between the global maximum and global minimum values of the time series of the system over sufficiently long interval. That is,

$$A = \sup\{x_1(t)\} - \inf\{x_1(t)\}. \tag{4.15}$$

For each system the value of A is calculated and their average $< A >$ is taken to be the index. The case where $< A >= 0$ represents the state of amplitude death, while $< A >\neq 0$ indicates oscillatory dynamics. The parameter value at which $< A >$ becomes ~ 0 is thus identified as the threshold for onset of stability of amplitude death states. Using this, the transition curves in the parameter plane $\epsilon_e - \epsilon_d$ are plotted in Fig. 4.4. We note that the points obtained from numerical simulations agree with the stability criteria Eq. (4.13) and Eq. (4.14) obtained in the previous section.

We also verify numerically the criteria for transition to the amplitude death state given in Eq. (4.12). For this, the numerically obtained values of ϵ_{ec}^2 are plotted against κ in Fig. 4.5. The line corresponds to the stability
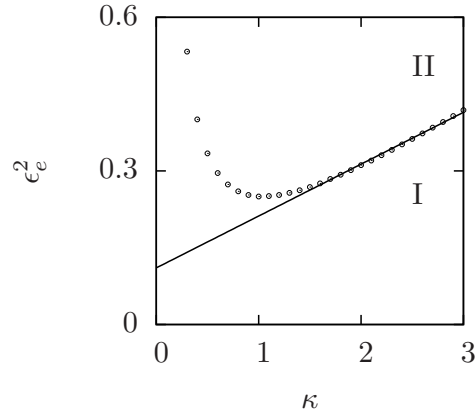
56

Figure 4.5: Transition from region of oscillations (I) to region of amplitude death (II) is shown in the parameter plane $\kappa - \epsilon_e^2$ for the coupled Rössler system. The points of amplitude death are obtained numerically when the index $< A >$ becomes zero. Solid curve is a linear fit corresponding to the stability condition Eq. (4.12), with the effective $\alpha = 0.1$. The deviation from straight line behavior for small values of κ is discussed in the text.

condition Eq. (4.12) and the points correspond to the threshold values obtained from numerical simulations. It is seen that the agreement is good for larger values of κ. However, for small values of κ, the points deviate from straight line behavior. The reason can be seen from Eq. (4.11) which gives the lower limit on κ. As κ decreases, the damping of the environment variable w, reduces. However, this damping is essential for the antisynchronizing tendency arising from the coupling to the environment. This leads to the deviations for small values of κ.

For two coupled Rössler systems as given in Eq. (4.2), we study the complete phase diagram in the parameter plane of coupling strengths for identifying the regions of different dynamic states such as amplitude death, complete synchronization and antisynchronization. Amplitude death states are identified using the index $< A >$ as mentioned above. To identify synchronized or antisynchronized states we use the asymptotic correlation values as the index, calculated using the equation 2.10. The phase diagram thus obtained for the coupled Rössler system is shown in Fig. 4.6. When the coupling strengths ϵ_d and ϵ_e are small, the systems are not synchronized (white region). For
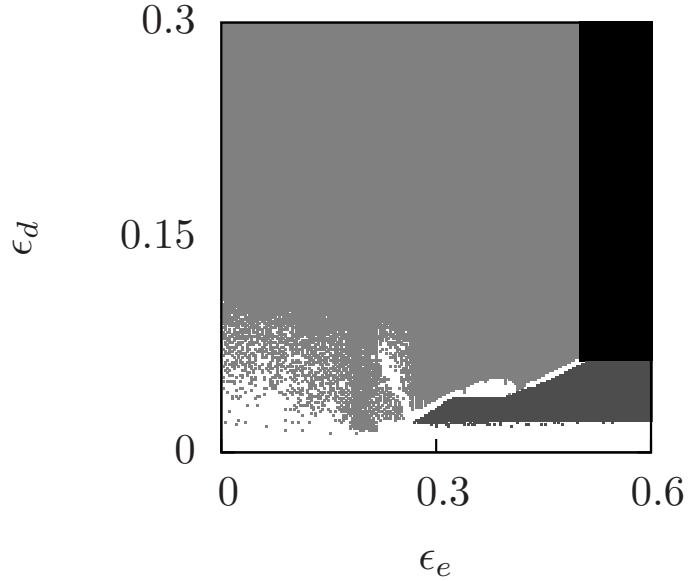
57

Figure 4.6: Regions of different dynamical states in the parameter plane of coupling strengths ϵ_e–ϵ_d in the case of two coupled Rössler systems. The indices used to identify the different regions are average correlation, C (Eq. (2.10)) and the index $< A >$. The black region corresponds to the state of amplitude death ($A \sim 0$), the light-grey region corresponds to the synchronized state ($C \sim 1$), the dark-grey region correspond to the antisynchronized state ($C \sim -1$) and the white region correspond to the state where $|C| < 1$. Here, the parameters are the same as in Fig. 4.1.

small values of ϵ_e, when ϵ_d is increased, the systems synchronize (light-grey region). When ϵ_e is increased, the systems become antisynchronized (dark-grey region). When both the coupling strengths are above a certain threshold as given by the stability conditions Eq. (4.13) and Eq. (4.14), the systems stabilize to the state of amplitude death (black region). We also note that the transition from complete synchronization to antisynchronization via a region of amplitude death corresponds to a phase transition where the average phase difference between the oscillators changes from 0 to nearly π. This is similar to the phase-flip bifurcation reported in the context of time-delay coupled systems [198, 200].

The nature of the transitions to the state of amplitude death is further characterized by fixing one of the parameters ϵ_e or ϵ_d and increasing the other.
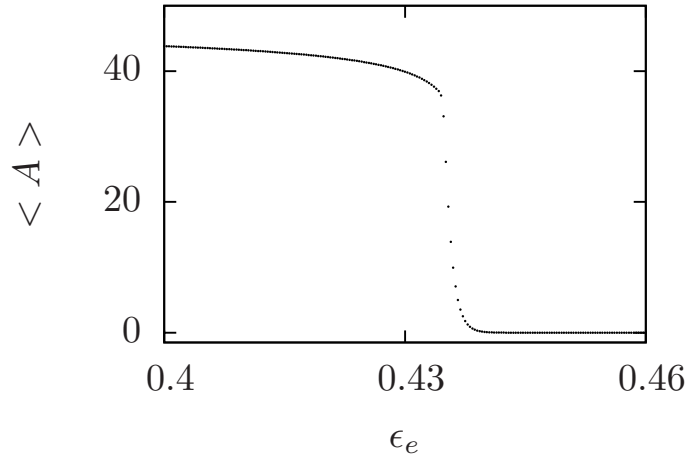
Figure 4.7: The index $< A >$ is plotted as a function of ϵ_e for a fixed value of $\epsilon_d = 0.2$ for two coupled Rössler systems. As ϵ_e is increased, we observe a continuous transition to the state of amplitude death ($\epsilon_{ec} \sim 0.45$).

This is shown in Fig. 4.7, where the index $< A >$ is plotted for increasing ϵ_e for a chosen value of ϵ_d. Here, the transition from oscillatory state to amplitude death state is continuous such that as the coupling strength is increased, the amplitude of the oscillations gradually decreases to zero. Similar transition is observed for the case where ϵ_e is kept fixed and ϵ_d is increased.

We also notice from the time series and phase space plots that as the coupling strength increases (ϵ_d or ϵ_e), the Rössler systems undergo the full reverse period doubling sequence to one-cycle before going to the amplitude death state. Then, the transition to the state of amplitude death occurs via a super-critical Hopf bifurcation. The bifurcation diagram for this transition is shown in Fig. 4.8. This is further confirmed by computing the fixed points of the coupled system and their stability near the transition region. Numerical simulations show that the coupled Rössler systems in Eq. (4.2) stabilize to the steady state corresponding to synchronized states of the subsystems. This
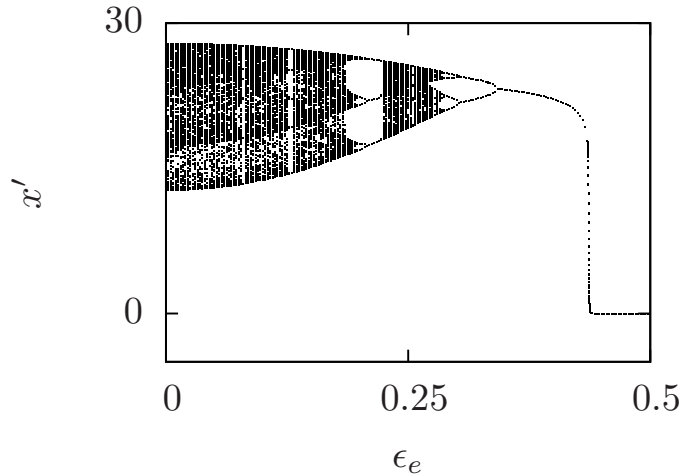
Figure 4.8: Bifurcation diagram obtained by plotting the maxima of x_{11}, (x') for sufficiently long period by increasing the coupling strength, ϵ_e for $\epsilon_d = 0.2$ and $\kappa = 1$. Here, the systems go through a reverse period doubling scenario as ϵ_e increases leading to a one-cycle (at $\epsilon_e \sim 0.35$) before amplitude death occurs $(\epsilon_{ec} \sim 0.45)$.

synchronized steady states are obtained from Eq. (4.2) as

$$
\begin{aligned}
x_{i1}^* &= (c \pm \sqrt{c^2 - 4ab\kappa/(\kappa - \epsilon_e^2 a)})/2 \\
x_{i2}^* &= -x_{i1}^*/a \\
x_{i3}^* &= -b/(x_{i1}^* - c) \\
w^* &= -\epsilon_e x_{i1}^*/\kappa
\end{aligned}
\tag{4.16}
$$

We note that the fixed point in the amplitude death state is different from the steady states of the intrinsic dynamics. It is one of the fixed points generated due to coupling with the environment. As the exact values of the fixed point depends on the environmental parameters like κ and ϵ_e, amplitude death state can be adjusted to a desired value within the stability region. Of the two fixed points, the one with plus sign in the second term of x_{i1}^* equation is unstable and the one with minus sign in the second term of x_{i1}^* equation becomes stable in the amplitude death state. The nature of the transition to the stable fixed point is determined by the eigenvalues of the corresponding
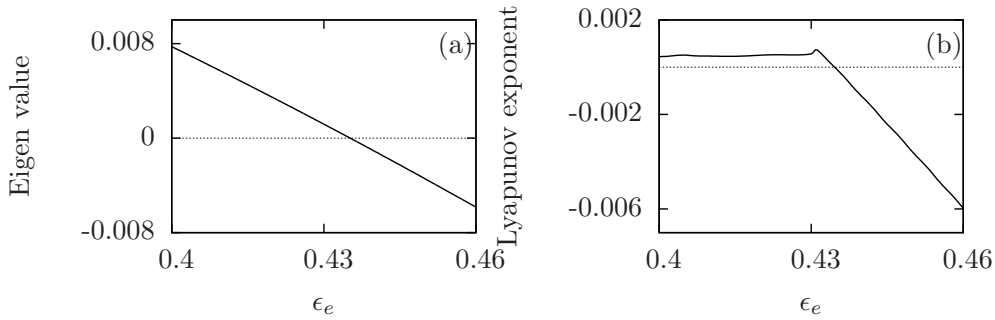
60

Figure 4.9: (a) Real part of the largest eigenvalues of the Jacobian obtained from Eq. (4.2), evaluated at the fixed point given in Eq. (4.16), for increasing ϵ_e and fixed values of $\epsilon_d = 0.2$ and $\kappa = 1$. At the transition ($\epsilon_{ec} \sim 0.435$), real parts of one pair of complex conjugate eigenvalues cross zero. (b) Largest Lyapunov exponent of the coupled Rössler system given in Eq. (4.2) as increasing ϵ_e for fixed values of $\epsilon_d = 0.2$ and $\kappa = 1$. The zero crossing of largest Lyapunov exponent ($\epsilon_{ec} \sim 0.435$) indicates transition to amplitude death state. In both figures, zero is shown as a dotted line.

Jacobian and we find that at the transition, real parts of complex conjugate pairs of eigenvalues become negative(Fig. 4.9(a)) , indicating super-critical Hopf bifurcation as described in Ref. [15]. In the amplitude death region, all the Lyapunov exponents of the coupled system (given in Eq. 4.2) are found to be negative. The largest Lyapunov exponent of the coupled system crosses zero at the transition and this is shown in Fig. 4.9(b). The nature of the transition is found to be the same when ϵ_e is kept fixed and ϵ_d is increased.

The above numerical results are presented for one set of parameters of Rössler system. We have varied the parameters and verified that the method works for other values of the parameters.

4.3.2   Coupled Lorenz systems

We repeat the same study in the case of two coupled Lorenz systems. It is interesting to note that in this case, the coupled systems stabilize to a fixed point that corresponds to antisynchronized states for the subsys-
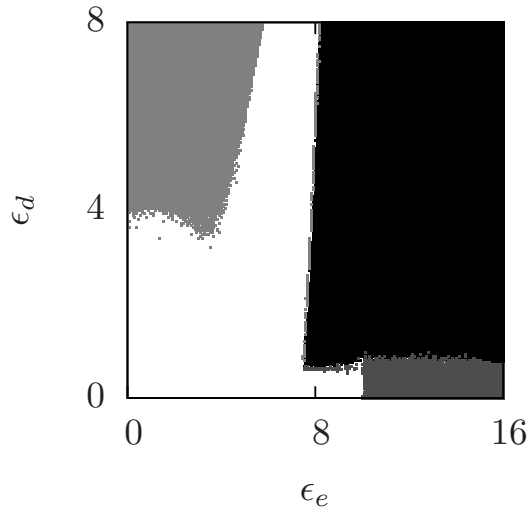
Figure 4.10: Regions of different dynamical states in the parameter plane of coupling strengths ϵ_e–ϵ_d in the case of Lorenz systems. The black region corresponds to the state of amplitude death ($A \sim 0$), the light-grey region corresponds to the synchronized state ($C \sim 1$), the dark-grey region correspond to the antisynchronized state ($C \sim -1$) and the white region correspond to the state where $|C| < 1$.

tems ($x_{11} = -x_{21}, x_{12} = -x_{22}, x_{13} = x_{23}$) as shown earlier in Fig. 4.2(c). The regions of different dynamical states in the parameter plane of coupling strengths in this case are shown in Fig. 4.10. When both ϵ_d and ϵ_e are small, the systems are not synchronized (white region). For very small values of ϵ_d and large values of ϵ_e, the systems are antisynchronized (dark-grey), and when ϵ_d is increased from this state, the systems go to the amplitude death state (black region). For small values of ϵ_e and large ϵ_d, the systems are synchronized (light-grey). As ϵ_e increases, the systems first lose synchronization and for larger values of ϵ_e, they stabilize to the state of amplitude death (black). In the de-synchronized state before the amplitude death state, the attractor in the phase space is highly distorted and the system goes through a state of frustration, trying to stabilize to antisynchronized state from the synchronized state before death occurs. This is shown in Fig. 4.11, where time series of the synchronization error between the two Lorenz systems is shown. Near this transition region, some initial conditions remain in a chaotic transient state for long time before getting stabilized to the fixed
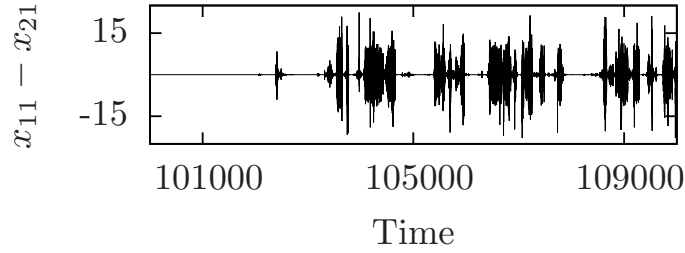
Figure 4.11: Synchronization error $(x_{11} - x_{21})$ as a function of time in the case of Lorenz systems for $\epsilon_d = 5$ and $\epsilon_e = 4.665$.
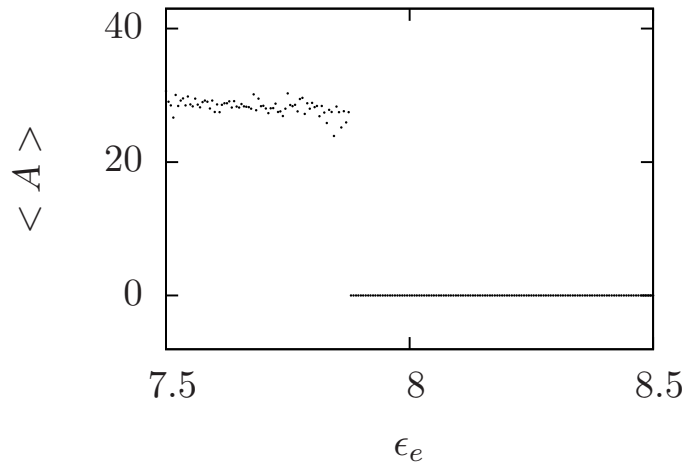

Figure 4.12: The index $< A >$ is plotted as a function of ϵ_e for a fixed value of $\epsilon_d = 5.0$ for two coupled Lorenz systems. Note that the transition to amplitude death is sudden ($\epsilon_{ec} \sim 7.88$) as opposed the case of coupled Rössler systems where the transition is continuous.

point. The phenomena of multi-stability and hysteresis are also observed in this region. The nature of transition to amplitude death in this case is shown in Fig. 4.12. Unlike the case of coupled Rössler systems, we see that the amplitude of oscillations drops suddenly at the critical strength of coupling. Thus, the transition is directly from chaotic state to amplitude death state. A similar type of transition from chaotic state to amplitude death state in case of delay coupled Lorenz systems has been reported in Ref. [179]. We further characterize this transition by computing the fixed points of the coupled system given in Eq. (4.3) and evaluating their stability near the transition region.

Numerical simulations show that the coupled Lorenz systems in Eq. (4.3) stabilize to the steady state corresponding to the antisynchronized state of the subsystems. These steady states are obtained from Eq. (4.3) as

$$
\begin{aligned}
x_{11}^* &= \pm\sqrt{\frac{((r-1)\sigma - 2\epsilon_d)b}{\sigma + 2\epsilon_d}} \\
x_{12}^* &= \frac{(\sigma + 2\epsilon_d)}{\sigma}x_{11}^* \\
x_{13}^* &= \frac{(\sigma + 2\epsilon_d)}{\sigma b}x_{11}^{*2} \\
x_{21}^* &= -x_{11}^* \\
x_{22}^* &= -x_{12}^* \\
x_{23}^* &= x_{13}^* \\
y^* &= 0
\end{aligned}
\tag{4.17}
$$

It is interesting to note that, unlike the case of two coupled Rössler systems, here the amplitude death state does not depend on the parameters of the environment. For both the solutions, we find that at the transition, real parts of complex conjugate pairs of eigenvalues of the corresponding Jacobian become negative (Fig. 4.13(a)). For $\epsilon_d > \epsilon_{dc}$, numerically an unstable limit cycle is found to coexist with the stable state of amplitude death for certain initial values. As there is no stable limit cycle before amplitude death, and an unstable fixed point becomes stable, it seems that this is a sub-critical Hopf bifurcation. All the Lyapunov exponents of the system (Eq. 4.3) are found to be negative at the amplitude death state. At the transition, the largest Lyapunov exponent of the coupled system becomes negative as shown in Fig. 4.13(b).

4.4   Summary

The notable features of the work presented in this chapter are

1. We have shown that indirect coupling through a dynamic environment
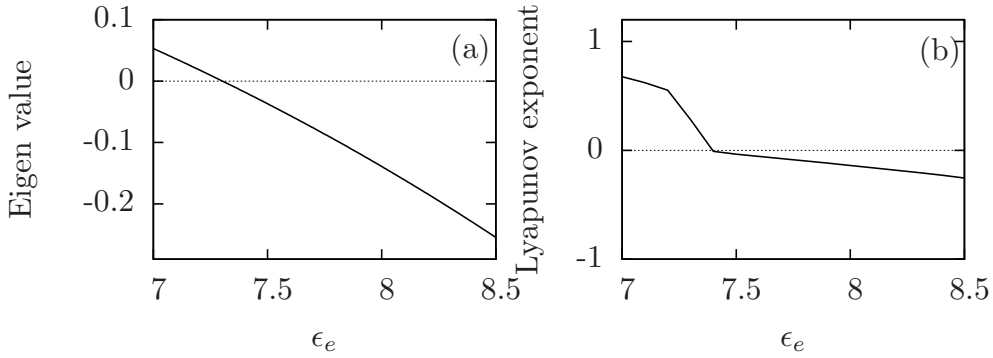
Figure 4.13: (a) Real part of the largest eigenvalue of the Jacobian obtained from Eq. (4.3), evaluated at the fixed point given in Eq. (4.17), for increasing ϵ_e and fixed values of $\epsilon_d = 5$ and $\kappa = 1$. At the transition ($\epsilon_{ec} \sim 7.31$), real parts of one pair of complex conjugate eigenvalues cross zero. (b) Largest Lyapunov exponent of the coupled Lorenz system given in Eq. (4.3) as increasing ϵ_e for fixed values of $\epsilon_d = 5$ and $\kappa = 1$. The zero crossing of largest Lyapunov exponent ($\epsilon_{ec} \sim 7.43$) indicates transition to amplitude death state. In both figures, zero is shown as a dotted line.

    in addition to direct coupling can lead to amplitude death.

2. The approximate stability analysis developed for general cases predicts the transition region in parameter space.

3. Results from direct numerical simulations agrees well with the threshold condition obtained from our theory.

4. The transitions to the state of amplitude death are found to be of two types - continuous and discontinuous.

    We have shown this in the context of two chaotic systems, namely coupled Rössler and coupled Lorenz systems. We also present the fixed point analysis for both cases studied here. In the next chapter, we further develop this mechanism and apply it to a variety of different dynamical systems to induce amplitude death.

Chapter 5

General mechanism for Amplitude Death

In chapter 4, we have presented a mechanism for inducing amplitude death in coupled systems due to competing effects of synchronizing and anti-synchronizing tendencies. We have shown this in the context of two chaotic systems, namely coupled Rössler and coupled Lorenz systems. In this chapter, we study the generality of the method. For this, we apply it to a variety of systems and find that for all cases which are synchronizable, the method works.

We also give an intuitive physical argument to support our claim of generality of the method. Our mechanism consists of having two types of couplings. The first is direct coupling which leads to synchronization. We know that, if the coupling constant is sufficiently large, the synchronization condition ensures that the largest Lyapunov exponent transverse to the synchronization manifold, is negative. Considering the space of coupled oscillators as a product of the individual systems and a network of two nodes, the synchronization manifold corresponds to the direction $e_s = (1, 1)^T$ in the network coordinates. Similarly the coupling through environment which ensures anti-synchronization, leads to the condition that the largest Lyapunov exponent transverse to the direction $e_a = (1, -1)^T$ is negative. Since we have coupled

only two systems, ensuring that the largest exponents transverse to both synchronizing and anti-synchronizing directions, i.e. e_s and e_a, are negative, implies that all the Lyapunov exponents are negative. Thus the system must converge to a fixed point.

In this chapter, we present the results of applying this method to periodic, hyperchaotic and driven systems and with different schemes of direct coupling, and different damped dynamics for the environment. The work presented in this chapter and chapter 4 has been published in Phys. Rev. E **84**, 046212 (2011) [215].

5.1 Amplitude death with alternative dynamics

Here, we present the results of our study on amplitude death in the case of periodic systems, time-delay systems, systems with different types of direct coupling and with different damped dynamics of the environment.

5.1.1 Amplitude death in periodic systems

We first study two standard limit cycle oscillators, namely Landau-Stuart oscillators and van der Pol oscillators, coupled using the scheme given in Eq. (4.1).

Landau-Stuart system is a nonlinear limit cycle oscillator, which has been previously used as a model system for studying the phenomenon of amplitude death [175, 178]. In our case, the dynamics of two coupled Landau-Stuart

systems is given by the following set of equations:

$$\begin{aligned}
\dot{x}_{i1} &= (1 - x_{i1}^2 - x_{i2}^2)x_{i1} - \omega x_{i2} + \epsilon_d(x_{j1} - x_{i1}) + \epsilon_e w, \\
\dot{x}_{i2} &= (1 - x_{i1}^2 - x_{i2}^2)x_{i2} + \omega x_{i1}, \\
\dot{w} &= -\kappa w - \frac{\epsilon_e}{2}\sum_i x_{i1}.
\end{aligned} \tag{5.1}$$

From numerical analysis of the above equations, we see that, when $\epsilon_e = 0$, and for suitable value of ϵ_d, the coupled systems synchronize. By increasing ϵ_e, the systems can be taken to a state of amplitude death. In Fig. 5.1, we show the regions of different dynamical states such as amplitude death, synchronized and anti-synchronized oscillations in the parameter plane of coupling strengths, ϵ_d–ϵ_e. For small values of ϵ_e and ϵ_d, the systems are synchronized (light-grey). For small values of ϵ_d and high values of ϵ_e, the systems are in anti-synchronized state (dark-grey). When the strengths of both ϵ_d and ϵ_e are sufficiently large, we observe amplitude death (black). We note that, here the transition to the state of amplitude death is sudden, similar to the case of Lorenz systems discussed in the preceding chapter. The case where ϵ_d is kept constant while increasing ϵ_e is shown in Fig. 5.2. Similar transition is observed in the case of increasing ϵ_d for a fixed value of ϵ_e.

However, in this case, for a given strength of coupling, the stability of amplitude death state depends on the initial conditions indicating multi-stability, that is, some initial conditions go to amplitude death state, while some other initial conditions remain in the oscillatory state. Such a multi-stability has also been reported for amplitude death phenomena in the case of Landau-Stuart oscillators using conjugate coupling [175]. In Fig. 5.1, for any pair of (ϵ_e, ϵ_d) values, we use the same initial conditions to obtain states of different phase space regions. The transition to amplitude death, as ϵ_d increases for fixed ϵ_e, does not appear to satisfy Eq. (4.14). This may be because of the multi-stability observed in the system. If we change the initial condition, then the curve representing transition to amplitude death as ϵ_d increases is found to change. In Fig. 5.3, basin of amplitude death is shown for a fixed value of ϵ_e and for increasing ϵ_d. Black regions represent the basin
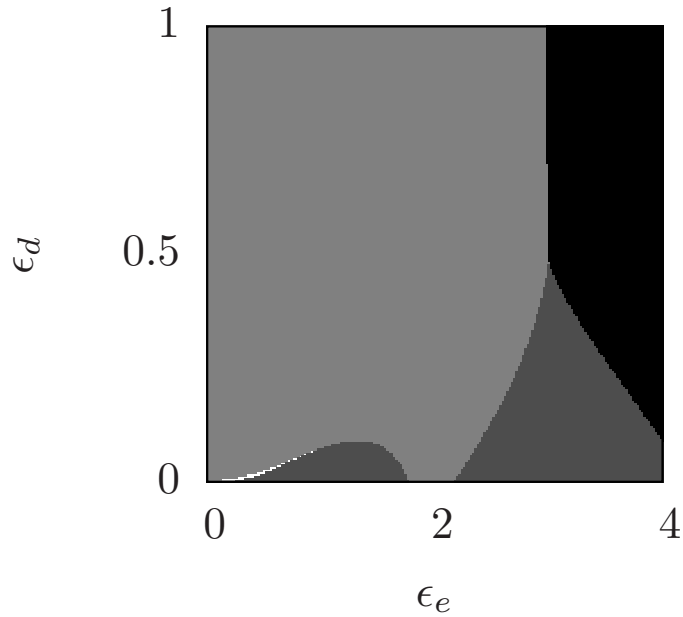
Figure 5.1: Regions of different dynamical states in the parameter plane of coupling strengths ϵ_e–ϵ_d in the case of Landau-Stuart systems. The black region corresponds to the state of amplitude deathidentified using index A (see Eq. 4.15 in Chapter 4 for the definition of A). The light-grey region corresponds to the synchronized state ($C \sim 1$), the dark-grey region correspond to the anti-synchronized state ($C \sim -1$) and the white region represents to the de-synchronized state. Numerical simulations are done with $\omega = 2$ and $\kappa = 1$.
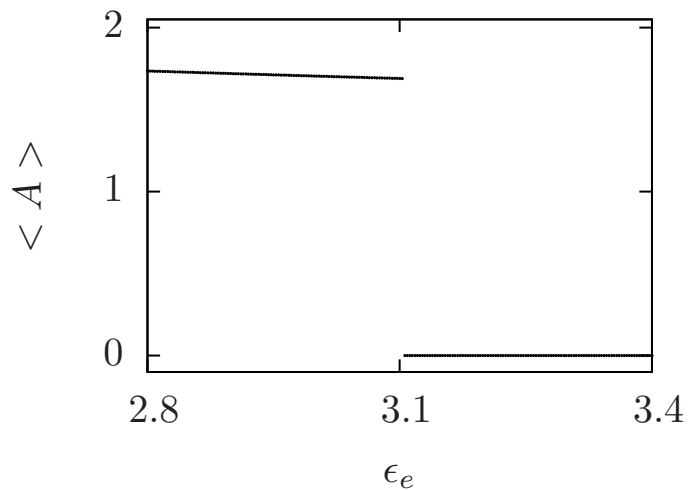
Figure 5.2: Here, we plot the index $< A >$, defined in Eq. 4.15 in Chapter 4 as a function of ϵ_e for constant $\epsilon_d = 0.5$ for two coupled Landau-Stuart oscillators. The transition to the state of amplitude death is sudden ($\epsilon_{ec} \sim 3.11$).

70
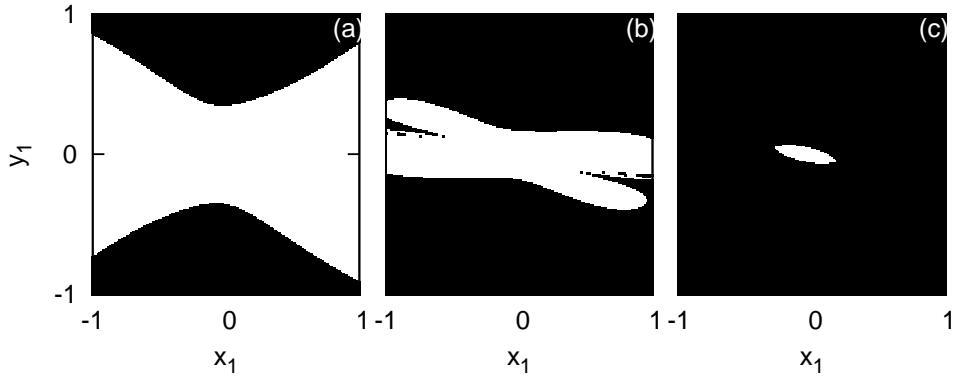
Figure 5.3: The basin for amplitude death in the plane of initial conditions x_1–y_1 of one of the two coupled Landau-Stuart systems. The initial condition of the other system is chosen to be $x_2 = x_1 + 0.1$, $y_2 = y_1$. The black regions indicate basin of attraction for the amplitude death state, where $< A >= 0$, and the white regions indicate the basin for oscillatory state ($< A >> 0$). The strength of indirect coupling is chosen to be $\epsilon_e = 3.8$, and the strength of direct coupling is varied as (a) $\epsilon_d = 0$ (b) $\epsilon_d = 0.2$ (c) $\epsilon_d = 0.4$. We see that the basin of amplitude death increases as ϵ_d increased.

for amplitude death and white regions represent the basin for oscillatory states. Fig. 5.3(a), shows the basin of amplitude death when $\epsilon_d = 0$. For some initial values, amplitude death occurs even in the absence of direct coupling. A possible explanation is that the α of the individual system is negative or zero such that, the stability condition $\kappa > \alpha$ given in Eq. (4.11) is always satisfied. It is seen that the area of the basin of amplitude death increases as ϵ_d is increased [Fig. 5.3(b) and (c)].

We repeat the same study for the case of two coupled periodic van der Pol systems given by the following equations:

$$\begin{aligned}
\dot{x}_{i1} &= x_{i2} + \epsilon_d(x_{j1} - x_{i1}) + \epsilon_e w, \\
\dot{x}_{i2} &= a(1 - x_{i1}^2)x_{i2} - x_{i1}, \\
\dot{w} &= -\kappa w - \frac{\epsilon_e}{2} \sum_i x_{i1}.
\end{aligned} \tag{5.2}$$

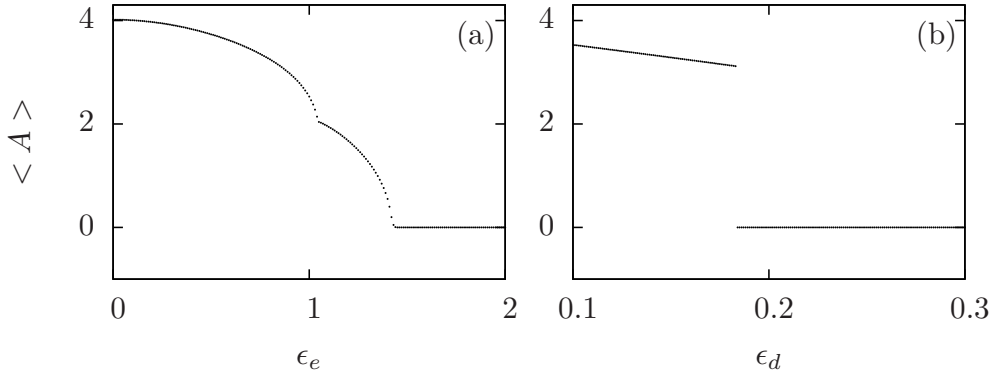We choose the parameter $a = 1$ such that the system has a stable limit

Figure 5.4: (a) The index $< A >$, defined in Eq. 4.15 in chapter 4 as a function of ϵ_e for a fixed $\epsilon_d = 1.5$ for two coupled van der Pol oscillators. Here, the transition to amplitude death is continuous. For $\epsilon_e < 1.05$, the coupled systems show synchronized limit cycles. At $\epsilon_e \sim 1.05$, we have a pitchfork bifurcation of the limit cycle and the two systems now have two different limit cycles. These limit cycles subsequently undergo super-critical Hopf bifurcation to the amplitude death state ($\epsilon_{ec} \sim 1.47$). (b) The index $< A >$ as a function of ϵ_d for a fixed $\epsilon_e = 2.0$ for two coupled van der Pol oscillators. Here, the transition to amplitude death is sudden ($\epsilon_{dc} \sim 0.18$) and is of sub-critical Hopf bifurcation. We note that the nature of the transition to the amplitude death state in the case of van der Pol oscillators is different from the other systems that we have studied. For the numerical simulations, the parameters are $a = 1$ and $\kappa = 1$.

cycle when both the couplings are absent (i.e., $\epsilon_e = \epsilon_d = 0$). For suitable strength of direct coupling ϵ_d, the systems synchronize and amplitude death is observed when both direct and indirect couplings are above their respective thresholds. As far as the nature of the transition to the state of amplitude death is concerned, the van der Pol oscillator shows a different behavior than other systems. We find that the nature of the transitions to amplitude death depends on the type of coupling parameter. Fixing ϵ_d and increasing ϵ_e, we see a smooth transition similar to the case of Rössler systems (Fig. 5.4 (a)) and by fixing ϵ_e and increasing ϵ_d, we get a sudden transition, similar to the case of Lorenz systems (Fig. 5.4(b)).

5.1.2 Amplitude death in time delay systems

The Mackey-Glass time-delay system is well studied as a model exhibiting hyperchaos. Stabilization to fixed point, or amplitude death in such systems has been reported using stabilization methods such as conventional feedback, tracking filter and delayed feedback [216]. Here we consider two Mackey-Glass systems coupled via both direct and indirect couplings as given by

$$
\begin{aligned}
\dot{x}_i &= -ax_i + \frac{bx_{\tau i}}{1 + x_{i\tau}^m} + \epsilon_d(x_j - x_i) + \epsilon_e w \\
\dot{w} &= -\kappa w - \frac{\epsilon_e}{2} \sum_{j=1,2} x_j
\end{aligned}
\tag{5.3}
$$

where x_i represents the Mackey-Glass system [23] and $x_{i\tau}$ is the value of the variable x_i at a delayed time $x_i(t - \tau)$. The parameters of the Mackey-Glass systems are chosen such that, the individual systems are in hyperchaotic regime. When $\epsilon_e = 0$, for sufficiently large coupling strength ϵ_d, the systems synchronize. By increasing ϵ_e we get amplitude death.

We show the different types of dynamical behavior of coupled Mackey-Glass systems in the parameter plane of coupling strengths in Fig. 5.5. For very small values of ϵ_d and ϵ_e, the two systems are not synchronized (white). The systems synchronize as ϵ_d is increased (light-grey). For large values of ϵ_d, if ϵ_e is increased, the systems go to a state of amplitude death (black). When ϵ_d is small and ϵ_e is large, the systems are in anti-synchronized state (dark-grey). As we increase ϵ_d, the systems go to the amplitude death state. However, for large values of ϵ_d and ϵ_e, the Mackey-Glass systems appear to show a different behavior than Rössler or Lorenz. We observe a re-entrant behavior to rhythmogenesis, both as ϵ_e increases, or as ϵ_d increases. This transition also satisfies our stability conditions Eq. (4.13) and Eq. (4.14). We find that the transition to the state of amplitude death in the case of two coupled Mackey-Glass systems is continuous and that the systems go through a reverse period doubling sequence reaching a limit cycle before the amplitude death occurs. This is similar to the case of Rössler systems discussed in the preceding chapter. Fig.5.6 shows the transition to amplitude
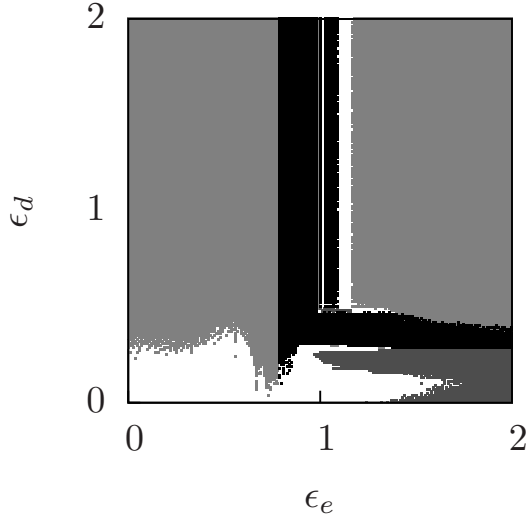
Figure 5.5: Regions of amplitude death (black), synchronized (light-grey) and anti-synchronized oscillations (dark-grey) in the parameter plane of coupling strengths ϵ_e–ϵ_d in the case of two coupled Mackey-Glass time-delay systems. For numerical analysis, we have chosen the following parameter values $a = 1$, $b = 2$, $\tau = 2.5$, $m = 10$ and $\kappa = 1$.

death from synchronized oscillatory state as ϵ_e is increased for a chosen value of ϵ_d.

5.1.3   Lorenz systems with replacement coupling

So far, we have studied direct coupling of the diffusive type. Synchronization is also possible by choosing the direct coupling of different types. Here we consider Lorenz systems coupled using a different scheme of coupling, namely replacement coupling, as given by the following equations:

$$
\begin{aligned}
\dot{x}_{i1} &= \sigma(x_{j2} - x_{i1}) + \epsilon_e w, \\
\dot{x}_{i2} &= (r - x_{i3})x_{i1} - x_{i2}, \\
\dot{x}_{i3} &= x_{i1}x_{i2} - bx_{i3}, \\
\dot{w} &= -\kappa w - \frac{\epsilon_e}{2}\sum_i x_{i1}.
\end{aligned}
\tag{5.4}
$$
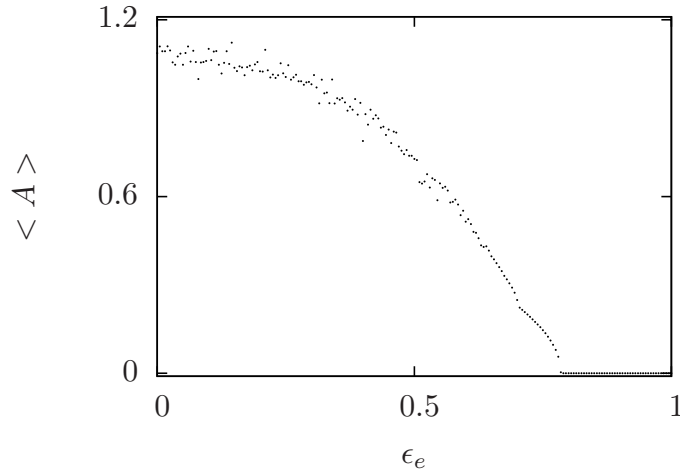
Figure 5.6: The index $< A >$ (defined in Eq. 4.15 in Chapter 4), as a function of ϵ_e for a fixed $\epsilon_d = 1.5$ for two coupled Mackey-Glass systems. The transition to amplitude death is continuous ($\epsilon_{ec} \sim 0.79$) .

Here, the direct coupling is of the replacement type, such that the x_2 variable in the first function of the first system is that of the second system and vice versa. This type of coupling leads to synchronization as reported in Ref. [33]. We introduce indirect coupling through variable w. We find that for suitable value of coupling strength ϵ_e, the systems stabilize to a state of amplitude death. This is shown in Fig. 5.7.
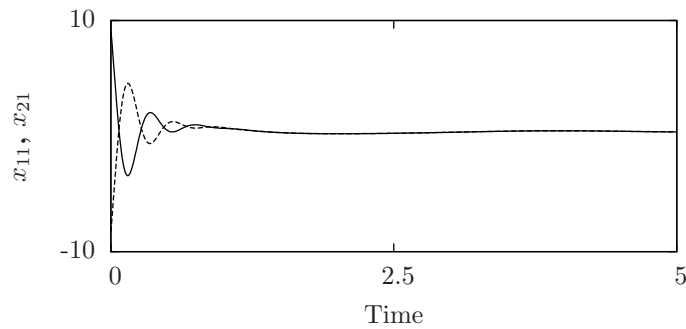
Figure 5.7: Time series of the variable x_{i1} of the coupled Lorenz systems where the direct coupling is of replacement type (see text) showing amplitude death for $\epsilon_e = 16.0$. The other parameters are $\sigma = 10$, $r = 28$, $b = 8/3$ and $\kappa = 1$.

5.1.4 Amplitude death with alternative dynamics for the environment

In previous sections, we have taken the intrinsic dynamics of the environment to be that of an overdamped harmonic oscillator. Here, we show that, amplitude death is possible with other intrinsic dynamics for the environment also.

For this, we consider the case of two Rössler systems coupled with a dynamic environment, where the intrinsic dynamics of the environment is that of a damped harmonic oscillator. The dynamics of the coupled system in this case is given by

$$
\begin{aligned}
\dot{x}_{i1} &= -x_{i2} - x_{i3} + \epsilon_d(x_{j1} - x_{i1}) + \epsilon_e w_1 \\
\dot{x}_{i2} &= x_{i1} + a x_{i2} \\
\dot{x}_{i3} &= b + x_{i3}(x_{i1} - c) \\
\dot{w}_1 &= w_2 - \frac{\epsilon_e}{2} \sum_i x_{i1} \\
\dot{w}_2 &= -w_2 - \kappa w_1
\end{aligned}
\tag{5.5}
$$

Here, the variables w_1 and w_2 represent a 2-dimensional environment together forming an underdamped harmonic oscillator. For very weak coupling ($\epsilon_d \sim 0, \epsilon_e \sim 0$), the two Rössler systems are not synchronized. When the coupling strength, ϵ_d, increased while ϵ_e is kept fixed at zero, the systems become synchronized. This is shown in the time series in Fig. 5.8(a). On the other hand, when ϵ_e, increased while ϵ_d is kept fixed at zero, the systems become anti-phase synchronized (Fig. 5.8(b)). When both ϵ_e and ϵ_d are above their respective thresholds, amplitude death is observed (Fig. 5.8(c)).

We repeat the same study by taking the intrinsic dynamics of the environment as that of an overdamped Duffing oscillator. The equations in this
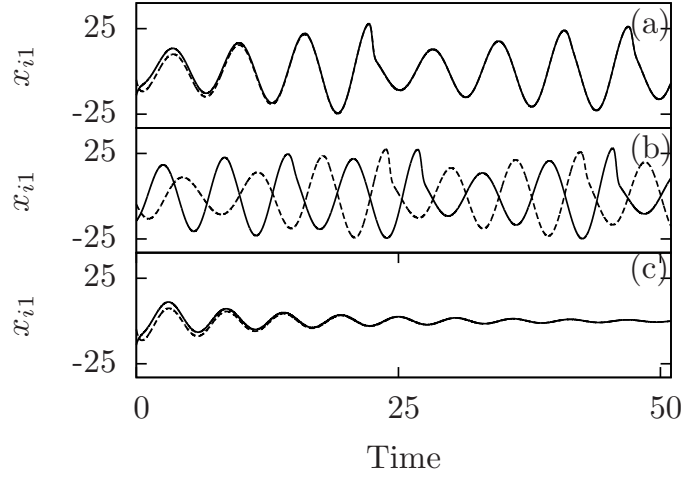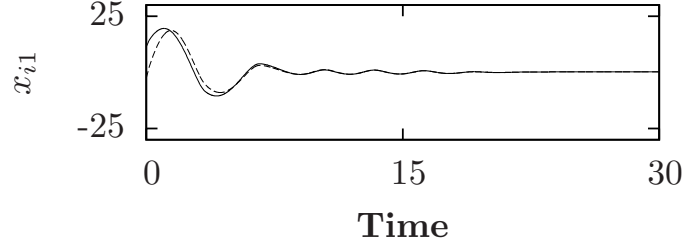
Figure 5.8: Time series of the first variables $x_{i1}, i = 1, 2$ of two coupled Rössler systems given in Eq. 5.5. (a) Synchronization for $(\epsilon_d, \epsilon_e) = (2.0, 0.0)$.(b) Anti-phase synchronization $(\epsilon_d, \epsilon_e) = (0.0, 0.5)$.(c) Amplitude death for $(\epsilon_d, \epsilon_e) = (2.0, 0.5)$.

case are

$$
\begin{aligned}
\dot{x}_{i1} &= -x_{i2} - x_{i3} + \epsilon_d(x_{j1} - x_{i1}) + \epsilon_e w \\
\dot{x}_{i2} &= x_{i1} + ax_{i2} \\
\dot{x}_{i3} &= b + x_{i3}(x_{i1} - c) \\
\dot{w} &= w - \kappa w^3 - \frac{\epsilon_e}{2} \sum_i x_{i1}
\end{aligned}
\tag{5.6}
$$

For small values of ϵ_e and ϵ_d, we see that the systems are not synchronized. They become synchronized as ϵ_d is increased from this state. For small values of ϵ_d and large values of ϵ_e, the systems are in anti-phase synchronized state. When the strengths of both ϵ_d and ϵ_e are sufficiently large, we observe amplitude death (Fig. 5.9). The phase diagram in this case is qualitatively similar to that given in Fig. 4.6.
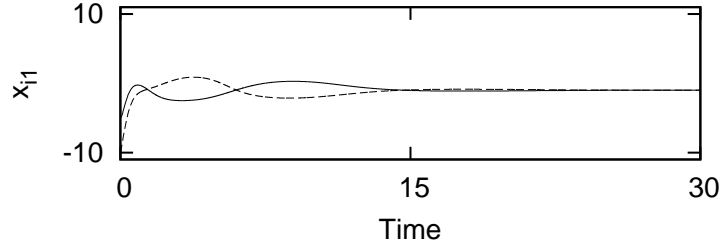
Figure 5.9: Time series of the first variables $x_{i1}, i = 1, 2$ of two coupled Rössler systems given in Eq. 5.6 showing amplitude death for $(\epsilon_d, \epsilon_e) = (2.0, 0.5)$.

5.2 Amplitude death in hyperchaotic Rössler systems

We also consider the case of two hyperchaotic Rössler systems as given by the following equations

$$
\begin{aligned}
\dot{x}_{i1} &= -x_{i2} - x_{i3} + \epsilon_e w_1 \\
&\quad -\epsilon_d \cos\theta(\sin\theta(x_{i1} - x_{j1}) + \cos\theta(x_{i3} - x_{j3})) \\
\dot{x}_{i2} &= x_{i1} + ax_{i2} + x_{i4} + \epsilon_e w_2 \\
\dot{x}_{i3} &= b + x_{i3}x_{i1} \\
&\quad -\epsilon_d \sin\theta(\sin\theta(x_{i1} - x_{j1}) + \cos\theta(x_{i3} - x_{j3})) \\
\dot{x}_{i4} &= -cx_{i3} + \sigma x_{i4} + \epsilon_e w_3 \\
\dot{w}_1 &= -\kappa w_1 - \frac{\epsilon_e}{2} \sum_i x_{i1} \\
\dot{w}_2 &= -\kappa w_2 - \frac{\epsilon_e}{2} \sum_i x_{i2} \\
\dot{w}_3 &= -\kappa w_3 - \frac{\epsilon_e}{2} \sum_i x_{i4}
\end{aligned}
\tag{5.7}
$$

where $i, j = 1, 2$ and $j \neq i$.

We choose parameters of the system such that, the intrinsic dynamics of the systems is hyperchaotic. For this system, the method of time-delay coupling is found ineffective for producing amplitude death [183]. In the absence of coupling via environment, the direct coupling via a scalar signal

78

Figure 5.10: Time series of the first variables $x_{i1}, i = 1, 2$ of the two coupled hyperchaotic Rössler systems given in Eq. 5.7 in amplitude death state. Parameters of the systems are chosen to be $a = 0.25$, $b = 3$, $c = 0.5$, $\sigma = 0.05$. Parameters used in the direct coupling term are $\epsilon_d = 2.5$, $\theta = \pi/3$ and in the indirect coupling terms are $\kappa = 10$ and $\epsilon_e = 4$.

results in synchronization of the two hyperchaotic systems for suitable values of parameters ϵ_d and θ as reported in Ref. [217]. We take the environment to be three-dimensional in this case. We find that amplitude death occurs in the coupled system for suitable value of coupling strengths ϵ_e and κ. This is shown in Fig. 5.10.

5.3 Small oscillations in driven systems

We also apply the scheme described in the preceding chapter to driven systems such as driven van der Pol and Duffing systems. In such driven systems, the fixed point is not a solution for the individual or coupled systems. Therefore, we interpret the equivalent of amplitude death state as the state having very small amplitude oscillations.

The driven van der Pol systems with direct diffusive coupling and indirect coupling through environment can be written as

$$
\begin{aligned}
\dot{x}_{i1} &= x_{i2} + \epsilon_d(x_{j1} - x_{i1}) + \epsilon_e w \\
\dot{x}_{i2} &= \alpha(1 - x_{i1}^2)x_{i2} - x_{i1} + \beta \cos(\omega t) \\
\dot{w} &= -\kappa w - \frac{\epsilon_e}{2}\sum_j x_{j1}
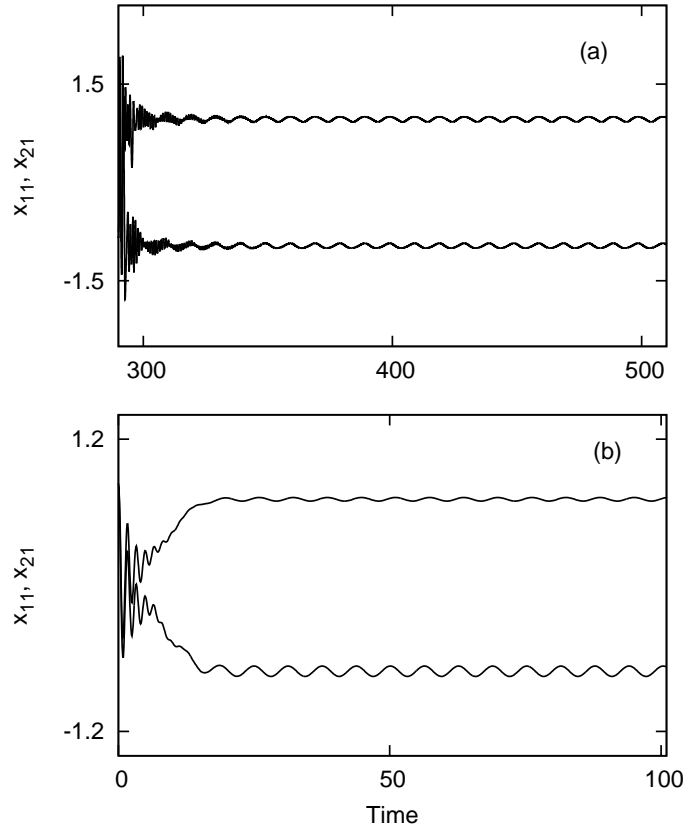\end{aligned}
\tag{5.8}
$$

Figure 5.11: Time series of the first variable x_{i1} of the coupled driven systems showing small oscillations. Here, we interpret the small oscillations as the state of amplitude death (see text). (a) driven van der Pol system for $(\epsilon_d, \epsilon_e) = (1.0, 3.5)$. The parameters of individual systems are taken to be $\alpha = 8.53$, $\omega = 0.63$ and $\beta = 1.2$ (b) driven Duffing system for $(\epsilon_d, \epsilon_e) = (1.0, 4.0)$. The parameters of individual systems are taken to be $\alpha = 0.25$, $\omega = 1$ and $\beta = 0.3$

We find that, when $\epsilon_e = 0$, and ϵ_d increases, the two systems become synchronized. In this state, if we start increasing ϵ_e, we get a state of small oscillations. Fig. 5.11(a) shows the time series for such a state.

Fig. 5.12(a) plots the index $< A >$ as a function of ϵ_e. We first see a transition from a limit cycle to two different limit cycles for the two systems. This state then subsequently goes to the state of small oscillations continuously as ϵ_e increases further. On the other hand, if we keep ϵ_e fixed and increase ϵ_d, the transition is sudden. As ϵ_d increases further, we find a

80
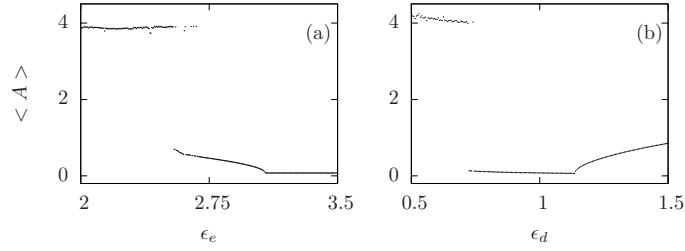
Figure 5.12: Transition to state of small oscillations in two coupled driven van der Pol oscillators. Here the death state corresponds to a state of small oscillations since fixed point is not a stable state. In this state, the index $< A >$ (see Eq. 4.15 in Chapter 4 for the definition) remains finite though very small. (a) The index $< A >$ as a function of ϵ_e for fixed $\epsilon_d = 1.0$. The transition is continuous ($\epsilon_{ec} \sim 3.08$). There is a sudden transition due to pitchfork bifurcation of the limit cycle observed at $\epsilon_e \sim 2.55$. (b) The index $< A >$ as a function of ϵ_d for fixed $\epsilon_e = 3.5$. The transition to the state of small oscillations is sudden ($\epsilon_{dc} \sim 0.72$). We also observe a re-entrant continuous transition to periodic oscillations with increasing amplitude at $\epsilon_d \sim 1.14$.

continuous transition to a state of increasing amplitude of oscillations. This is shown in Fig. 5.12(b).

The same study is repeated for the case of two coupled Duffing systems given by the following equations

$$
\begin{aligned}
\dot{x}_{i1} &= x_{i2} + \epsilon_d(x_{j1} - x_{i1}) + \epsilon_e w \\
\dot{x}_{i2} &= -\alpha x_{i2} + x_{i1} - x_{i1}^3 + \beta \cos(\omega t) \\
\dot{w} &= -\kappa w - \frac{\epsilon_e}{2} \sum_j x_{j1}
\end{aligned}
\tag{5.9}
$$

We find that a regime of small oscillations is possible in this case also. This is shown in Fig. 5.11(b).

Thus, we have illustrated the method for inducing amplitude death in coupled systems introduced in this paper works for periodic systems, hyper-chaotic and driven systems. It is effective in quenching the dynamics even with different forms of direct coupling such as replacement coupling.

5.4   Summary

In summary, the method for amplitude death introduced in the preceding chapter is found to be quite general and works for different types of systems such as periodic, chaotic and time-delay systems. The regions of different dynamic states in the parameter plane of coupling strengths and the nature of transitions to the state of amplitude death are also found to be in agreement with the theory developed in the preceding chapter.

Thus,

1. In this chapter, we have extended the study to include environment with different dynamics.

2. The method is found effective in diverse dynamics of systems like periodic, chaotic, hyperchaotic etc.

3. We have also shown that amplitude death is possible with different types of direct coupling.

4. An effect similar to amplitude death with suppressed dynamics with small oscillations is also observed in the case of driven systems.

5. Hence, the method is established as general and effective for controlling the dynamics and inducing amplitude death in connected systems.

In the next chapter, we further extend our mechanism for suppression of dynamics in complex network of dynamical systems.

Chapter 6

Amplitude death in complex networks induced by environment

In chapters 4 and 5, we have discussed a mechanism for inducing amplitude death in coupled synchronizable systems. In this chapter, we extend this to the case of a complex network of N systems. We develop the stability analysis following the approach given in Ref. [218]. The stability conditions are obtained for the general case. We consider different network structures and show that, the critical strength of coupling needed for amplitude death has a universal relation with the largest non-zero eigenvalue of the coupling matrix. This is verified by extensive numerical studies on many networks like chain, ring, tree, lattice, all-to-all, star and random topologies. The work presented in this chapter has been published in Phys. Rev. E **85**, 046211 (2012) [219].

6.1 Amplitude death via direct and indirect coupling

We consider the dynamics of N systems $x_i, i = 1, 2, \ldots, N$, in a network, coupled with two types of couplings, namely a direct diffusive coupling and an indirect coupling through an environment as an extension of the model given in chapter 4 which gave a general model for amplitude death in two coupled systems. The dynamics of such a model is given by

$$
\begin{aligned}
\dot{x}_i &= f(x_i) + \sum_j \beta G_{ij} \epsilon_d x_j + \epsilon_e \gamma w \\
\dot{w} &= -\kappa w - \frac{\epsilon_e}{N} \gamma^T \sum_i x_i
\end{aligned}
\tag{6.1}
$$

where $i, j = 1, 2, \ldots N$. Here, x_i represents m-dimensional nonlinear oscillators whose intrinsic dynamics is given by $f(x_i)$. G is the coupling matrix of dimension $N \times N$. We choose the elements of G such that, the row-sum, $\sum_j G_{ij} = 0$, for every j. This ensures that the largest eigenvalue of the coupling matrix μ_1, is zero. β is a matrix $(m \times m)$ with elements 0 and 1 and defines the components of x_i which take part in the coupling. For simplicity, we take β to be diagonal, $\beta = diag(\beta_1, \beta_2, \ldots, \beta_m)$ and in numerical simulations, only one component, β_1 is assumed to be non-zero. The environment is considered to be common to all nodes and modelled by a one-dimensional over-damped oscillator w, with damping parameter κ. It is clear that without feedback from the systems, the environment can not remain dynamic and will rapidly settle to a steady state. However, the feedback from all the systems keeps it active. All the systems, in turn, get feedback from the environment. γ is a column matrix $(m \times 1)$, with elements 0 or 1, and it decides the components of x_i that get feedback from the environment. γ^T is the transpose of γ and decides the components of x_i which gives feedback to the environment. The strength of this feedback coupling between the systems and the environment is given by ϵ_e.

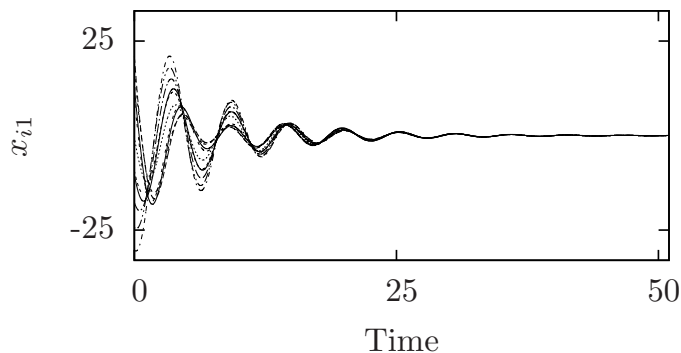We illustrate our scheme using a network of coupled chaotic Rössler sys-

Figure 6.1: Time series of the first variables x_{i1} of 10 coupled Rössler systems in all-to-all coupled network [Eq. (6.2)] showing amplitude death for $(\epsilon_d, \epsilon_e) = (0.05, 0.8)$. Here, the Rössler parameters are $a = b = 0.1, c = 18$. The damping parameter of the environment is taken to be $\kappa = 1$.

tems represented by the following equations:

$$
\begin{aligned}
\dot{x}_{i1} &= -x_{i2} - x_{i3} + \epsilon_d \sum_j G_{ij} x_{j1} + \epsilon_e w, \\
\dot{x}_{i2} &= x_{i1} + a x_{i2}, \\
\dot{x}_{i3} &= b + x_{i3}(x_{i1} - c), \\
\dot{w} &= -\kappa w - \frac{\epsilon_e}{N} \sum_i x_{i1}.
\end{aligned}
\tag{6.2}
$$

Here, we choose G to be an all-to-all connected network of 10 nodes, that is, $G_{ij} = 1$, if $j \neq i$ and $G_{ii} = -9$. We find that amplitude death is possible for suitable values of coupling strengths. The time series for the amplitude death state is shown in Fig. 6.1.

As noted from Eq. (6.2), our model has two types of coupling. The first is direct diffusive coupling which tends to synchronize the systems $x_1 = x_2 = x_3 = \ldots = x_N$. We find that, the coupling via environment has a tendency to decrease the sum, $\sum_i x_i$. When both these tendencies work together the systems converge to a fixed point. This is explicitly seen in the context of two systems coupled through the environment discussed in Chapter 4, where the environmental coupling reduces the sum to a small value, corresponding to antiphase synchronization.

6.2 Linear stability analysis

The stability of the steady state of the network of coupled systems given in Eq. (6.1) can be analysed by writing the variational equations formed by linearising Eq. (6.1) as

$$
\begin{aligned}
\dot{\xi}_i &= f'(x_i)\xi_i + \sum_j \beta G_{ij}\epsilon_d\xi_j + \epsilon_e\gamma z, \\
\dot{z} &= -\kappa z - \frac{\epsilon_e}{N}\gamma^T \sum_i \xi_i,
\end{aligned}
\tag{6.3}
$$

where ξ_i and z are small deviations from the respective values of x_i and y, f' is the $m \times m$ Jacobian matrix.

Let us introduce the $m \times N$ state function [218]

$$
\Xi = (\xi_1, \xi_2, \ldots, \xi_N).
\tag{6.4}
$$

Then, Eq. (6.3) for the synchronized state $[x_1 = x_2 = \ldots = x_N]$ can be written as

$$
\dot{\Xi} = f'\Xi + \beta\epsilon_d\Xi G^T + \epsilon_e z\Gamma,
\tag{6.5}
$$

$$
\dot{z} = -\kappa z - \frac{\epsilon_e}{N}\gamma^T \sum_i \xi_i,
\tag{6.6}
$$

where G^T is the transpose of the coupling matrix, Γ is a $m \times N$ matrix, $\Gamma = (\gamma, \gamma, \ldots, \gamma)$.

Let e_k be an eigenvector of G^T such that

$$
G^T e_k = \mu_k e_k,
\tag{6.7}
$$

where μ_k is an eigenvalue of G^T. Right-multiplying both sides of Eq. (6.5) with e_k, we get

$$
\dot{\Xi}e_k = f'\Xi e_k + \mu_k\beta\epsilon_d\Xi e_k + \epsilon_e z\Gamma e_k.
\tag{6.8}
$$

Let

$$\Phi_k = \Xi e_k. \tag{6.9}$$

Then, Eq. (6.8) can be written as

$$\dot{\Phi}_k = f'\Phi_k + \mu_k\beta\epsilon_d\Phi_k + \epsilon_e z\Gamma e_k. \tag{6.10}$$

We note that $e_1 = (1, 1, \ldots, 1)^T$ is the synchronization manifold and $\Phi_1 = \Xi e_1 = \sum_i \xi_i$. Since one could write Γ as the product $\Gamma = \gamma e_1^T$, Eq. (6.10) and (6.5) can be written as

$$\dot{\Phi}_k = f'\Phi_k + \mu_k\beta\epsilon_d\Phi_k + \epsilon_e z\gamma e_1^T e_k, \tag{6.11}$$

$$\dot{z} = -\kappa z - \frac{\epsilon_e}{N}\gamma^T\Phi_1. \tag{6.12}$$

First, we consider the case where G is taken to be a symmetric matrix. In this case, the remaining eigenvectors span a $(N-1)$-dimensional subspace orthogonal to the eigenvector e_1 . Consequently, this subspace is orthogonal to the synchronization manifold. For $k = 1$, Eq. (6.11) and becomes

$$\dot{\Phi}_1 = f'\Phi_1 + \epsilon_e z N\gamma. \tag{6.13}$$

Since e_i are orthogonal, $\Gamma e_k = \gamma e_1^T e_k = 0$ for $k \neq 1$. Therefore, For $k \neq 1$, Eq. (6.11) reduces to

$$\dot{\Phi}_k = f'\Phi_k + \mu_k\beta\epsilon_d\Phi_k. \tag{6.14}$$

We note that Eqs. (6.13) and (6.12) are coupled while Eq. (6.14) is independent of the other two. Moreover, Eq. (6.14) is equivalent to the Master Stability Equation introduced by Pecora and Carrol in Ref. [141]. Therefore, the stability function for any given system will be obtained as a function of $\epsilon_d\mu_k$ in the same way. This therefore ensures the stability of the synchronized state $x_1 = x_2 = x_3 = \ldots = x_N$. As noted in the previous section, for the amplitude death state to be stable, we need one more condition to be satisfied. That is, the synchronized state should be a fixed point. For this, the eigenvalues of the Jacobian corresponding to the coupled system given

in Eqs. (6.13) and (6.12) should be negative.

So far, we have discussed the case where the coupling matrix, G is symmetric. The same analysis can be extended to the asymmetric case as well. In this case, the eigenvectors of G are, in general, not orthogonal to the synchronization manifold.

Let e_k, for $k \neq 1$ be split to two components, one parallel and the other perpendicular to e_1. That is,

$$e_k = e_k^\perp + q_\| e_1, \tag{6.15}$$

where, $e_k^\perp$ is orthogonal to e_1. Substituting e_k from Eq. (6.15) in Eq. (6.10), we find that the dynamics of Φ_1 and z will again be the same as given in Eqs. (6.13) and (6.12) . The dynamics of $\Phi_k, k > 1$ are given by

$$\dot{\Phi}_k = f'\Phi_k + \mu_k \beta \epsilon_d \Phi_k + \epsilon_e z N \gamma q_\| \tag{6.16}$$

since, $\Gamma e_k^\perp = \gamma e_1^T e_k^\perp = 0$. In principle, the coupled equations, Eqs. (6.13), (6.16) and (6.12) can be considered as Master Stability Equation in this case also. However, in this case it is not practically useful since the Master Stability function will be a function of four parameters ϵ_d, a, b and ϵ_e, with $\mu_k = a + ib$.

To continue the analysis of the stability of the amplitude death states from Eqs. (6.13), (6.12) and (6.14), we assume that the time average values of f' are approximately the same and can be replaced by an effective constant value α. Thus, Eq. (6.14) becomes

$$\dot{\Phi}_k = \alpha \Phi_k + \mu_k \epsilon_d \Phi_k, \tag{6.17}$$

and the corresponding Lyapunov exponent is given by

$$\lambda_1 = \alpha + \mu_2 \epsilon_d, \tag{6.18}$$

where μ_2 is the largest μ_k for $k \neq 1$.

The Jacobian corresponding to the coupled Eqs. (6.13) and (6.12) is

$$J = \begin{pmatrix} \alpha & \epsilon_e N \\ -\epsilon_e/N & -\kappa \end{pmatrix},$$

and the eigenvalues are

$$\lambda_{2,3} = \frac{(\alpha - \kappa) \pm \sqrt{(\kappa + \alpha)^2 - 4\epsilon_e^2}}{2}. \tag{6.19}$$

For the stability of the amplitude death state, the real parts of the eigenvalues should be negative. Thus Eq. (6.18) gives the condition

$$\alpha + \mu_2 \epsilon_d < 0, \tag{6.20}$$

while from Eq. (6.19) we get the following conditions.
(1) If $(\kappa - \alpha)^2 < 4(\epsilon_e^2 - \alpha\kappa)$, $\lambda_{2,3}$ are complex and the condition of stability is

$$\kappa > \alpha. \tag{6.21}$$

(2) If $(\kappa - \alpha)^2 > 4(\epsilon_e^2 - \alpha\kappa)$, $\lambda_{2,3}$ are real and the stability condition becomes

$$\kappa > (\alpha) \quad \text{and} \quad \epsilon_e^2 > (\alpha\kappa). \tag{6.22}$$

Thus, if Eqs. (6.20) and (6.21) or (6.22) are simultaneously satisfied, the oscillations can not occur and the systems stabilize to a steady state of amplitude death.

For a given κ, α and μ_2, the transition to amplitude death occurs at critical coupling strengths ϵ_{dc} and ϵ_{ec} independent of each other. That is

$$\epsilon_{dc} = const \tag{6.23}$$

and

$$\epsilon_{ec} = const \tag{6.24}$$

For different network configurations μ_2 is different and the transition occurs at the critical coupling strength

$$\epsilon_{dc} = \frac{-\alpha}{\mu_2}. \tag{6.25}$$

In the case where G is asymmetric, using the approximation $f' \sim \alpha$ as explained above, we can write the Jacobian corresponding to Eqs. (6.13), (6.16) and (6.12) as

$$J = \begin{pmatrix} \alpha + \mu_2 \beta \epsilon_d & \epsilon_e z N \gamma q_\| & \epsilon_e N \gamma q_\| \\ 0 & \alpha + \mu_2 \epsilon_d & \epsilon_e N \\ 0 & -\epsilon_e/N & -\kappa \end{pmatrix},$$

and the eigenvalues are the same as given in Eq.(6.19). Thus, we get the same stability relations as in Eqs. (6.20), (6.21) and (6.22).

6.3   Numerical analysis

In this section, we apply our scheme to different network topologies, taking the Rössler system as a standard nodal dynamics.

6.3.1   Network of Rössler systems

First, we apply the scheme of coupling introduced in Eq. (6.1) to the case of regular networks of coupled chaotic Rössler systems. Here, we take the coupling to be of diffusive type [Eq. 6.2]. The occurrence of amplitude death in the case of regular all-to-all coupled network is illustrated in Fig. 6.1.

To characterize the state of amplitude death, we use an index A intro-

duced in Chapter 4. It is defined as the difference between the global maximum and global minimum values of the time series of the system over a sufficiently long interval. The value of A is found out for each system, and their average $<A>$ is calculated. The case where $<A> = 0$ represents the state of amplitude death, while $<A> \neq 0$ indicates oscillatory dynamics. The parameter value at which $<A>$ becomes ~ 0 is thus identified as the threshold for onset of stability of amplitude death states.

For a given network topology, the threshold value of coupling strengths for the onset of amplitude death is given by Eqs. (6.23) and (6.24). This is verified for the case of all-to-all coupled network of Rössler systems by direct numerical simulations. Using the index $<A>$ the regions of amplitude death states are identified in the parameter plane of coupling strengths, ϵ_e–ϵ_d, and is shown in Fig. 6.2. The transition curves from the stability analysis given in Eq. (6.23) and (6.24) are also plotted. We see that the agreement is good.

We also verify numerically the criteria for transition to amplitude death given in Eq. (6.22). For this, the numerically obtained values of ϵ_{ec}^2 are plotted against κ in Fig. 6.3. The line correspond to the stability condition Eq. (6.22) and the points are obtained from numerical simulations. As we can see from Fig. 6.3, the agreement is good for larger values of κ. However, for small values of κ, the points deviate from straight line behaviour. The reason is clear from Eq. (6.21) which gives the lower limit on κ.

The nature of the transitions to the state of amplitude death is further characterized by fixing one of the parameters ϵ_e or ϵ_d and increasing the other. In Fig. 6.4 $<A>$ of the coupled system given in Eq. 6.2 for increasing ϵ_e for a chosen value of ϵ_d. Here, the transition from oscillatory state to amplitude death state is continuous such that, as the coupling strength is increased, the amplitude of oscillations gradually decreases to zero. Numerically, we also observe that, at each node the sub-systems undergo a reverse period-doubling sequence to limit cycle before undergoing a transition to the amplitude death state, similar to the case of two coupled Rössler systems reported earlier in
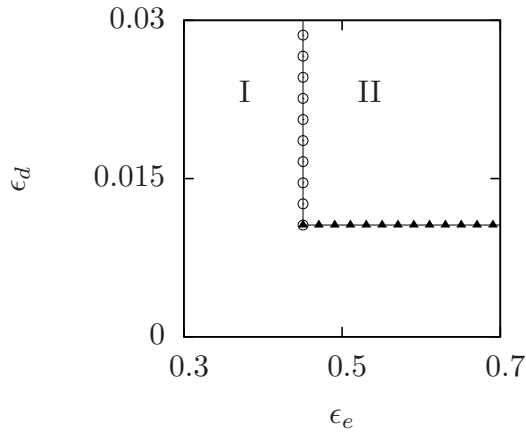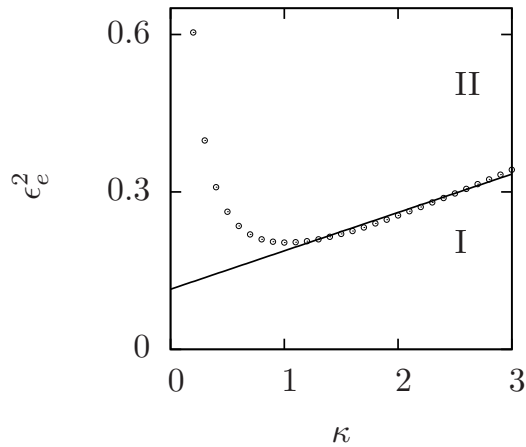
Figure 6.2: Transition from region of oscillations (I) to region of amplitude death (II) is shown in the parameter plane ϵ_e–ϵ_d for the coupled Rössler systems. Numerical simulations are done on a symmetric, all-to-all coupled network of 10 nodes. The points mark the parameter values $(\epsilon_{ec}, \epsilon_{dc})$ at which the transition to amplitude death occurs. Solid triangles show the transition to amplitude death as ϵ_d is increased for a constant ϵ_e. The horizontal line formed by these triangles confirms the stability condition Eq. (6.23). Similarly, circles correspond to transition to amplitude death state as ϵ_e is increased for a constant ϵ_d and confirm the stability condition of Eq. (6.24).

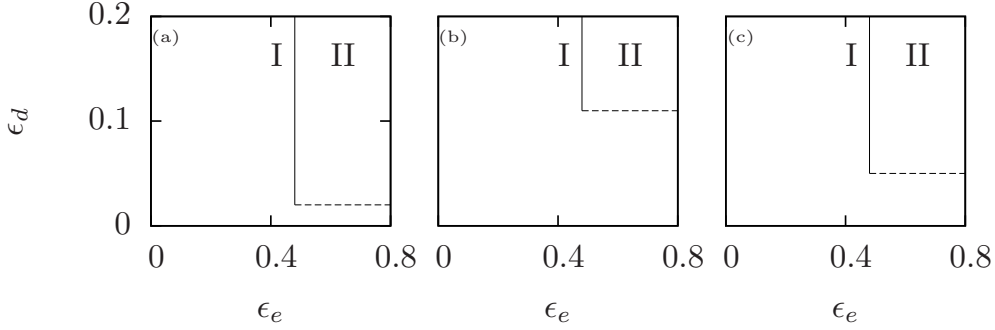
Figure 6.3: Transition from region of oscillations (I) to region of amplitude death (II) is shown in the parameter plane $\kappa - \epsilon_e^2$ for the coupled Rössler systems given in Eq. (6.2). Here, an all-to-all coupled network of 10 nodes is used. The points of amplitude death are obtained numerically when the index $<A>$ becomes zero. Solid curve is a linear fit corresponding to the stability condition Eq. (6.22). The deviation from straight line behaviour for small values of κ is discussed in the text.
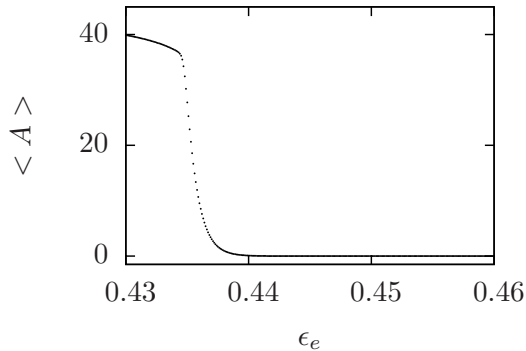
Figure 6.4: The index $< A >$ as a function of ϵ_e for a fixed value of $\epsilon_d = 0.4$ for an all-to-all coupled network of 10 Rössler systems. As ϵ_e is increased, we observe a continuous transition to the state of amplitude death ($\epsilon_{ec} \sim 0.45$).

chapter 4. Similar transition is observed for the case where ϵ_e is kept fixed and ϵ_d is increased.

So far, we have presented the results from numerical simulations of Eq. (6.2) in an all-to-all coupled network. We have repeated the study in other network configurations such as chain, ring, tree, lattice, star and random topologies. These different types of networks are illustrated in Fig. 6.5. In Fig. 6.6, we show the regions of amplitude death states in the parameter plane of coupling strengths, ϵ_e–ϵ_d for three networks of different topologies. We see that, the critical strength of coupling via environment ϵ_{ec} is independent of the network topology. On the other hand, the critical strength of direct coupling for amplitude death, ϵ_{dc} varies with the largest non-zero eigenvalue of the coupling matrix G, as given in Eq. (6.25).

To verify this, we consider symmetric and asymmetric matrices of different topologies and sizes. With each network considered, the largest non-zero eigenvalue, μ_2 of the corresponding coupling matrix G is calculated. The critical value of coupling, ϵ_{dc} is obtained from numerical simulations of Eq. (6.2) and is plotted against the corresponding μ_2 in Fig. 6.7. A universal relation between the critical coupling strength and largest non-zero eigenvalue of the coupling matrix, as given by Eq. (6.25) is clearly seen. A similar insensitivity of the transition to amplitude death, to the network structure is reported in

93
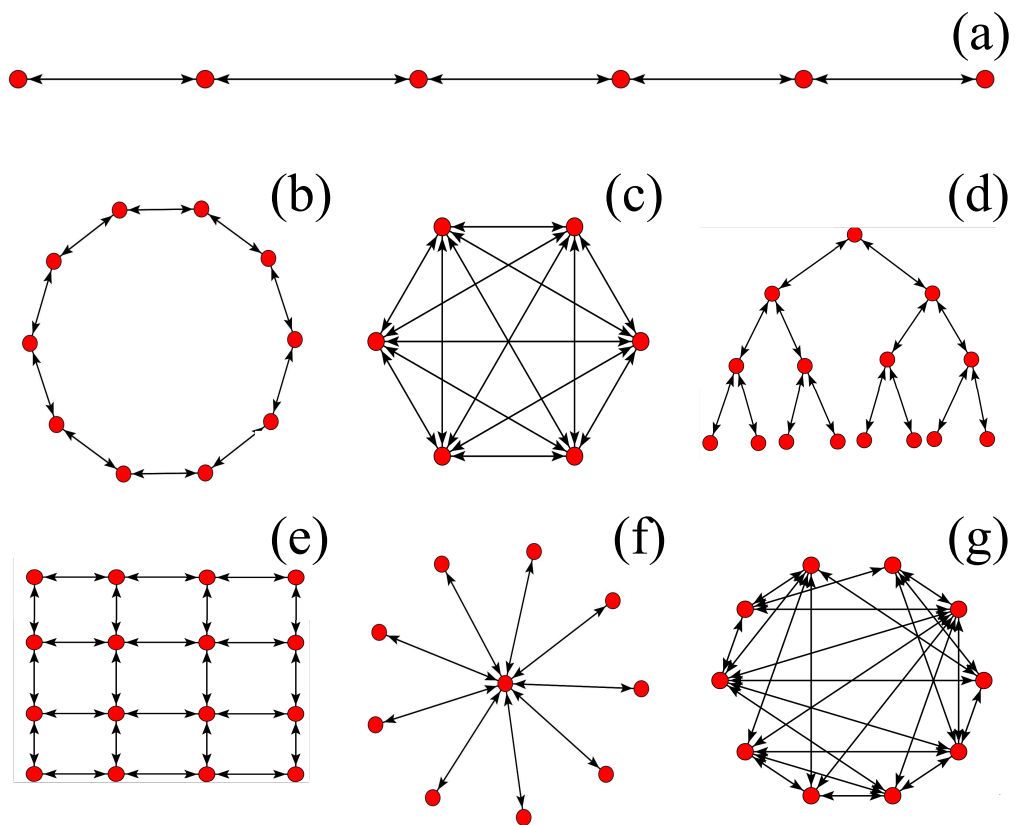
Figure 6.5: Schematic illustrations for some networks used in the study (a) a chain network ($N = 6$), (b) a ring network with nearest neighbour coupling ($N = 10$),(c) an all-to-all coupled network ($N = 6$), (d) a tree network ($N = 15$), (e) a lattice ($N = 16$), (f) a star network ($N = 10$), and (g) a random network ($N = 10$).

Figure 6.6: Transition from region of oscillations (I) to region of amplitude death (II) is shown in the parameter plane ϵ_e–ϵ_d for coupled Rössler systems in three different networks. (a) all-to-all coupled network of 6 nodes (Fig. 6.5(c)), (b) Star network of 10 nodes (Fig. 6.5(f)), and (c) Random network of 10 nodes (Fig. 6.5(g)). We note that, ϵ_{ec} is independent of the network topology while ϵ_{dc} varies from network to network.

the case of time-delay coupled Rössler systems in Ref. [196] where, the smallest eigenvalue of the adjacency matrix of the network is found to determine the size of the death island.

The study reported above have been carried out using networks of size up to 16 nodes. However we have repeated the study for random networks up to size $N = 100$ and amplitude death is found to occur in such large networks also.

6.3.2 Network of Landau-Stuart oscillators

We repeat the study with a network of Landau-Stuart oscillators, given by the following equations,

$$
\begin{aligned}
\dot{x}_{i1} &= (1 - x_{i1}^2 - x_{i2}^2)x_{i1} - 2x_{i2} + \epsilon_d \sum_j G_{ij} x_{j1} + \epsilon_e w, \\
\dot{x}_{i2} &= (1 - x_{i1}^2 - x_{i2}^2)x_{i2} + 2x_{i1}, \\
\dot{w} &= -\kappa w - \frac{\varepsilon_e}{N} \sum_i x_{i1}.
\end{aligned}
\tag{6.26}
$$
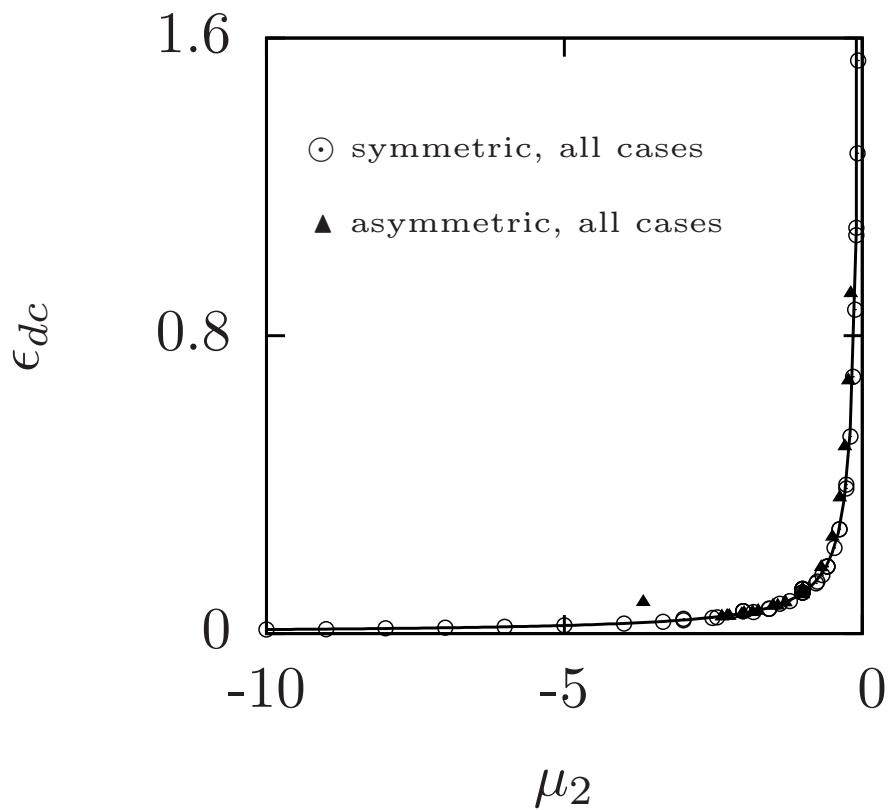
Figure 6.7: Critical strength of direct coupling ϵ_{dc} for amplitude death as a function of the largest non-zero eigenvalue of the coupling matrix, μ_2. Here points correspond to values obtained from numerical simulations, while the line correspond to the stability condition in Eq. (6.25). Open circles represent symmetric networks of different topologies such as chain, ring, all-to-all-coupled, tree, lattice, star and random. Similarly, filled triangles represent asymmetric networks of different topologies such as chain, ring, tree, star and random. For the asymmetric networks, μ_2 is, in general, complex. Hence, the real part of μ_2 is plotted here. The parameters of the Rössler system are the same as that used in Fig. 6.1. The parameters in the coupling terms are $\epsilon_e = 0.8$ and $\kappa = 1$.

96
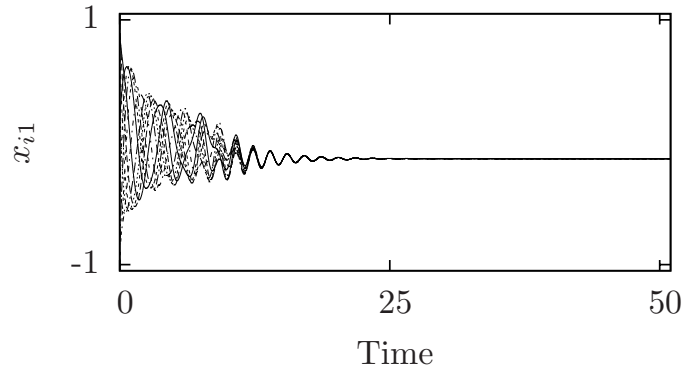
Figure 6.8: Time series of the variable x_{i1} of the 10 Landau-Stuart network in an all-to-all coupled network in amplitude death state $(\epsilon_d, \epsilon_e, \kappa) = (0.2, 3.5, 1)$.

For numerical simulations, we take an all-to-all coupled network of 10 nodes. We find that amplitude death is possible in this case also. This is illustrated in the time series shown in Fig. 6.8. The region of amplitude death in the parameter plane of coupling strengths, ϵ_e–ϵ_d, is identified using the index $< A >$ and is shown in Fig. 6.9.

We repeat the study with many networks of different topologies and sizes. We find that, the stability condition given by Eq. (6.25) is satisfied in this case as well. This is shown in Fig. 6.10.

6.4 Discussion

In this chapter, we have discussed the occurrence and characterization of amplitude death in complex network of nonlinear oscillators, caused by interactions with a common environment. We have developed a stability analysis to obtain the criteria for the onset of amplitude death. The transition curves obtained from the stability analysis matches well with those obtained from direct numerical simulations.

However, we note that exact agreement with stability theory as shown in Fig. 6.2 is seen only for Rössler type nodal dynamics. For a network of
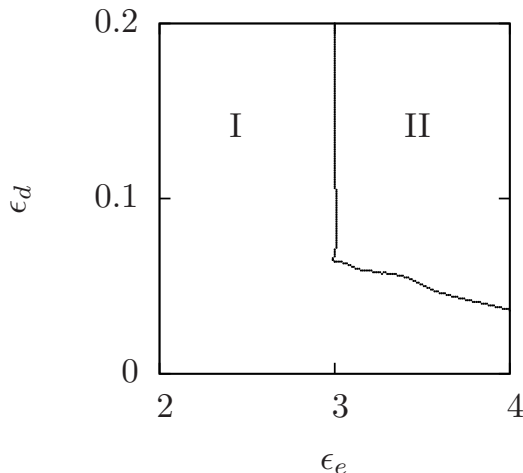
Figure 6.9: Transition from region of oscillations (I) to region of amplitude death (II) is shown in the parameter plane ϵ_e–ϵ_d for 10 coupled Landau systems on a symmetric, all-to-all coupled network [Eq. (6.26)]. The points mark the parameter values (ϵ_{ec},ϵ_{dc}) at which the transition to amplitude death occurs. Here, the intrinsic parameter of the systems and the damping parameter of the environment are chosen to be $\omega = 2$ and $\kappa = 1$ respectively. We use the same set of initial conditions for any pair of (ϵ_e,ϵ_d) values.

coupled Landau-Stuart oscillators, we observe some deviations between theoretical and numerical transition curves (Fig. 6.9). This can be explained as follows. Towards the end of the stability analysis, we have used an approximation of constant Jacobian f', which masks the system-specific details of the transition, but gives the overall features of the phase diagram. Hence the conditions Eqs. (6.23) and (6.24) are approximate and one must investigate in a specific case to see any departures from them.

For both Rössler and Landau-Stuart in the amplitude death state, the Jacobian f' depends on ϵ_e, but not on ϵ_d. Hence, the condition (6.24), i.e. $\epsilon_{ec} = const$, obtained from Eq. (6.22) which is derived from Eqs. (6.12) and (6.13), is independent of ϵ_d for both Rössler and Landau-Stuart as can be seen from Figs. 6.2 and 6.9.

The other condition Eq. (6.23), i.e. $\epsilon_{dc} = const$, is obtained from Eq. (6.20) which is derived from Eq. (6.14). Since Eq. (6.14) depends both on ϵ_d and
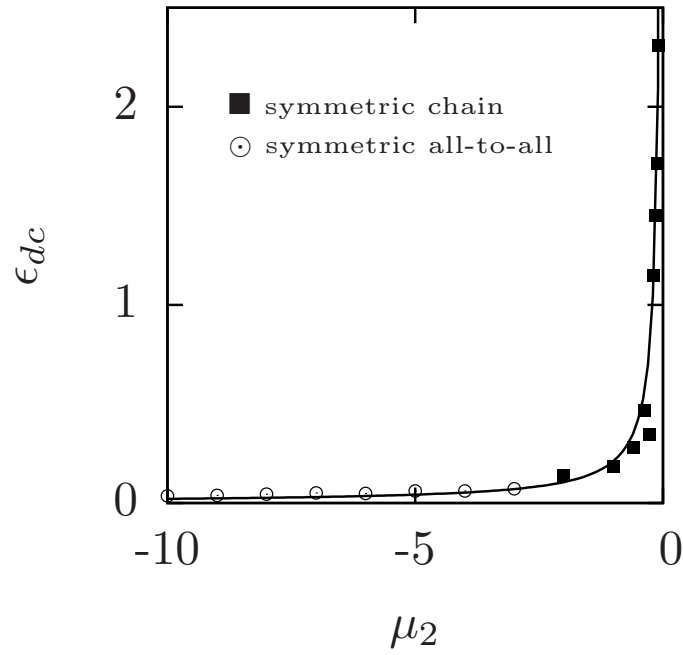
Figure 6.10: Critical strength of direct coupling ϵ_{dc} for amplitude death as a function of the largest non-zero eigenvalue of the coupling matrix, μ_2 for Landau-Stuart oscillators. Here points correspond to values obtained from numerical simulations, while the line correspond to the stability condition in Eq. (6.25). Open circles represent symmetric all-to-all coupled networks of different sizes and filled squares represent symmetric networks of chain topology of different sizes. The parameters in the coupling terms are $\epsilon_e = 4.0$ and $\kappa = 1$.

indirectly on ϵ_e through the Jacobian f', ϵ_{dc} will now depend on ϵ_e for both Rössler and Landau-Stuart. In the case of Rössler network, as explained earlier, the Jacobian has a simple structure and the dependence of ϵ_{dc} on ϵ_e is weak giving almost a straight line as in Fig. 6.2.

In the case of coupled Rössler systems, we note from numerical simulations that the amplitude death state correspond to the stable fixed point of Eq. (6.2), given by

$$
\begin{aligned}
x_{i1}^* &= (c - \sqrt{c^2 - 4ab\kappa/(\kappa - \epsilon_e^2 a)})/2, \\
x_{i2}^* &= -x_{i1}^*/a, \\
x_{i3}^* &= -b/(x_{i1}^* - c), \\
w^* &= -\epsilon_e x_{i1}^*/\kappa.
\end{aligned}
\tag{6.27}
$$

The Jacobian corresponding to Eq. (6.2) is given by

$$
J = \begin{pmatrix}
\mu\epsilon_d & -1 & -1 \\
1 & a & 0 \\
\frac{2b}{c+\sqrt{c^2-4ab\kappa/(\kappa-\epsilon_e^2 a)}} & 0 & -\frac{c+\sqrt{c^2-4ab\kappa/(\kappa-\epsilon_e^2 a)}}{2}
\end{pmatrix}.
$$

and the corresponding characteristic equation is

$$
\begin{aligned}
0 &= -\lambda^3 + (\mu\epsilon_d + a + x_1^* - c)\lambda^2 \\
&\quad + (-\mu\epsilon_d(a + x_1^* - c) - a(x_1^* - c) + x_3^* - 1)\lambda \\
&\quad + (\mu\epsilon_d a(x_1^* - c) + (x_1^* - c) - ax_3^*)
\end{aligned}
\tag{6.28}
$$

In the amplitude death state, the real parts of all the eigenvalues of this Jacobian are negative. Therefore, at the transition to amplitude death state ($\epsilon_e = \epsilon_{ec}$ and $\epsilon_d = \epsilon_{dc}$), the largest eigenvalue is pure imaginary, given by

$$
\lambda = i\beta.
\tag{6.29}
$$

Substituting Eq. (6.29) in Eq. (6.28) and equating both the real and imagi-

nary parts to separately we get

$$-\beta^3 = \beta(-\mu\epsilon_d(a + x_1^* - c) - a(x_1^* - c) + x_3^* - 1) \tag{6.30}$$

and

$$
\begin{aligned}
0 &= (\mu\epsilon_d + a + x_1^* - c)(-\mu\epsilon_d(a + x_1^* - c) - a(x_1^* - c) + x_3^* - 1) \\
&\quad + (\mu\epsilon_d a(x_1^* - c) + (x_1^* - c) - ax_3^*). \tag{6.31}
\end{aligned}
$$

Substituting the value of the fixed point from Eq. (6.27) and solving for ϵ_{dc} numerically, we see that the dependence of ϵ_{dc} on ϵ_e is weak, giving almost a straight line as in Fig. 6.2.

In the case of Landau-Stuart network, the amplitude death state corresponds to the fixed point of the coupled system Eq. (6.26), given by

$$x_{i1}^* = \pm \frac{\sqrt{1 + \frac{8}{\epsilon_e^2} - \epsilon_e^2 + \sqrt{-16 + \epsilon_e^4} - \frac{\sqrt{-16+\epsilon_e^4}}{\epsilon_e^2}}}{\sqrt{2}}$$

$$
\begin{aligned}
x_{i2}^* = \frac{1}{-2 + 2\epsilon_e^2}\Bigg(&\pm 2\sqrt{2}\sqrt{1 + \frac{8}{\epsilon_e^2} - \epsilon_e^2 + \sqrt{-16 + \epsilon_e^4} - \frac{\sqrt{-16 + \epsilon_e^4}}{\epsilon_e^2}} \\
&\pm \frac{\epsilon_e^2\sqrt{1 + \frac{8}{\epsilon_e^2} - \epsilon_e^2 + \sqrt{-16 + \epsilon_e^4} - \frac{\sqrt{-16+\epsilon_e^4}}{\epsilon_e^2}}}{\sqrt{2}} \\
&\mp \frac{\epsilon_e^4\sqrt{1 + \frac{8}{\epsilon_e^2} - \epsilon_e^2 + \sqrt{-16 + \epsilon_e^4} - \frac{\sqrt{-16+\epsilon_e^4}}{\epsilon_e^2}}}{\sqrt{2}} \\
&\mp \frac{\epsilon_e^2(1 + \frac{8}{\epsilon_e^2} - \epsilon_e^2 + \sqrt{-16 + \epsilon_e^4} - \frac{\sqrt{-16+\epsilon_e^4}}{\epsilon_e^2})^{3/2}}{2\sqrt{2}}\Bigg) \tag{6.32}
\end{aligned}
$$

and the Jacobian corresponding to Eq. 6.13 is given by

$$J = \begin{pmatrix} 1 - 3x_{i1}^{*2} - x_{i2}^{*2} + \mu\epsilon_d & -2x_{i1}^* x_{i2}^* - 2 \\ -2x_{i1}^* x_{i2}^* + 2 & 1 - x_{i1}^{*2} - 3x_{i2}^{*2} \end{pmatrix}.$$

Here also, we proceed to find the eigenvalues of this Jacobian and substitute

101

the value to be $\lambda = i\beta$, as in the case of coupled Rössler systems. We find that, the dependence of ϵ_{dc} on ϵ_e is a polynomial relation explaining the curve obtained for numerical simulations (Fig. 6.9).

In the context of Landau-Stuart oscillators, there is an additional complexity due to bistability, with oscillations and amplitude death co-existing with different basins. This bistability has been reported earlier in the case of amplitude death in Landau-Stuart oscillators [175, 215]. Such a bistability does not exist for Rössler systems. In Fig. 6.9, we have used the same set of initial conditions for any pair of (ϵ_e, ϵ_d) values. For a different set of initial conditions, the critical coupling curve in Fig. 6.9 can shift slightly though the general features will remain the same.

Thus,

1. We show that coupling via a dynamic environment induces amplitude death in a complex network of coupled nonlinear systems.

2. Our method involves a single damped dynamical system coupled to all nodes equally

3. The method introduced here works in complex networks of different topologies.

4. Using the master stability formalism, the threshold values of the coupling strengths for amplitude death are obtained for the general case.

5. A universal relation between the largest eigenvalue of the coupling matrix and the critical value of coupling is shown to exist, independent of the coupling topology.

Chapter 7

Effect of the environment on the dynamics of coupled neurons

7.1   Introduction

In chapter 3, we have described a simple coupling scheme to realize in-phase or antiphase synchronization in two chaotic systems. We have introduced a mechanism for inducing amplitude death in coupled synchronizable systems in chapter 4. Later, we have extended this mechanism for amplitude death to the case of a complex network of coupled oscillators. In all these cases, the emergent dynamics was brought about by the interactions with a common medium which had its dynamics modulated by the feedback from the systems. This type of coupling is very relevant in the case of biological systems where they interact through chemicals in the surrounding medium. In this chapter, we present the effects of indirect coupling via a dynamic environment on the dynamics of coupled neurons. In the context of neurons, the environment can be extracellular fields or charges or chemicals that can alter the synapses. The dynamics of a single neuron can be modeled by an excitable system of the

type introduced in chapter 1.

7.2 Coupled neurons

Here we consider the case where two uncoupled neurons are interacting with a common medium. We show that, both in-phase and antiphase synchronization are possible for suitable choice of parameters. In this context, we mention that most studies on synchronization of neurons include direct interaction between them [220–224]. There are studies where neurons are driven to synchronization by a common noisy background [148]. Here, we report how synchronization is possible by indirect interaction through a common shared environment or medium.

7.2.1 In-phase and antiphase synchronization due to indirect coupling via environment

We consider two neurons whose dynamics is represented by the Hindmarsh-Rose model [26]. They are coupled through a common medium as given by the following equations

$$
\begin{aligned}
\dot{x}_{i1} &= x_{i2} + ax_{i1}^2 - x_{i1}^3 - x_{i3} + I + \epsilon_1\beta_i w, \\
\dot{x}_{i2} &= 1 - bx_{i1}^2 - x_{i2}, \\
\dot{x}_{i3} &= -rx_{i3} + sr(x_{i1} + c), \\
\dot{w} &= -\kappa w - \frac{\epsilon_2}{2}\sum_{i=1,2}\beta_i x_{i1}.
\end{aligned}
\tag{7.1}
$$

Here, x_{i1}, x_{i2} and x_{i3} represents the variables of the Hindmarsh-Rose neuron model, w represent the environment, with κ as its damping parameter. We choose the intrinsic parameters a, I, b, ρ, s and χ of the neuron model such that the system is in chaotic bursting state. We find that, both in-phase and antiphase synchronization are possible for suitable values of ϵ_1, ϵ_2, β_1
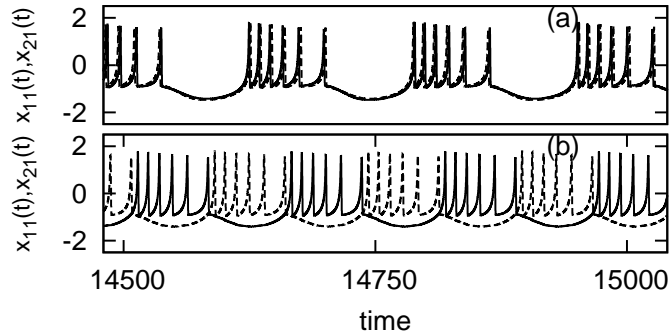
Figure 7.1: Time series of the first variable x_{i1} of two environmentally cou-
pled Hindmarsh Rose neurons showing synchronization of bursts (a) In-phase
synchronization ($\epsilon_1 = \epsilon_2 = 0.4$, $\beta_1 = -\beta_2 = 1$)(b) antiphase synchronization
($\epsilon_1 = \epsilon_2 = 0.4$, $\beta_1 = \beta_2 = 1$). Here, the parameters of the individual neuron are
$a = 3$,$b = 5$,$r = 0.005$,$s = 4$,$c = 1.6$,$I = 3.05$ such that their intrinsic dynamics is
chaotic. The synchronized state obtained is periodic in this case.

and β_2. When $\beta_1 = +1$ and $\beta_2 = -1$, we observe in-phase synchronization of
bursts, as shown in the time series in Fig. 7.1(a). When the coupling strength
is increased, we see that the spikes becomes synchronized, corresponding
to complete synchronization. When $\beta_1 = \beta_2 = +1$, we observe antiphase
synchronization of bursts, as shown in the time series in Fig. 7.1(b).

To identify states of in-phase and antiphase synchronization precisely, we
need to define the phase of the systems. Since the synchronization is with
respect to the bursts, the instantaneous phase is defined [225] as

$$\phi(t) = 2\pi \frac{t - \tau_k}{\tau_{k+1} - \tau_k}, \tag{7.2}$$

where, τ_k is the time of the kth burst. To find τ_k from the time series of the
variable x_{i1} is not easy. However, we find that, oscillations in the slow variable
x_{i3} corresponds to the bursts in x_{i1}, as shown in Fig. 7.2. Therefore, we take
τ_k to be the time the kth oscillation in x_{i3} begins, defined in simulations as
the time the variable x_{i3} crosses a chosen Poincaré plane. (Fig. 7.2). The
phase $\phi(t)$ and the phase difference $\psi(t)$ between the two Hindmarsh-Rose
systems coupled through environment are calculated using Eq. (7.2). The

105
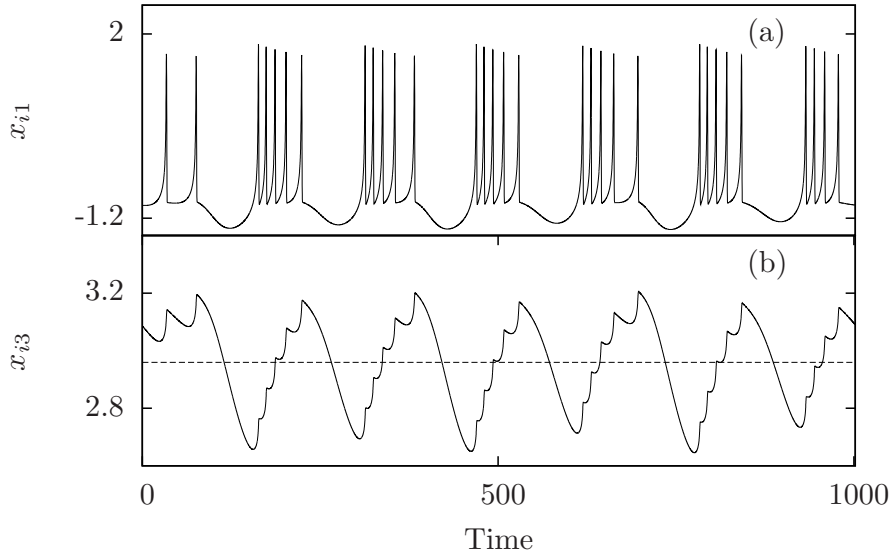
Figure 7.2: (a) Time series of the x_{i1} variable of the Hindmarsh-Rose system showing bursting behavior. (b) Time series of the slow variable, x_{i3}, of the Hindmarsh-Rose system showing oscillations corresponding to the bursts in x_{i1}. The dashed line represents a suitable Poincaré section.

mean phase difference over many cycles $< \psi(t) >$ is then calculated, for the the full parameter plane ϵ_1–ϵ_2 . The states with $< \psi(t) >\sim 0$ are identified as states of in-phase synchronization. Similarly, the states with $< \psi(t) >\sim \pi$ corresponds to antiphase synchronization of bursts. This is shown in Fig. 7.3. We see that, there are bands of synchronized and unsynchronized regions in the parameter plane of coupling strengths. Transitions between these bands follow the stability criterion given in Eq. 3.10, i.e. $\epsilon_{2c} \propto 1/\epsilon_{1c}$. The qualitative features of the burst changes as coupling strength ($\epsilon_1 = \epsilon_2 = \epsilon$) increases. Time series of the representative states from each band is shown in Fig. 7.4.
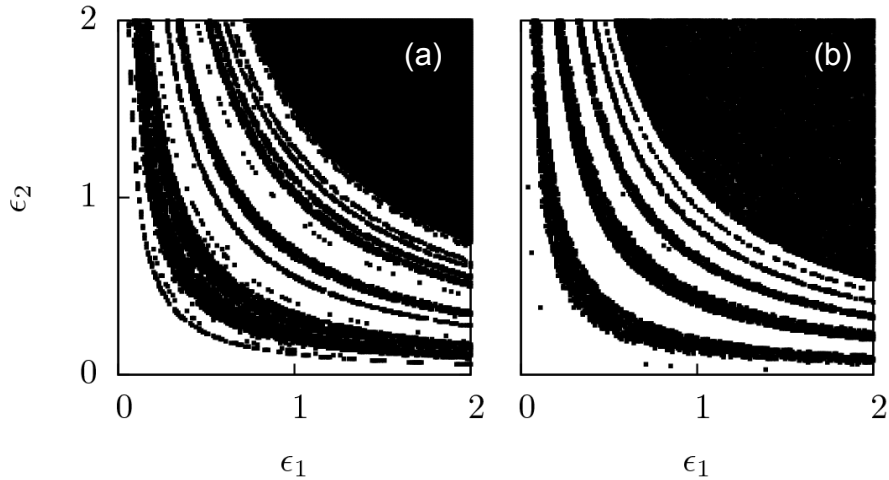
Figure 7.3: (a) Regions of in-phase synchronization in the parameter plane of coupling strengths ϵ_1–ϵ_2 in the case of two Hindmarsh-Rose neuron systems coupled via environment ($\beta_1 = -\beta_2 = 1$). Points mark the parameter values at which $< \psi(t) > \sim 0$. (b)Regions of antiphase synchronization in the parameter plane of coupling strengths ϵ_1–ϵ_2 in the case of two Hindmarsh-Rose neuron systems coupled via environment ($\beta_1 = \beta_2 = 1$). Points mark the parameter values at which $< \psi(t) > \sim \pi$.

7.2.2 Amplitude death via direct and indirect coupling in two neurons

Neurons make functional contact with other neurons or other cells of the muscles and glands through what are called synapses. Synapses can be electrical or chemical. The coupling due to electrical interactions is linear and depends on the difference between the membrane potentials. In the synaptic case, the coupling is pulsative and is modeled as a static sigmoid input-output function with a threshold and saturation [226].

Here, we consider how an environment can affect the dynamics of the neurons which are also coupled directly by electrical or chemical connections.
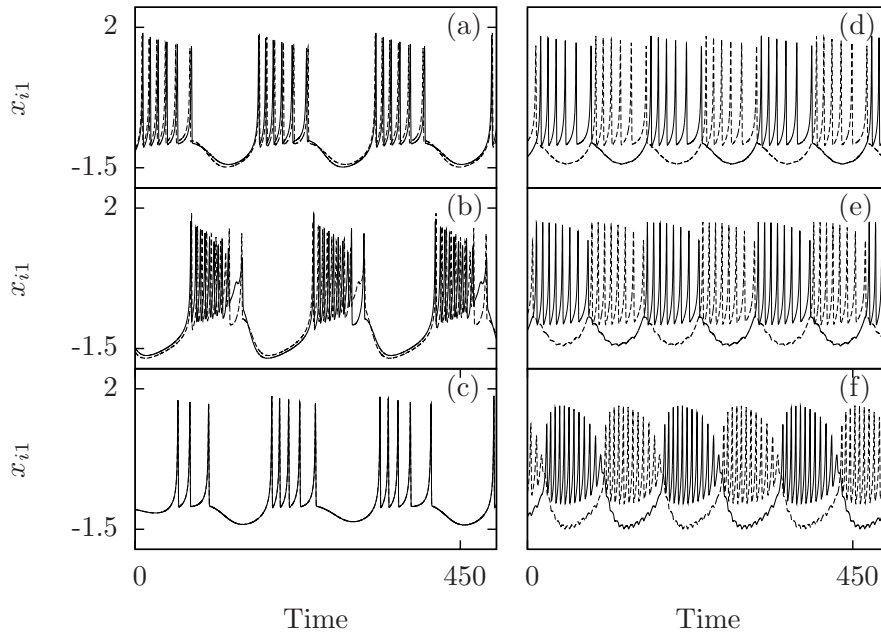
Figure 7.4:   Time series of the x_{i1} variable of the two coupled Hindmarsh-Rose systems showing in-phase (a–c) and antiphase (d–f) synchronization. (a) In-phase synchronization of bursts for $\epsilon_1 = \epsilon_2 = 0.5$ and $\beta_1 = -\beta_2 = 1$, (b) in-phase synchronization of bursts for $\epsilon_1 = \epsilon_2 = 1.0$ and $\beta_1 = -\beta_2 = 1$, (c) in-phase synchronization of bursts for $\epsilon_1 = \epsilon_2 = 1.5$ and $\beta_1 = -\beta_2 = 1$, (d) antiphase synchronization of bursts for $\epsilon_1 = \epsilon_2 = 0.4$ and $\beta_1 = \beta_2 = 1$, (e) antiphase synchronization of bursts for $\epsilon_1 = \epsilon_2 = 0.8$ and $\beta_1 = \beta_2 = 1$, and (f) antiphase synchronization of bursts for $\epsilon_1 = \epsilon_2 = 1.2$ and $\beta_1 = \beta_2 = 1$.

Gap-junction or electrical coupling

Neurons in many parts of the nervous system as well as in certain cells of the heart and pancreas interact by gap junctions. Electrical synapses via gap-junctions are bidirectional and is suitable for high speed transfer of signals. They are thus used mostly for defensive reflexes [227, 228].

We now consider the dynamics of two Hindmarsh-Rose systems coupled mutually with two types of couplings, namely a direct diffusive coupling and an indirect coupling through an environment, given by the following equations.

$$
\begin{aligned}
\dot{x}_{i1} &= x_{i2} - x_{i1}^3 + ax_{i1}^2 - x_{i3} + I + \epsilon_e w + \epsilon_g(x_{j1} - x_{i1}) \\
\dot{x}_{i2} &= 1 - bx_{i1}^2 - x_{i2} \\
\dot{x}_{i3} &= \rho(s(x_{i1} + \chi) - x_{i3}) \\
\dot{w} &= -\kappa w - \frac{\epsilon_e}{2} \sum_i x_{i1}
\end{aligned}
\tag{7.3}
$$

Here, ϵ_g is the strength of the gap-junction coupling. This type of coupling via gap-junction is reported to synchronize the neurons [223, 229]. We take the strength of the coupling via environment to be $\epsilon_1 = \epsilon_2 = \epsilon_e$. We see that, when both ϵ_e and ϵ_g are sufficiently large, the systems stabilize to a state of amplitude death. This is illustrated in the time series given in Fig. 7.5.

To identify states of amplitude death, we use the index $< A >$ defined earlier in chapter 4. The case where $< A > \sim 0$ indicates states of amplitude death, while $< A > \neq 0$ indicates oscillatory dynamics. The regions of amplitude death in the parameter plane of coupling strengths, $\epsilon_e - \epsilon_g$ is shown in Fig. 7.6. Further, we study the nature of the transition to amplitude death state. In Fig. 7.7, the average value of the index $< A >$ is plotted as one of the coupling strengths is increased, while keeping the other fixed. In Fig. 7.7(a) we see that, as the coupling strength, ϵ_e, is increased keeping ϵ_g fixed, the index $< A >$ gradually decreases and becomes zero at the amplitude death state. Thus, the transition is continuous. Similar transition is
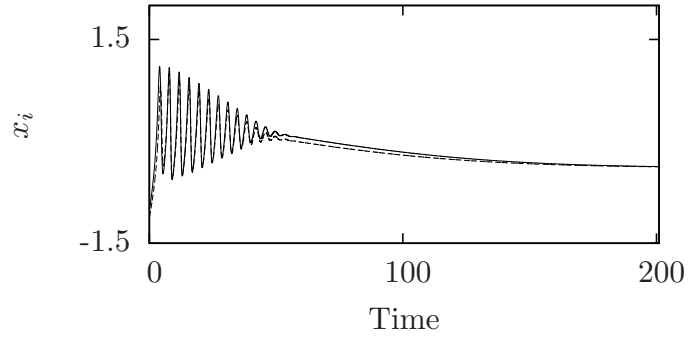
Figure 7.5: Time series of the first variable x_{i1} of the two coupled Hindmarsh-Rose systems showing amplitude death for $(\epsilon_g, \epsilon_e, \kappa) = (1.0, 1.5, 1.0)$. Here, the parameters of the individual neuron are taken to be $a = 3$, $b = 5$, $r = 0.006$, $s = 4$, $c = 1.6$, $I = 3.2$.
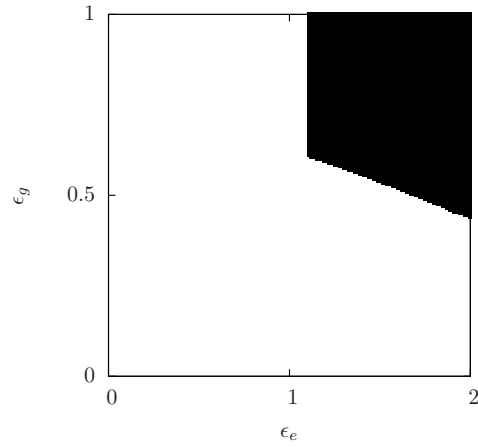
Figure 7.6: Regions of amplitude death in the parameter plane of coupling strengths ϵ_e–ϵ_g for the coupled Hindmarsh-Rose neurons (Eq. 7.3).
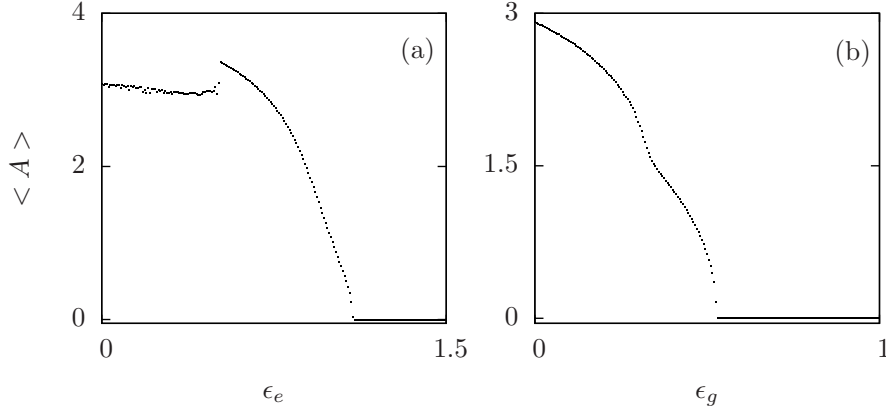
Figure 7.7: (a) The index $< A >$ plotted as a function of ϵ_e for a fixed value of $\epsilon_g = 1.0$ for two coupled Hindmarsh-Rose systems (Eq. 7.4). (b) The index $< A >$ plotted as a function of ϵ_g for a fixed value of $\epsilon_e = 1.5$. As ϵ_e or ϵ_g is increased, we observe a continuous transition to the state of amplitude death.

seen in Fig. 7.7(b), where ϵ_e is kept fixed and ϵ_g is increased.

Synaptic coupling

Chemical synapses are the primary means of signal transmission between neurons. It is known that activity driven modification in synaptic connections accounts for development and learning [230, 231]. So also, disruptions to the synaptic connections can lead to neuronal dysfunctions and neuronal disorders [232, 233].

Here, we consider two neurons with excitatory synaptic coupling between them and introduce an indirect coupling as given by the following equations

$$
\begin{aligned}
\dot{x}_{i1} &= x_{i2} - x_{i1}^3 + ax_{i1}^2 - x_{i3} + I + \\
&\quad \epsilon_e w + \epsilon_s \frac{V_r - x_{i1}}{1 + \exp(-\lambda(x_{j1} - \theta))}, \\
\dot{x}_{i2} &= 1 - bx_{i1}^2 - x_{i2}, \\
\dot{x}_{i3} &= \rho(s(x_{i1} + \chi) - x_{i3}), \\
\dot{w} &= -\kappa w - \frac{\epsilon_e}{2} \sum_i x_{i1}.
\end{aligned}
\tag{7.4}
$$

111
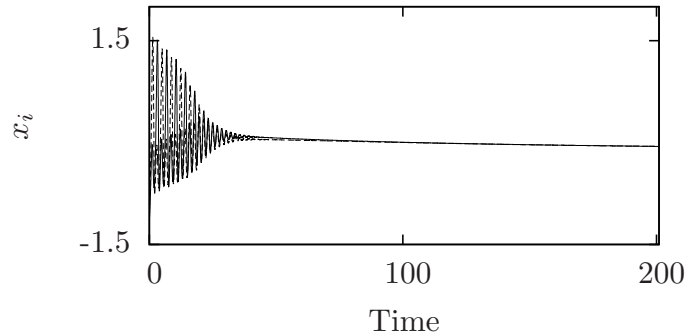
Figure 7.8: Time series of the variable x_{i1} of two Hindmarsh-Rose systems given in Eq. 7.4 showing amplitude death for the coupling strengths $(\epsilon_s, \epsilon_e) = (0.2, 3.5)$. Here, the parameters of the intrinsic system are the same as that in Fig. 7.5. The parameters in the coupling terms are chosen to be $V_r = 3$, $\theta = -0.25$, $\lambda = 10$ and $\kappa = 1$.

Here, the direct coupling is of synaptic type, given by the sigmoidal term in the first equation. The parameters of the synaptic coupling term are chosen such that, the synapse is excitatory [224]. The strength of synaptic coupling is given by ϵ_s. When $\epsilon_e = 0$, and ϵ_s is sufficiently large, the bursts of both neurons become synchronized. For larger values of ϵ_s and ϵ_e, we observe amplitude death. This is illustrated in the time series in Fig. 7.8. The region of amplitude death in the parameter plane of coupling strengths is shown in Fig. 7.9. As we keep one of the coupling parameters fixed (ϵ_e or ϵ_s), and increase the other, we observe transition to amplitude death state and again re-entrant behavior to spikes.

7.3   Neuronal networks

Gap-junction coupling

We consider the dynamics of N Hindmarsh-Rose neuron models $x_i, i = 1, 2, \ldots, N$, in a network, coupled with two types of couplings, namely a coupling via gap junction and an indirect coupling via an environment. The
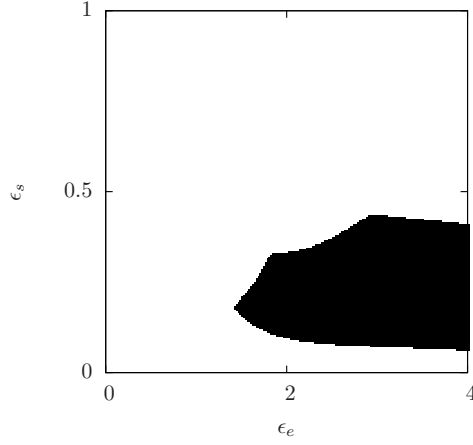
Figure 7.9: Region of amplitude death (black) in the parameter plane of coupling strengths ϵ_e–ϵ_s for two coupled Hindmarsh-Rose neurons.

dynamics of such a model is given by

$$
\begin{aligned}
\dot{x}_{i1} &= x_{i2} - x_{i1}^3 + ax_{i1}^2 - x_{i3} + I \\
&\quad + \sum_j G_{ij}\epsilon_g x_{j1} + \epsilon_e w \\
\dot{x}_{i2} &= 1 - bx_{i1}^2 - x_{i2} \\
\dot{x}_{i3} &= \rho(s(x_{i1} + \chi) - x_{i3}) \\
\dot{w} &= -\kappa w - \frac{\epsilon_e}{N}\sum_i x_{i1}.
\end{aligned}
\tag{7.5}
$$

The neurons are coupled among themselves via gap junction coupling, with coupling constant ϵ_g. The $N \times N$ coupling matrix G decides the coupling among the neurons. The elements of G are chosen in a way so that the row-sum, $\sum_j G_{ij} = 0$, for every j, and thus the largest eigenvalue of the coupling matrix μ_1, is zero. The variable w represents the environment, whose intrinsic dynamics is that of a one-dimensional over-damped oscillator with damping parameter κ.The strength of this feedback coupling between the systems and the environment is given by ϵ_e.

First, we choose G to be an all-to-all connected network of 10 nodes, that is, $G_{ij} = 1$, if $j \neq i$ and $G_{ii} = -9$. The occurrence of amplitude death in this case is illustrated the time series in Fig. 7.10. The average of index A

113
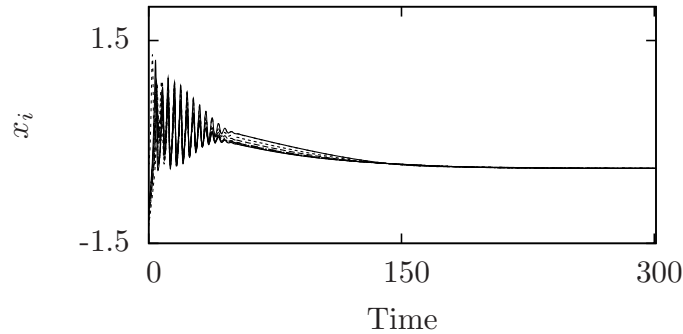
Figure 7.10: The time series of the x variable of all the 10 HR neurons in an all-to-all network given in Eq. 7.5 showing amplitude death at coupling strength $(\epsilon_g, \epsilon_e) = (1.0, 1.5)$. Other parameters are the same as in Fig. 7.5.

is calculated for the full parameter plane $\epsilon_e - \epsilon_g$ and the points where the index $<A>$ becomes nearly zero are shown in black in Fig. 7.11.

We observe that the nature of the transition to the state of amplitude death in continuous, similar to the case of 2-coupled Hindmarsh-Rose systems discussed earlier. We also notice from the time series and phase space plot that as the coupling strength (ϵ_d or ϵ_e) increases, the coupled Hindmarsh-Rose systems undergo many transitions from bursting state to oscillatory dynamics before going to the AD state. From the time series, we observe that, when $\epsilon_e \sim 0$, the systems are in chaotic bursting state. As ϵ_e is increased, the systems go to a periodic bursting state and then to a limit cycle state. As ϵ_e is increased from this state, amplitude of this limit cycle decreases gradually. When ϵ_e is increased above a threshold value, the systems reach the state of amplitude death. Similarly, for a fixed value of ϵ_e, when ϵ_g is increased from zero, the systems go from chaotic bursting state to periodic bursting state to limit cycle state before reaching amplitude death when $\epsilon_g > \epsilon_{gc}$.

So far, we have presented the results from numerical simulations of Eq. (7.5). Now, we consider many networks of various topologies and sizes. From numerical simulations with networks of different topology, we see that the critical strength of coupling via environment,ϵ_{ec}, remains constant while the critical strength of coupling via gap-junction,ϵ_{gc}, varies. For each network topology considered, we calculate the eigenvalues of the corresponding cou-
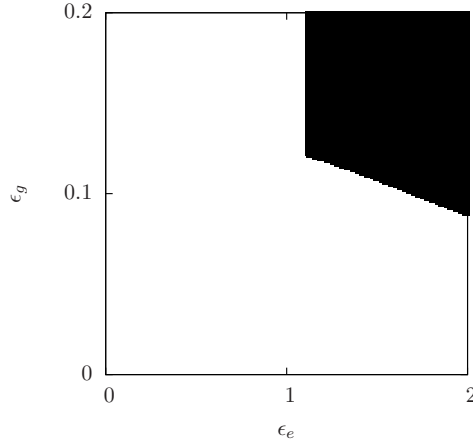
Figure 7.11: Regions of amplitude death in the parameter plane of coupling strengths, ϵ_e–ϵ_g, for the coupled Hindmarsh-Rose systems. Numerical simulations are done on a symmetric, random network of 10 nodes. If we change the network topology, then the curve representing transition to amplitude death as ϵ_g increases, is found to change.

pling matrix G. From numerical simulations of Eq. 7.5 on these networks, we obtain ϵ_{gc}. In Fig. 7.12, this is plotted against the largest non-zero eigenvalue μ_2 of the corresponding coupling matrix.

Synaptic coupling

We now extend the work to a network of synaptically coupled neurons given by the following equations.

$$
\begin{aligned}
\dot{x}_{i1} &= x_{i2} - x_{i1}^3 + ax_{i1}^2 - x_{i3} + I + \\
&\quad \epsilon_e w + \epsilon_s \sum_j G_{ij} \frac{V_r - x_{i1}}{1 + \exp(-\lambda(x_{j1} - \theta))}, \\
\dot{x}_{i2} &= 1 - bx_{i1}^2 - x_{i2}, \\
\dot{x}_{i3} &= \rho\big(s(x_{i1} + \chi) - x_{i3}\big), \\
\dot{w} &= -\kappa w - \frac{\epsilon_e}{2} \sum_i x_{i1}.
\end{aligned}
\tag{7.6}
$$
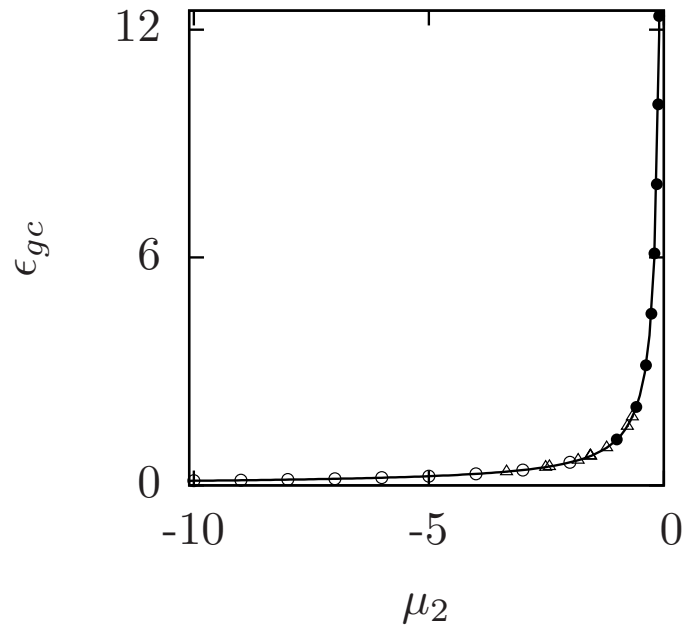
Figure 7.12: Critical strength of coupling via gap junction for amplitude death as a function of the largest non-zero eigenvalue of the coupling matrix, μ_2. Here, points are obtained from numerical simulations and the line correspond to a numerical fit to Eq. 6.25 with $\alpha \sim 1.2$. Open circles correspond all-to-all networks of different sizes ($N = 2$–10), filled circles correspond to chain of different sizes ($N = 3$–10) and open triangles correspond to random networks of 10 nodes. The parameters of the individual systems are the same as given in Fig. 7.5. The parameters in the coupling terms are $\kappa = 1$ and $\epsilon_e = \epsilon_{ec} = 1.105$.
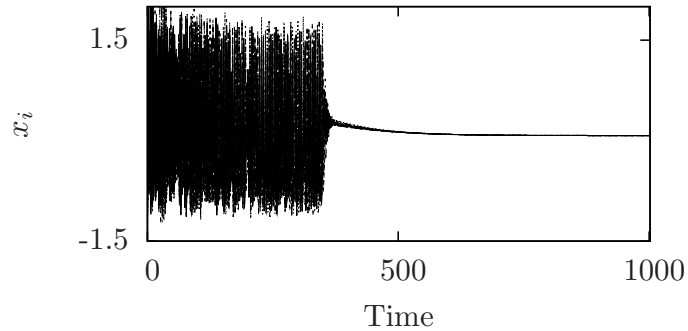
Figure 7.13: The time series of the x_1 variable of all the 10 Hindmarsh-Rose neurons given in Eq. 7.6 showing amplitude death $(\epsilon_s, \epsilon_e, \kappa) = (1.0, 2.0, 1.0)$.

From numerical analysis of the above equations, we see that, the systems can be taken to a state of amplitude death for suitable values of coupling strengths. The amplitude death state in this case is illustrated in Fig. 7.13. In Fig. 7.14, we show the regions of amplitude death in the parameter plane of coupling strengths, ϵ_d–ϵ_e. Black patches in Fig. 7.14 corresponds to regions of amplitude death. White region includes synchronized bursts, desynchronized states and sub-threshold oscillations.

The range of values of the three parameters ϵ_e, ϵ_s and κ for which amplitude death can occur is analysed by studying the bifurcation diagram in which around fifty maxima in the voltage of the ith neuron, obtained by keeping two of these parameters fixed and varying the third, are plotted in Fig. 7.15. We note that, by tuning the decay parameter of the environment or the coupling strengths, the suppression of neuronal activity or amplitude death can be prevented.

7.3.1 Neuronal network with alternative models

So far, we have presented the results of numerical simulations of Hindmarsh-Rose model neurons. We find that this method of inducing amplitude death works in other models of neurons as well. In this section, we apply our model to two other neuron models, namely, Hodgkin-Huxley [24] model and

117
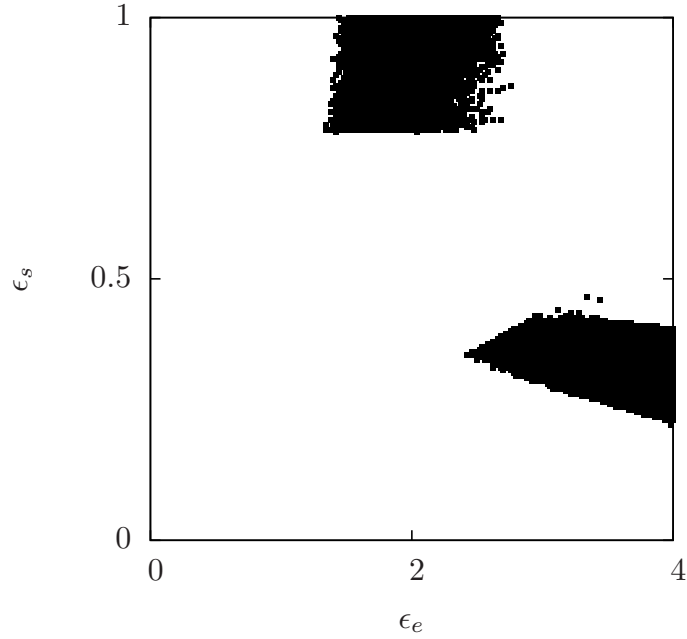
Figure 7.14: Regions of amplitude death in the parameter plane ϵ_e–ϵ_s for a network of synaptically coupled Hindmarsh-Rose systems.

FitzHugh-Nagumo [25] model.

We now consider a network of 10 Hodgkin-Huxley neurons interacting with a dynamic environment as given by the following equations

$$
\begin{aligned}
\dot{v}_i &= \frac{g_K n^4 (V_K - v_i) + g_{Na} m^3 h (V_{Na} - v_i) + g_L (V_L - v_i) + I}{C_m} \\
&\quad + \epsilon_e w + \frac{\epsilon_s}{n_i} \sum_j A_{ij} \frac{V_r - v_i}{1 + \exp(-\lambda(v_j - \theta))} \\
\dot{n}_i &= \alpha_n(v_i)(1 - n_i) - \beta_n(v_i) n_i \\
\dot{m}_i &= \alpha_m(v_i)(1 - m_i) - \beta_m(v_i) m_i \\
\dot{n}_i &= \alpha_h(v_i)(1 - h_i) - \beta_h(v_i) h_i \\
\dot{w} &= -\kappa w - \frac{\epsilon_e}{n} \sum_j v_j
\end{aligned}
$$

(7.7)
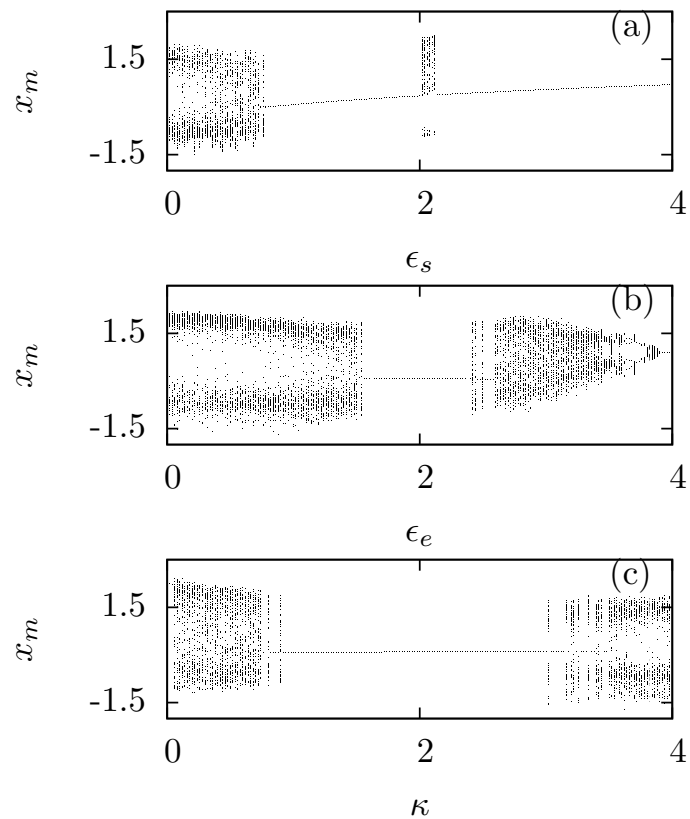
Figure 7.15: Bifurcation diagram obtained by plotting the maxima of x_i for sufficiently long time. Here two of the three coupling parameters (κ, ϵ_e, ϵ_s) are kept constant at a chosen value, and the other parameter is increased in steps of 0.02. (a) increasing ϵ_s for $(\epsilon_e, \kappa) = (2, 1)$ (b) increasing ϵ_e for $(\epsilon_s, \kappa) = (1, 1)$ (c) increasing κ for $(\epsilon_e, \epsilon_s) = (2, 1)$. We see that quiescent states (amplitude death) occurs only for suitable combinations of the parameters.
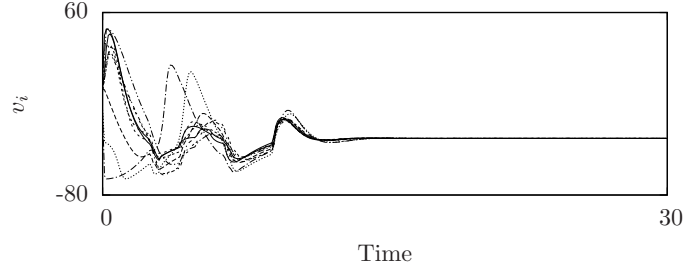
Figure 7.16: Time series of the voltage of 10 Hodgkin-Huxley neurons in a network showing amplitude death for $(\kappa, \epsilon_e, \epsilon_S) = (1,2,1)$.

where,

$$
\begin{aligned}
\alpha_n(v) &= \frac{0.01(v + 55)}{1 - \exp(\frac{-(v+55)}{10})} \\
\beta_n(v) &= 0.125 \exp(\frac{-(v + 65)}{80}) \\
\alpha_m(v) &= \frac{0.1(v + 40)}{1 - \exp(\frac{-(v+40)}{10})} \\
\beta_m(v) &= 4 \exp(\frac{-(v + 65)}{18}) \\
\alpha_h(v) &= 0.07 \exp(\frac{-(v + 65)}{20}) \\
\beta_h(v) &= \frac{1}{1 + \exp(\frac{-(v+35)}{10})}
\end{aligned}
$$

(7.8)

We choose the intrinsic parameters of the systems to be $I = 10$, $C_m = 1$, $V_{Na} = 50$, $V_K = -77$, $V_L = -54.4$, $g_{Na} = 120$, $g_K = 36$ and $g_L = 0.3$ such that the neurons are in spiking state. The parameters in synaptic coupling term are chosen to be $V_r = 40$, $\lambda = 10$ and $\theta = -40$. Amplitude death is observed for suitable values of the coupling constants. This state is shown in Fig. 7.16.

120
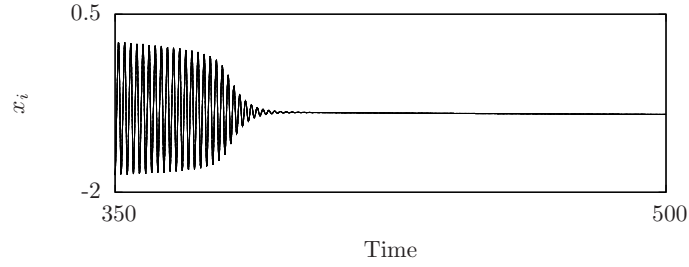
Figure 7.17: Time series of the x_i variable of 10 coupled FitzHugh-Nagumo neurons in a network showing amplitude death for $(\kappa, \epsilon_e, \epsilon_s) = (1, 4, 0.5)$.

Network of FitzHugh-Nagumo neurons

We repeat the study with a network of FitzHugh-Nagumo neurons as given by the following equations

$$
\begin{aligned}
\dot{x}_i &= x_i - \frac{x_i^3}{3} - y_i \\
&\quad + \epsilon_e w + \frac{\epsilon_s}{n_i} \sum_j A_{ij} \frac{V_r - x_i}{1 + \exp(-\lambda(x_j - \theta))} \\
\dot{y}_i &= \mu(x_i + a) \\
\dot{w} &= -\kappa w - \frac{\epsilon_e}{n} \sum_j x_j
\end{aligned}
$$

(7.9)

We simulate the above equations choosing the intrinsic parameters of the systems to be $a = 0.95$, $\mu = 0.08$. We find that amplitude death is possible in this case as well. This is shown in the time series in Fig. 7.17.

7.4   Summary

In this chapter, we have reported the application of the method introduced in the earlier chapters to the specific context of coupled neurons and neuronal networks.

121

1. We have shown that, the indirect interactions via a common medium can take two uncoupled neurons to in-phase or antiphase synchronized states.

2. This indirect interaction, when present with a direct interaction between the neurons is effective in inducing amplitude death in the systems.

3. By considering networks of neurons with different models, we show that, the dynamics of the network will be suppressed due to its interaction with a common environment or medium.

4. Also, this suppression of activity can be controlled by tuning the parameters of the environment.

The interaction with a dynamic environment is particularly relevant in the context of neurons since extracellular fields, charges or chemicals can alter the synapses. As shown here, the disruption of collective activity can lead to pathological cases like Alzheimer's disease where, the dynamic environment mimics interactions of neurons through proteins such as amyloid beta in the surrounding medium.

Chapter 8

Conclusions

This thesis is a study on the effects of a dynamic environment in controlling, monitoring and influencing the dynamics of systems. We study this in the context of two uncoupled chaotic systems interacting only through a dynamic environment and suppression of dynamics in coupled systems when they are influenced by a common environment. We extend this to complex networks and show how the environment can drive the network to a state of amplitude death. This is applied to a network of neurons with gap-junction and synaptic coupling.

The novel features of the research reported in this thesis are

1. The decisive role played by the environment in the dynamics of connected systems is brought out and the resultant emergent phenomena studied for a variety of dynamics and interactions.

2. General stability analysis is developed in all cases, whose results are supported by detailed and direct numerical simulations.

3. In the context of complex networks, the stability analysis developed leads to a universal relation independent of network topology, connecting the eigenvalue of the coupling matrix and the critical value of direct coupling. This is verified by direct numerical simulations also.

4. We propose that the method of inducing amplitude death introduced here is a very general mechanism that is easy to implement to obtain desirable steady states in many contexts.

5. We find that the role of the environment is especially relevant in the context of neuronal networks where disruption of collective activity can lead to pathological cases. Therefore, studies in this direction can contribute to a comprehensive understanding of such cases and possible prevention of undesirable effects.

We note that the work presented in this thesis has opened scope for further research in various directions. Some of them are

1. In the work presented here, the environment is modeled by a single shared variable. It will be more realistic to consider non-local effects and heterogeneity in the environment.

2. Different types of dynamics like discrete systems and the corresponding environmental effects will be interesting for further study for understanding diverse phenomena.

3. The investigations if further extended can help in understanding clinical problems related to Alzheimer's disease or other neurological disorders. In this context, possibility of experimental measurements to establish the interaction of neuron with amyloid beta is being investigated.

4. The ideas presented in this thesis can find applications in engineering, one such case being the possibility of synchronizing large number of electronic systems or power systems through electromagnetic interference mediated interactions.

Bibliography

[1] K. M. Cuomo and A. V. Oppenheim, Phys. Rev. Lett. **71**, 65 (1993).

[2] K. Murali. and M. Lakshmanan, Phys. Rev. E **48**, R1624 (1993).

[3] E. Klein, R. Mislovaty, I. Kanter and W. Kinzel, Phy.Rev. E **72**, 016214 (2005).

[4] R. He and P. G. Vaidya, Phy. Rev. E **57**, 1532 (1998).

[5] S. Sinha and W.L. Ditto, Phys. Rev. E **60**, 363 (1999).

[6] S. Sinha, T. Munakata, and W.L. Ditto, Phys. Rev. E **65**, 036216 (2002).

[7] R. Zhang, H.L.D. de S.Cavalcante, Z. Gao, D.J. Gauthier, J.E.S. Socolar, M.M. Adams, and D.P. Lathrop, Phys. Rev. E **80**, 045202 (2009).

[8] K. Murali, A. Miliotis, W.L. Ditto, S. Sinha, Phys. Lett. A **373**, 1346 (2009).

[9] K. Murali, S. Sinha, and W.L. Ditto, Phys. Rev. E **68**, 016205 (2003).

[10] L. Gammaitoni, P. Hänggi, P. Jung, and F. Marchesoni, Rev. Mod. Phys. **70**, 223 (1998).

[11] M. Soljačić, M. Ibanescu, S.G. Johnson, Y. Fink, and J.D. Joannopoulos, Phys. Rev. E **66**, 055601 (2002).

[12] C. Wargitsch and A. Hübler, Phys. Rev. E **51**, 1508 (1995).

[13] R. C. Hilborn, *Chaos and Nonlinear Dynamics* , (Oxford University Press, New York, 1994).

[14] M. Lakshmanan and S. Rajasekar, *Nonlinear Dynamics: Integrability, Chaos and Patterns*, (Springer, New York, 2003).

[15] S. H. Strogatz, *Nonlinear dynamics and chaos: with applications to physics, biology, chemistry, and engineering*, (Westview Press, 1994) .

[16] E. N. Lorenz, J. Atmos. Sci. **20** 130 (1963).

[17] A. Wolf, J. B. Swift, H. L. Swinney, and J. A. Vastano, Physica D **16**, 285 (1985).

[18] O. E. Rössler, Phys. Lett. **57A**, 397 (1976).

[19] H. Haken, Physics Letters A, **53**, 77 (1975).

[20] E. Knobloch, Physics Letters A,**82**, 439 (1981).

[21] S. Novak, and R.G. Frehlich, Phys. Rev. A, **26**, 3660 (1982).

[22] O. E. Rössler, Phys. Lett. A **71**, 155 (1979).

[23] M.C. Mackey, and L. Glass, Science **197**, 287 (1977).

[24] A.L. Hodgkin, A.F. Huxley, J. Physiol. **117**, 500 (1952).

[25] R. FitzHugh, Biophys J. **1**, 445 (1961).

[26] J.L. Hindmarsh and R.M. Rose, Proc. R. Soc. London, Ser. B **221**, 87 (1984) .

[27] M. Storace, D. Linaro, and E. de Lange, Chaos 18, 033128 (2008).

[28] G. Innocenti, A. Morelli, R. Genesio, and A. Torcini, Chaos **17**, 043128 (2007).

[29] J. M. González-Miranda, Chaos **13**, 845 (2003).

[30] X.J. Wang, Physica D **62**, 263 (1993).

[31] M. Ding and E. Ott, Phys. Rev. E **49**, R945 (1994).

[32] T. Kapitaniak, Phys. Rev. E **50**, 1642 (1994).

[33] J. Güémez and M.A. Matías, Phys. Rev. E **52**, R2145 (1995).

[34] L.M. Pecora, and T. L. Carroll, Phys. Rev. Lett. **64**, 821 (1990).

[35] L.M. Pecora and T.L. Carroll, Phys. Rev. A **44**, 2374 (1991).

[36] U. Parlitz, L. Kocarev, T. Stojanovski, and H. Preckel, Phys. Rev. E **53**, 4351 (1996).

[37] W. Jinlan, C. Guangzhi, Q. Tuanfa, N. Wansun, and W. Xuming, Phys. Rev. E **58**, 3017 (1998).

[38] T. Fukai and M. Shiino, Phys. Rev. Lett. **64**, 1465 (1990).

[39] P. C. Bressloff and S. Coombes, Phys. Rev. Lett. **81**, 2168 (1998).

[40] J.F. Heagy, T.L. Carroll, and L.M. Pecora, Phys. Rev. E **50**, 1874 (1994).

[41] D. Golomb, D. Hansel, B. Shraiman, and H. Sompolinsky, Phys. Rev. A **45**, 3516 (1992).

[42] M.G. Rosenblum and A.S. Pikovsky, Phys. Rev. Lett. **92**, 114102 (2004).

[43] D.J. Watts and S.H. Strogatz, Nature (London) **393**, 440 (1998).

[44] A.L. Barabási and R. Albert, Science, **286**, 509 (1999).

[45] J. Camacho, R. Guimerá, and L.A.N. Amaral, Phys. Rev. Lett. **88**, 228102 (2002).

[46] A. Pękalski, J. Szwabiński, I. Bena, and M. Droz, Phys. Rev. E **77**, 031917 (2008).

[47] J. García-Ojalvo, M. Elowitz, S. Strogatz, Proc. Natl. Acad. Sci., **101**, 10955 (2004).

[48] A. S. Pikovsky, M. G. Rosenblum, and J. Kurths, *Synchronization: A Universal Concept in Nonlinear Sciences* , Cambridge Nonlinear Science Series, (Cambridge University Press, London, 2003).

[49] H. Fukuda, N. Nakamichi, M. Hisatsune, H. Murase, T. Mizuno, Phys. Rev. Lett. **99** 098102 (2007).

[50] J. Karbowski, Phys. Rev. Lett., **86**, 3674 (2001)

[51] L. Zemanová, C. Zhou, J. Kurths, Physica D **224**, 202 (2006).

[52] C. Zhou, L. Zemanová, G. Zamora, C.C. Hilgetag, and J. Kurths, Phys. Rev. Lett. **97**, 238103 (2006).

[53] M.E.J. Newman, SIAM Rev. **45** , 167 (2003).

[54] R. Pastor-Satorras and A. Vespignani, Phys. Rev. Lett. **86**, 3200 (2001).

[55] R.M. May and A.L. Lloyd, Phys. Rev. E **64**, 066112 (2001).

[56] F.C. Santos, J.F. Rodrigues, and J.M. Pacheco, Phys. Rev. E **72**, 056128 (2005).

[57] L.D. Valdez, P.A. Macri, and L.A. Braunstein, Phys. Rev. E **85**, 036108 (2012).

[58] D. Smilkov and L. Kocarev, Phys. Rev. E **85**, 016114 (2012).

[59] R. Yang, W. Wang, Y.C. Lai, and G. Chen, Phys. Rev. E **79**, 026112 (2009).

[60] L. Zhao, Y.C. Lai, K. Park, and N. Ye, Phys. Rev. E **71**, 026125 (2005).

[61] M.E.J. Newman, Phys. Rev. E **66**, 016128 (2002).

[62] A.E. Motter and Y.C. Lai, Phys. Rev. E **66**, 065102 (2002)

[63] R. Albert, I. Albert, and G.L. Nakarado, Phys. Rev. E **69**, 025103 (2004).

[64] R.V. Solé, M. Rosas-Casals, B. Corominas-Murtra, and S. Valverde, Phys. Rev. E **77**, 026102 (2008).

[65] L. Zdeborová, A. Decelle, and M. Chertkov, Phys. Rev. E **80**, 046112 (2009).

[66] A. Arenas, A. Díaz-Guilera, J. Kurths, Y. Moreno, and C. Zhou, Phys. Rep. **469**, 93 (2008).

[67] S. Boccaletti, V. Latora, Y. Moreno, M. Chavez, and D.U. Hwang, Phys. Rep. **424**, 175 (2006).

[68] K. Kaneko, *Theory and Applications of Coupled Map Lattices* (Wiley, New York, 1993).

[69] E. Ott, *Chaos in Dynamical Systems* (Cambridge University Press, Cambridge, 1993).

[70] C. Schäfer, M.G. Rosenblum, H.H. Abel, and J. Kurths, Phys. Rev. E **60**, 857 (1999).

[71] A. Stefanovska, H. Haken, P. V. E. McClintock, M. Hožič, F. Bajrović, and S. Ribarič, Phys. Rev. Lett. **85**, 4831 (2000).

[72] C. Liu, S.M. Reppert, Neuron, **25**, 123 (2000).

[73] H. Fujisaka, and T. Yamada, Prog. Theor. Phys. **69**, 32 (1983).

[74] N.F. Rulkov, M.M. Sushchik, L.S. Tsimring, and H.D.I. Abarbanel, Phys. Rev. E **51**, 980 (1995).

[75] L. Kocarev, and U. Parlitz, Phys. Rev. Lett. **76**, 1816 (1996).

[76] M.G. Rosenblum, A.S. Pikovsky, and J. Kurths, Phys. Rev. Lett. **76**, 1804 (1996).

[77] E.R. Rosa, E. Ott, and M.H. Hess, Phys. Rev. Lett. **80**, 1642 (1998).

[78] M.G. Rosenblum, A.S. Pikovsky, and J. Kurths, Phys. Rev. Lett. **78**, 4193 (1997).

[79] S. Taherion, and Y.C. Lai, Phys. Rev. E. **59**, R6247 (1999).

[80] C.M. Kim, S. Rim, W.H. Kye, J.W. Ryu, and Y.J. Park, Phys. Lett. A, **320**, 39 (2003).

[81] S. Camargo, R.L. Viana, and C. Anteneodo, Phys. Rev. E **85**, 036207 (2012).

[82] I. Grosu, E. Padmanaban, P.K. Roy, and S.K. Dana, Phys. Rev. Lett. **100**, 234102 (2008).

[83] I. Grosu, R. Banerjee, P.K. Roy, and S.K. Dana, Phys. Rev. E **80**, 016212 (2009).

[84] G.L. Oppo, A. Politi, G.L. Lippi, and F.T. Arecchi, Phys. Rev. A **34**, 4000 (1986).

[85] S. Sivaprakasam, E. M. Shahverdiev, P. S. Spencer, and K. A. Shore, Phys. Rev. Lett. **87**, 154101 (2001).

[86] S. Sivaprakasam, I. Pierce, P. Rees, P. S. Spencer, K. A. Shore and A. Valle, Phys. Rev. A **64** ,013805 (2001).

[87] I. Wedekind, and U. Parlitz, Phys. Rev. E **66**, 026218 (2002).

[88] A. Uchida, K. Higa, T. Shiba, S. Yoshimori, F. Kuwashima, and H. Iwasawa, Phys. Rev. E **68**, 016215 (2003).

[89] D.W. Sukow, A. Gavrielides, T. McLachlan, G. Burner, J. Amonette, and J. Miller, Phys. Rev. A **74**, 023812 (2006).

[90] H. Zhu, and B. Cui, Chaos **17**, 043122 (2007).

[91] H.D.I. Abarbanel, N.F. Rulkov, and M.M. Sushchik, Phys. Rev. E **53**, 4528 (1996).

[92] A.S. Pikovsky, M. G. Rosenblum, G. V. Osipov, and J. Kurths, Physica D **104**, 219 (1997).

[93] A.S. Pikovsky, M. Zaks, M. Rosenblum, G. Osipov, and J. Kurths, Chaos **7**, 680 (1997).

[94] E.H. Park, M. A. Zaks, and J. Kurths, Phys Rev E **60**, 6627 (1999).

[95] Y. Braiman and K. Wiesenfeld, Phys. Rev. B **49**, 15223 (1994).

[96] P.Hadley and M.R. Beasley, App. Phys. Lett. **50**, 621 (1987).

[97] J. Liu, C. Ye, S. Zhang, and W. Song, Phys. Lett. A **274**, 27 (2000).

[98] A. V. Rangan, and D. Cai, Phys. Rev. Lett. **96** ,178101 (2006).

[99] S. Sinha, and S. Sinha, Phys. Rev. E **71**, 020902(R) (2005).

[100] X. Chen and J. E. Cohen, J. Theo. Biol. **212** , 223 (2001).

[101] H. Fujigaki, M. Nishi, and T. Shimada, Phys. Rev. E **53**, 3192 (1996).

[102] P. Tass, M.G. Rosenblum, J. Weule, J. Kurths, A. Pikovsky, J. Volkmann, A. Schnitzler, and H.J. Freund, Phys. Rev. Lett. **81**, 3291 (1998).

[103] R.C. Elson, A.I. Selverston, R. Huerta, N.F. Rulkov, M.I. Rabinovich, and H.D.I. Abarbanel, Phys. Rev. Lett. **81**, 5692 (1998).

[104] A. Neiman, L. Schimansky-Geier, F. Moss, B. Shulgin, and J.J. Collins, Phys. Rev. E **60**, 284 (1999).

[105] K.J. Lee, Y. Kwak, and T.K. Lim, Phys. Rev. Lett. **81**, 321 (1998).

[106] S. Boccaletti and D.L. Valladares, Phys. Rev. E **62**, 7497 (2000).

[107] I.V. Koryukin and P. Mandel, Phys. Rev. E **65**, 026201 (2002).

[108] F. Mormann, R.G. Andrzejak, T. Kreuz, C. Rieke, P. David, C.E. Elger, and K.Lehnertz, Phys. Rev. E **67**, 021912 (2003).

[109] H.U.Voss, Phys. Rev. E **61**, 5115 (2000).

[110] D.V. Senthilkumar and M. Lakshmanan, Phys. Rev. E **71**, 016211 (2005).

[111] C. Masoller, Phys. Rev. Lett. **86**, 2782 (2001).

[112] L.M. Pecora, T.L. Carroll, G.A. Johnson, D.J. Mar, and J.F. Heagy, Chaos **7**, 520 (1997).

[113] J.M. González-Miranda, *Synchronization and Control of Chaos*, (Imperial College Press, 2004).

[114] D.V. Senthilkumar, J. Kurths, and M. Lakshmanan, Chaos **19**, 023107 (2009).

[115] S. Boccaletti, J. Kurths, G. Osipov, D. L. Valladares, and C. S. Zhou Phys. Rep. **366**, 1 (2002).

[116] P.M. Gade, C.K. Hu, Phys. Rev. E **62**, 6409 (2000) .

[117] H. Hong, M.Y. Choi, B.J. Kim, Phys. Rev. E **65** 026139 (2002) .

[118] M. Barahona, L.M. Pecora, Phys. Rev. Lett. **89**, 054101 (2002).

[119] J. Gómez-Gardeñes, S. Gómez, A. Arenas, and Y. Moreno, Phys. Rev. Lett. **106**, 128701 (2011).

[120] T. Nishikawa, A.E. Motter, Y.C. Lai, F.C. Hoppensteadt, Phys. Rev. Lett. **91**, 014101 (2003) .

[121] L.F. Lago-Fernández, R. Huerta, F. Corbacho, J.A. Sigüenza, Phys. Rev. Lett. **84**, 2758 (2000).

[122] J. Jost, M.P. Joy, Phys. Rev. E **65**, 016201 (2002) .

[123] K.S. Fink, G. Johnson, T.L. Carroll, L.M. Pecora, Phys. Rev. E **61**, 5080 (2000) .

[124] J. Gómez-Gardeñes, Y. Moreno, and A. Arenas, Phys. Rev. Lett. **98**, 034101 (2007).

[125] M. Chavez, D.U. Hwang, A. Amann, H.G. Hentschel, and S. Boccaletti, Phys. Rev. Lett. **94**, 218701 (2005).

[126] C. Zhou, A.E. Motter, and J. Kurths, Phys. Rev. Lett. **96**, 034101 (2006).

[127] C. Li, W. Sun, and J. Kurths, Phys. Rev. E **76**, 046204 (2007)

[128] Y. Shang, M. Chen, and J. Kurths, Phys. Rev. E **80**, 027201 (2009).

[129] F.M. Atay, J. Jost, and A. Wende, Phys. Rev. Lett. **92**, 144101 (2004).

[130] M. Rosenblum and A. Pikovsky, Phys. Rev. Lett. **98**, 064101 (2007).

[131] H.G. Winful, L. Rahman, Phys. Rev. Lett. **65**, 1575 (1990).

[132] G. Kozyreff, A.G. Vladimirov, and P. Mandel, Phys. Rev. Lett. **85**, 3809 (2000).

[133] W. Wang, I.Z. Kiss, and J.L. Hudson, Phys. Rev. Lett. **86**, 4954 (2001)

[134] A. Takamatsu, T. Fujii, and I. Endo, Phys. Rev. Lett. **85**, 2026 (2000).

[135] R. Bartsch, J.W. Kantelhardt, T. Penzel, and S. Havlin, Phys. Rev. Lett. **98**, 054102 (2007).

[136] B. Blasius, A. Huppert, and L. Stone, Nature 399, 354 (1999).

[137] E. Sismondo, Science 249, 55 (1990).

[138] D. Rybski, S. Harlin, and A. Bunde, Physica A 320, 601 (2003).

[139] J.A. Acebrón, L.L. Bonilla, C.J.P. Vicente, F. Ritort, and R. Spigler, Rev. Mod. Phys. **77**, 137 (2005).

[140] M. Chen, Y. Shang, Y. Zou, and J. Kurths, Phys. Rev. E **77**, 027101 (2008) .

[141] L.M. Pecora and T.L. Carroll, Phys. Rev. Lett. **80**, 2109 (1998).

[142] Y. Chen, G. Rangarajan, M. Ding, Phys. Rev. E **67**, 026209 (2003) .

[143] K. Wiesenfeld, P. Colet, and S.H. Strogatz, Phys. Rev. Lett. **76**, 404 (1996).

[144] C. van Vreeswijk, Phys. Rev. E **54**, 5522 (1996).

[145] Y. Zhang, G. Hu, H.A. Cerdeira, S. Chen, T. Braun, and Y. Yao, Phys. Rev. E **63**, 026211 (2001)

[146] R. Toral, C.R. Mirasso, E. Hernandez-Garcia, and O. Piro, Chaos **11**, 665 (2001).

[147] C.S. Zhou, and J. Kurths, Phys. Rev. Lett. **88** 230602 (2002)

[148] D. He, P. Shi, and L. Stone, Phys. Rev. E **67**, 027201 (2003).

[149] R. Mainieri and J. Rehacek, Phys. Rev. Lett. **82**, 3042 (1999).

[150] J. Yan, and C. Li, Chaos, Solitons and Fractals, **26**, 1119 (2005).

[151] Z. Li and D. Xu, Chaos, Solitons and Fractals, **22**, 477 (2004).

[152] S. Boccaletti, A. Farini, and F. T. Arecchi, Phys. Rev. E **55**, 4979 (1997).

[153] F. Sorrentino and E. Ott, Phys. Rev. Lett. **100**, 114101 (2008).

[154] B. Ravoori, A.B. Cohen, A.V. Setty, F. Sorrentino, T.E. Murphy, E. Ott, and R. Roy, Phys. Rev. E **80**, 056205 (2009).

[155] A. Bergner, M. Frasca, G. Sciuto, A. Buscarino, E.J. Ngamga, L. Fortuna, and J. Kurths, Phys. Rev. E **85**, 026208 (2012).

[156] G. Ambika and R. E. Amritkar, Phys. Rev. E **79**, 056206 (2009).

[157] G. Ambika, R.E. Amritkar, Pramana, **77**, 891 (2011).

[158] G. Ambika, R.E. Amritkar, Chaos Solitons Fract. **44**, 1035 (2011).

[159] M. Dolnik and M. Marek, J. Phys. Chem. **92**, 2452 (1988).

[160] M.F. Crowley and I.R. Epstein, J. Phys. Chem. **93**, 2496 (1989).

[161] K. Bar-Eli, Physica D **14**, 242 (1985).

[162] M. Dolnik and I. R. Epstein, Phys. Rev. E 54, 3361 (1996).

[163] K. Tsaneva-Atanasova, C. L. Zimliki, R. Bertram, and A. Sherman, Biophys. J. **90**, 3434 (2006).

[164] A. Koseska, E. Volkov, and J. Kurths, Chaos **20**, 023132 (2010).

[165] I. Ozden, S. Venkataramani, M. A. Long, B. W. Connors, and A. V. Nurmikko, Phys. Rev. Lett. **93**, 158102 (2004).

[166] E. Ullner, A. Zaikin, E. I. Volkov, and J. Garcia-Ojalvo, Phys. Rev. Lett. 99, 148103 (2007).

[167] R. Herrero, M. Figueras, J. Rius, F. Pi, and G. Orriols, Phys. Rev. Lett **84**, 5312 (2000).

133

[168] M. Wei and J. Lun , Appl. Phys. Lett. **91**, 061121 (2007).

[169] J. Benford, H. Sze, W. Woo, R.R. Smith, and B. Harteneck, Phys. Rev. Lett. **62**, 969 (1989).

[170] M.Y. Kim, R. Roy, J.L. Aron, T.W. Carr, and I.B. Schwartz, Phys. Rev. Lett. **94**, 088101 (2005).

[171] P. Kumar, A. Prasad, and R. Ghosh, J. Phys. B **41**, 135402 (2008).

[172] R.E. Mirollo and S. H. Strogatz, J. Stat. Phys. **60**, 245 (1990).

[173] B. Ermentrout, Physica D **41**, 219 (1990).

[174] Y. Zhai, I. Z. Kiss, and J. L. Hudson, Phys. Rev. E 69, 026208 (2004).

[175] R. Karnatak, R. Ramaswamy and A. Prasad, Phys. Rev. E **76**, 035201 (2007).

[176] M. Dasgupta, M. Rivera, and P. Parmananda, Chaos **20**, 023126 (2010).

[177] K. Konishi, Phys. Rev. E 68, 067202 (2003).

[178] D.V. Ramana Reddy, A. Sen, and G.L. Johnston, Phys. Rev. Lett. **80**, 5109 (1998).

[179] A. Prasad, Phys. Rev. E **72**, 056204 (2005).

[180] K. Konishi, K. Senda, and H. Kokame, Phys. Rev. E **78**, 056216 (2008).

[181] C. U. Choe, V. Flunkert, P. Hövel, H. Benner, and E. Schöll, Phys. Rev. E **75**, 046206 (2007).

[182] R. Dodla, A. Sen, and G. L. Johnston, Phys. Rev. E **69**, 056217 (2004).

[183] K. Konishi, Phys. Lett. A **341**, 401 (2005).

[184] F.M. Atay, Phys. Rev. Lett. **91**, 094101 (2003).

[185] Y. Chen, J. Xiao, W. Liu, L. Li, and Y. Yang, Phys. Rev. E **80**, 046206 (2009).

[186] P.C. Matthews, and S.H. Strogatz, Phys. Rev. Lett. **65**, 1701 (1990).

[187] L. Rubchinsky and M. Sushchik, Phys. Rev. E **62**, 6440 (2000).

[188] L.L. Rubchinsky, M.M. Sushchik, and G.V.Osipov, Mathematics and Computers in Simulation **58**, 443 (2002).

[189] J. Yang, Phys. Rev. E **76**, 016204 (2007).

[190] Z. Hou, and H. Xin, Phys. Rev. E **68**, 055103(R), 2003.

[191] W. Liu, X. Wang, S. Guan, and C.H. Lai, New Journal of Physics **11** 093016 (2009).

[192] A. Sen, R. Dodla, and G.L. Johnston, Pramana - journal of physics **64**, 465 (2005).

[193] K. Konishi, Phys. Rev. E **70**, 066201 (2004).

[194] Y.Song, J. Xu, and T. Zhang, Chaos **21**, 023111 (2011).

[195] K. Konishi, and H. Kokame, Phys. Lett. A **366**, 585 (2007).

[196] W. Zou, X. Zheng, and M. Zhan, Chaos **21**, 023130 (2011).

[197] A. Prasad, M. Dhamala, B.M. Adhikari, and R. Ramaswamy, Phys. Rev. E **81**, 027201 (2010).

[198] R. Karnatak, N. Punetha, A. Prasad, and R. Ramaswamy, Phys. Rev. E **82**, 046219 (2010).

[199] N. Punetha, R. Karnatak, A. Prasad, J. Kurths, and R. Ramaswamy, Phys. Rev. E **85**, 046204 (2012).

[200] A. Prasad, S.K. Dana, R. Karnatak, J. Kurths, B. Blasius, and R. Ramaswamy, Chaos **18**, 023111 (2008).

[201] W. Liu, J. Xiao, and J. Yang, Phys. Rev. E **72**, 057201 (2005).

[202] B.F. Kuntsevich and A.N. Pisarchik, Phys. Rev. E **64**, 046221 (2001)

[203] M. Bennett, M.F. Schatz, H. Rockwood, and K. Wiesenfeld, Proc. R. Soc. London A **458**, 563 (2002).

[204] M. Miller and B. Bassler, Annu. Rev. Microbiol. **55**, 165 (2001).

[205] C. Nadell, B. Bassler, and S. Levin, J. Biol. **7**, 27 (2008).

[206] W. Ng and B. Bassler, Annu. Rev. Genet. **43**, 197 (2009).

[207] D. Gonze, S. Bernard, C. Waltermann, A. Kramer and H. Herzel, Biophys. J. **89**, 120 (2005).

[208] A. Kuznetsov, M. Kærn and N. Kopell, SIAM J. Appl. Math. **65**, 392 (2004).

[209] R. Wang, and L. Chen, J. Biol. Rhythms **20**, 257 (2005).

[210] R. Toth, A.F. Taylor, and M.R. Tinsley, J. Phys. Chem. B **110**, 10170 (2006)

[211] J. Javaloyes, M. Perrin, and A. Politi, Phys. Rev. E **78**, 011108 (2008).

[212] K. Wiesenfeld, C. Bracikowski, G. James, and R. Roy, Phys. Rev. Lett. **65**, 1749 (1990).

[213] G. Katriel, Physica D. **237**, 2933 (2008).

[214] V. Resmi, G. Ambika, and R.E. Amritkar, Phys. Rev. E **81**, 046216 (2010).

[215] V. Resmi, G. Ambika, and R.E. Amritkar, Phys. Rev. E **84**, 046212 (2011).

[216] A. Namajūnas, K. Pyragas, and A. Tamaševičius, Phys. Lett. A **204**, 255 (1995).

[217] J.H. Peng, E.J. Ding, M. Ding, and W. Yang, Phys. Rev. Lett. **76**, 904 (1996).

[218] G. Rangarajan, and M. Ding, Phys. Lett. A **296**, 204 (2002).

[219] V. Resmi, G. Ambika, R.E. Amritkar, and G. Rangarajan, Phys. Rev. E **85**, 046211 (2012).

[220] M. Rosenblum and A. Pikovsky, Phys. Rev. E **70**, 041904 (2004).

[221] R. D. Pinto, P. Varona, A.R. Volkovskii, A. Szücs, H.D.I. Abarbanel, and M.I. Rabinovich, Phys. Rev. E **62**, 2644 (2000) .

[222] N. Burić, K. Todorović, and N. Vasović, Phys. Rev. E **78**, 036211 (2008).

[223] R. Erichsen, Jr. and L.G. Brunnet, Phys. Rev. E **78**, 061917 (2006).

[224] I. Belykh , E. de Lange, and M. Hasler, Phys Rev Lett **94**, 188101 (2005) .

[225] B. Hu, and C. Zhou, Phys. Rev. E **61**, R1001 (2000).

[226] M.I. Rabinovich, P. Varona, A.I. Selverston, and H.D.I. Abarbanel, Rev. Mod. Phys. **78**, 1213 (2006).

[227] S.G. Hormuzdi, M.A. Filippov, G. Mitropoulou, H. Monyer, R. Bruzzone, Biochim. Biophys. Acta **1662** 113 (2004).

[228] M.V.L Bennett and R.S. Zukin, Neuron, **41**, 495 (2004).

[229] M. Yoshioka, Phys. Rev. E **71**, 065203 (2005)

[230] J.J. Letzkus, B.M. Kampa, and G.J. Stuart, J. Neurosci., **26**, 10420 (2006).

[231] V. Booth and A. Bose, J. N. Physiol. ,**85**, 2432 (2001).

[232] D.J. Selkoe, Science,**298**, 789 (2002).

[233] D.M. Walsh and D.J. Selkoe, Neuron, **44** , 181 (2004).

Index